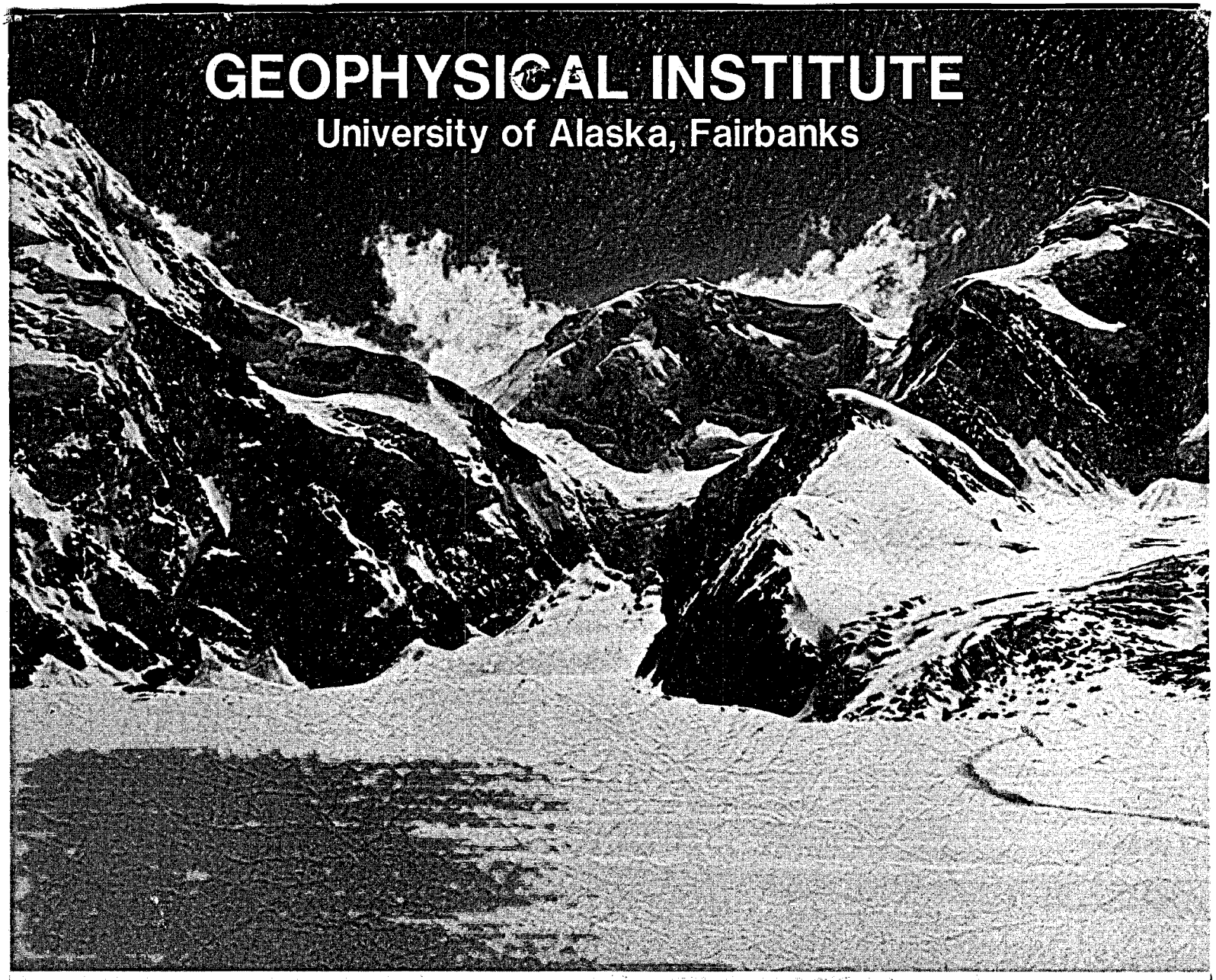

UAG R-271

A GEOLOGICAL AND GEOPHYSICAL STUDY OF THE GEOTHERMAL ENERGY POTENTIAL OF PILGRIM SPRINGS, ALASKA

Donald L. Turner and Robert B. Forbes, Editors

Report to:

U.S. Department of Energy
and
Alaska Division of Energy and Power Development

January 1980

DISCLAIMER

A GEOLOGICAL AND GEOPHYSICAL STUDY OF THE GEOTHERMAL ENERGY POTENTIAL OF PILGRIM SPRINGS, ALASKA

Donald L. Turner and Robert B. Forbes, Editors

Prepared for:

The Division of Geothermal Energy of the U.S. Department of Energy
Cooperative Agreement DE-FC07-79ET27034
Principal Investigator: Donald L. Turner
Co-Principal Investigators: Eugene M. Wescott
Juergen Kienle

and:

The State of Alaska
Division of Energy and Power Development
Contract 79-580
Principal Investigator: Robert B. Forbes
Co-Principal Investigators: Eugene M. Wescott
Juergen Kienle

Participating Scientists:

Thomas Osterkamp, Jeffrey Kline[1], Daniel Hawkins, Samuel Swanson, William Harrison, Joan Gosink, Richard Reger[1], Roman Motyka[1], Laurence Lawver[2]

Research Assistants:

Jerry Peace, Andrew Lockhart, Richard Sydora, Rena McFarlane[1], Thomas Williams[1], Richard Gaffi, Danita Maynard, J. Hanscom, M. Kane, Camille Stephens, Mary Moorman, Jeffrey Morehouse

[1]Alaska Division of Geological and Geophysical Surveys
[2]U.S. Geological Survey, Menlo Park, California

Geophysical Institute Report UAG R-271

January 1980

TABLE OF CONTENTS

	Page
SUMMARY	iv
INTRODUCTION	1
REFERENCES	5
ACKNOWLEDGEMENTS	6
BEDROCK GEOLOGY OF THE PILGRIM SPRINGS GEOTHERMAL AREA, ALASKA by S.E. Swanson, D.L. Turner, R.B. Forbes, and D. Maynard	7
Introduction	7
Previous Work	8
Metamorphic and Intrusive Rocks of Probable Precambrian Age	8
Calc-Silicate Rocks	9
Metaquartzite	9
Gneissic Rocks	10
Paragneiss	10
Chlorite-Biotite Schist	11
Gneissic Granite	11
Intrusive Igneous Rocks of Probable Mesozoic Age	12
Biotite Granodiorite	13
Biotite Quartz Monzonite/Granodiorite	13
Granite Pegmatites	13
Metamorphism	14
Structure	16
Faults	17
References	20
SURFICIAL GEOLOGY AND TEST DRILLING AT PILGRIM SPRINGS, ALASKA by J.T. Kline, R.D. Reger, R.M. McFarlane and T. Williams	21
Surficial Geology	21
Preliminary Drilling Results	22
References	28
LOCAL AND REGIONAL GEOTHERMAL GRADIENTS AND RADIOGENIC HEAT PRODUCTION IN CRYSTALLINE BASEMENT ROCKS by R.B. Forbes	29
Radiogenic Heat and Geothermal Gradients	29
Near Surface Heat Production in Crystalline Rocks	29
Sample Location and Distribution	30
Uranium-Thorium Concentration and Heat Production Calculations	30

TABLE OF CONTENTS (Cont'd)

	Page
Local and Regional Geothermal Gradients	33
Test Wells in the Baldwin Peninsula-Cape Espenberg Areas	35
The Nimiuk Pt. #1 Well	37
The Cape Espenberg #1 Well	37
Summary	41
Acknowledgements	42
References	42
GEOCHEMISTRY OF PILGRIM SPRINGS THERMAL WATERS by R.J. Motyka, R.B. Forbes and M. Moorman	43
Introduction	43
Water Chemistry	45
Geothermometry	47
Dissolved Gases	48
Discussion	49
Acknowledgements	50
References	51
SEISMIC REFRACTION SURVEY OF THE PILGRIM SPRINGS GEOTHERMAL AREA, ALASKA by J. Kienle, A. Lockhart and J. Peace	53
Objectives	53
Background and Previous Work	53
Methods and Instrumentation	54
Results	57
Stratigraphic Interpretation	70
Summary and Conclusions	71
References	72
GRAVITY SURVEY OF THE PILGRIM SPRINGS GEOTHERMAL AREA, ALASKA by J. Kienle and A. Lockhart	73
Objectives	73
Methods	73
Results	76
References	79
ELECTRICAL RESISTIVITY SURVEY OF THE PILGRIM SPRINGS GEOTHERMAL AREA, ALASKA by E. Wescott, R. Sydora, J. Peace and A. Lockhart	81
Theory	81
Methods	81
Previous Work	82
1979 Survey	82
References	100

TABLE OF CONTENTS (Cont'd)

	Page
WATER AND HEAT FLOW MEASUREMENTS AND THEIR RELATIONSHIP TO POWER ESTIMATES AT PILGRIM SPRINGS, ALASKA by W. Harrison and D. Hawkins	101
Introduction	101
Procedures and Results	101
Surface Measurements	101
Borehole Measurements	104
Discussion	110
Surface Measurements	110
Borehole Measurements	110
Power Budget	112
Acknowledgement	112
References	112
A RECONNAISSANCE STUDY OF THE HYDROTHERMAL CHARACTERISTICS AND ACCESSIBLE POWER OF PILGRIM SPRINGS, ALASKA by T.E. Osterkamp, J.P. Gosink, R.B. Forbes, R.G. Gaffi, J.T. Hanscom, M.L. Kane, C.A. Stephens, J. Kline	113
Introduction	113
Temperature Measurements	114
Electrical Conductivity Measurements	124
Hydrological Measurements	136
Discussion, Models, Energy and Power	146
Acknowledgements	153
Appendix A	154
References	156
CONCLUSIONS AND RECOMMENDATIONS FOR PHASE-TWO GEOPHYSICS, HYDROLOGY, EXPLORATORY DRILLING, AND GEOCHEMISTRY AT PILGRIM SPRINGS, ALASKA by D.L. Turner, R.B. Forbes, T.E. Osterkamp, E.M. Wescott and J. Kienle	157
Conclusions	157
Recommendations	159
Hydrothermal Studies of the Pilgrim River	159
Geophysical Surveys	160
Exploratory Drilling	161
Recommended Work Schedule	164
References	165
PLATE I	

SUMMARY

The Pilgrim Springs geothermal area, located about 75 km north of Nome, was the subject of an intensive, reconnaissance-level geophysical and geological study during a 90-day period in the summer of 1979. The thermal springs are located in a northeast-oriented, oval area of thawed ground approximately 1.5 km^2 in size, bordered on the north by the Pilgrim River. A second, much smaller, thermal anomaly was discovered about 3 km northeast of the main thawed area. Continuous permafrost in the surrounding region is on the order of 100 m thick.

Present surface thermal spring discharge is $\approx 4.2 \times 10^{-3}$ m^3 s^{-1} (67 gallons/minute) of alkali-chloride-type water at a temperature of 81°C. The reason for its high salinity is not yet understood because of conflicting evidence for seawater vs. other possible water sources. Preliminary Na-K-Ca geothermometry suggests deep reservoir temperatures approaching 150°C, but interpretation of these results is difficult because of their dependence on an unknown water mixing history. Based on these estimates, and present surface and drill hole water temperatures, Pilgrim Springs would be classified as an intermediate-temperature, liquid-dominated geothermal system.

The springs are located in the Pilgrim River Valley, a fault-bounded tectonic depression, or graben, flanked on the north and south by mountains composed of highly-deformed, upper amphibolite facies metamorphic rocks of probable Precambrian age, cut by discordant granitic plutons of probable Mesozoic age. Seismic, gravity and resistivity surveys indicate that the crystalline basement of the valley floor is at least 200 m beneath Pilgrim Springs, much deeper than was previously believed. The gravity data also suggest that Pilgrim Springs is near

the intersection of two inferred fault zones forming the corner of a deep, downdropped basement block.

The seismicity of the area indicates currently active normal faulting. Mapped north-south trending faults in the Kigluaik Mountains south of Pilgrim Springs may extend through the downdropped crystalline basement under the Pilgrim River Valley. One or more of these faults could possibly provide a deep conduit for the geothermal system. Surficial geologic mapping indicates considerable subsidence of the Pilgrim River Valley during Quaternary time. A north-south trending Quaternary fault extends across the valley and appears to coincide with the western boundary of the main thawed area. Resistivity studies confirm the presence of this fault but do not suggest that it is presently serving as a hot water conduit in the vicinity of our resistivity profile.

Geologic evidence suggests that the low-lying region extending from the Imuruk Basin through the Kuzitrin Valley to the Imuruk lava fields may represent an incipient rift through the Seward Peninsula. We therefore propose that the mainifestations of anomalous heat flow (young volcanism and alkali-chloride hot springs) in this region may be associated with tensional tectonics and active rifting.

Resistivity surveys have located a shallow, 50 m-thick, pancake-shaped reservoir of hot, saline water about 1 km^2 in area under Pilgrim Springs. Shallow ground electromagnetic surveys (used here for the first time in a geothermal area), ground temperature surveys and modelling of convection cells have been used in conjunction with deep resistivity surveys to determine drilling targets within the area of this reservoir. Thermal, hydrologic and geologic models of the total geothermal system suggest that hotter reservoirs could be present at greater depths. Computer modelling of resistivity data does not rule out this possibility.

Two 50 m exploratory test holes, separated by 100 meters, were drilled in November, 1979, in the area of the primary drilling target recommended in our preliminary report. Artesian aquifers were encountered in a 20-30 m depth interval. Flow rates were estimated at 200 and 300-400 gallons per minute, respectively, at a temperature of 90°C.

Preliminary hydrologic studies involving a Pilgrim River temperature survey and ground water flow estimates calculated from temperature profiles have resulted in a proposed water balance model and power estimates for the geothermal system. Our analysis suggests that the power presently being dissipated from the upper 50 m of the system is a minimum of 350 megawatts (MW), with more than 300 MW of this amount in subsurface groundwater discharge beneath the Pilgrim River. The accessible resource base for the upper 50 m of the system referenced to 0°C is estimated at 500 MW. The beneficial power available for direct (nonelectric) use is estimated at 30 MW. Referencing these estimates to 15°C would reduce them to 2/3-3/4 of the above values. Quantitative estimates of the electrical power potential will depend on engineering and reservoir parameters which are presently unknown. It is clear, however, that the electrical power potential will probably be a small fraction of the 30 MW beneficial power estimate.

We emphasize that many hydrologic measurements are preliminary, based on reconnaissance-level studies, and that our preliminary power estimates should be viewed with caution until they can be tested by more extensive field measurements and analysis. A follow-on program of more extensive geophysical surveys, hydrologic studies, exploratory drilling and geochemical studies is proposed in order to achieve a more complete understanding of the Pilgrim Springs geothermal system and to provide a basis for future power estimates, production drilling, engineering studies and commercial site development.

INTRODUCTION

Pilgrim Springs, Alaska was the subject of an intensive geophysical and geological survey during June-August, 1979. The springs are located on the Seward Peninsula, about 75 km north of Nome (Figure 1). Earlier studies, including a reconnaissance geological and geophysical survey by Forbes, et al. (1975), and geochemical studies of Pilgrim Springs waters by the U.S. Geological Survey (Waring, 1917; Miller, et al., 1975) had indicated that Pilgrim Springs might be an important geothermal target.

Geophysical Institute personnel were responsible for project management, bedrock mapping, geophysical surveying, analysis and integration of field data, and preparation of the final report. Alaska Division of Geological and Geophysical Surveys (A.D.G.G.S.) personnel were responsible for surficial mapping, geologic supervision and logging of test drill holes, geochemical analyses, and preparation of the sections of this report covering these areas.

Base camp was established at Pilgrim Springs, Alaska on June 16, 1979. The field program was initiated with the thermal gradient measurements which were accomplished with driven probes on a 100 meter grid (Figure 2). Helicopter supported mapping produced a 1:63,360 scale geologic map of the surrounding area (Plate I). A surficial geologic map of the area is being prepared at a scale of 1:14,000 by the A.D.G.G.S. Mapping, temperature measurement and electrical conductivity work was completed by July 15, 1979. Seismic, resistivity, and gravity studies were completed on July 29, 1979, and the camp was closed on July 31, 1979.

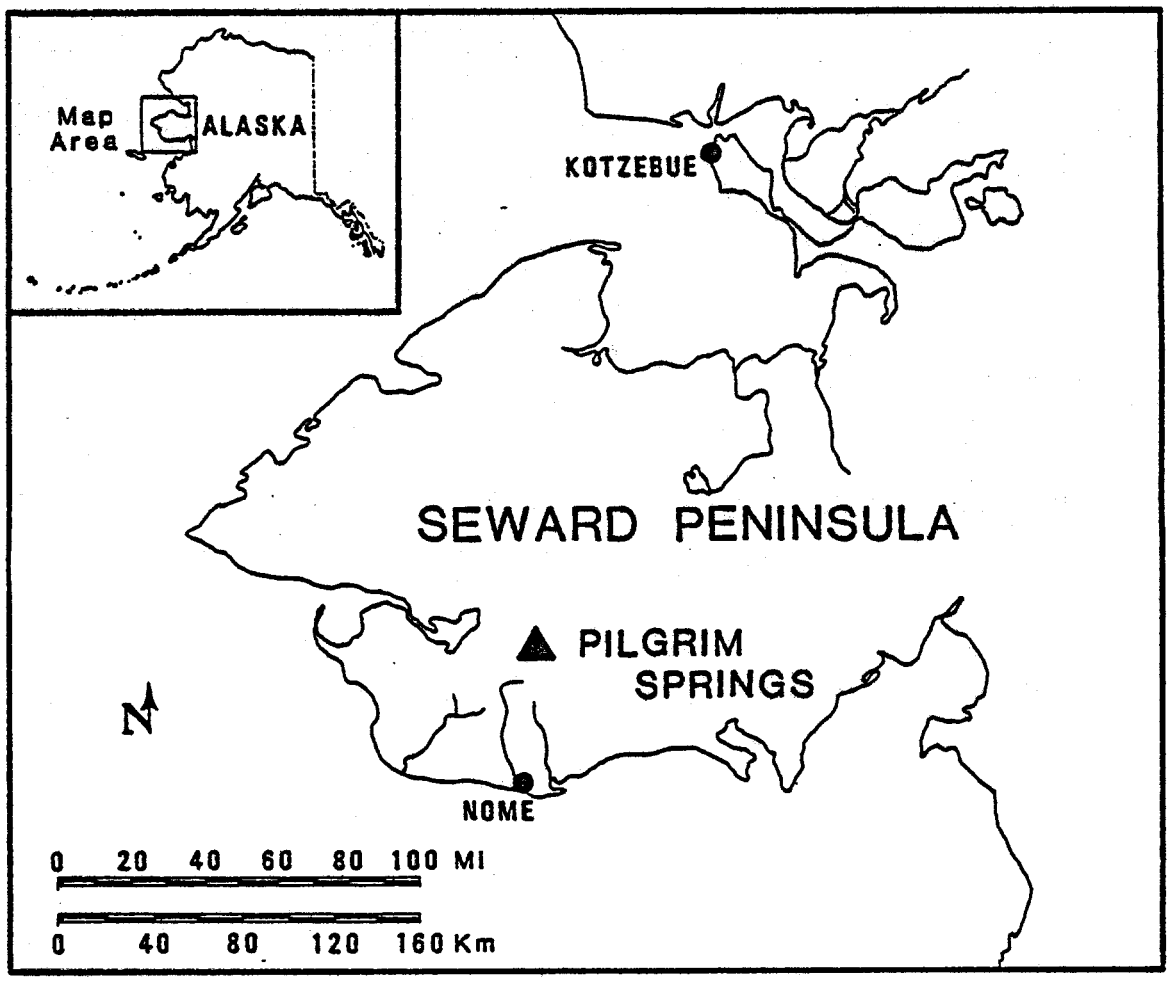

Figure 1. Location of Pilgrim Springs.

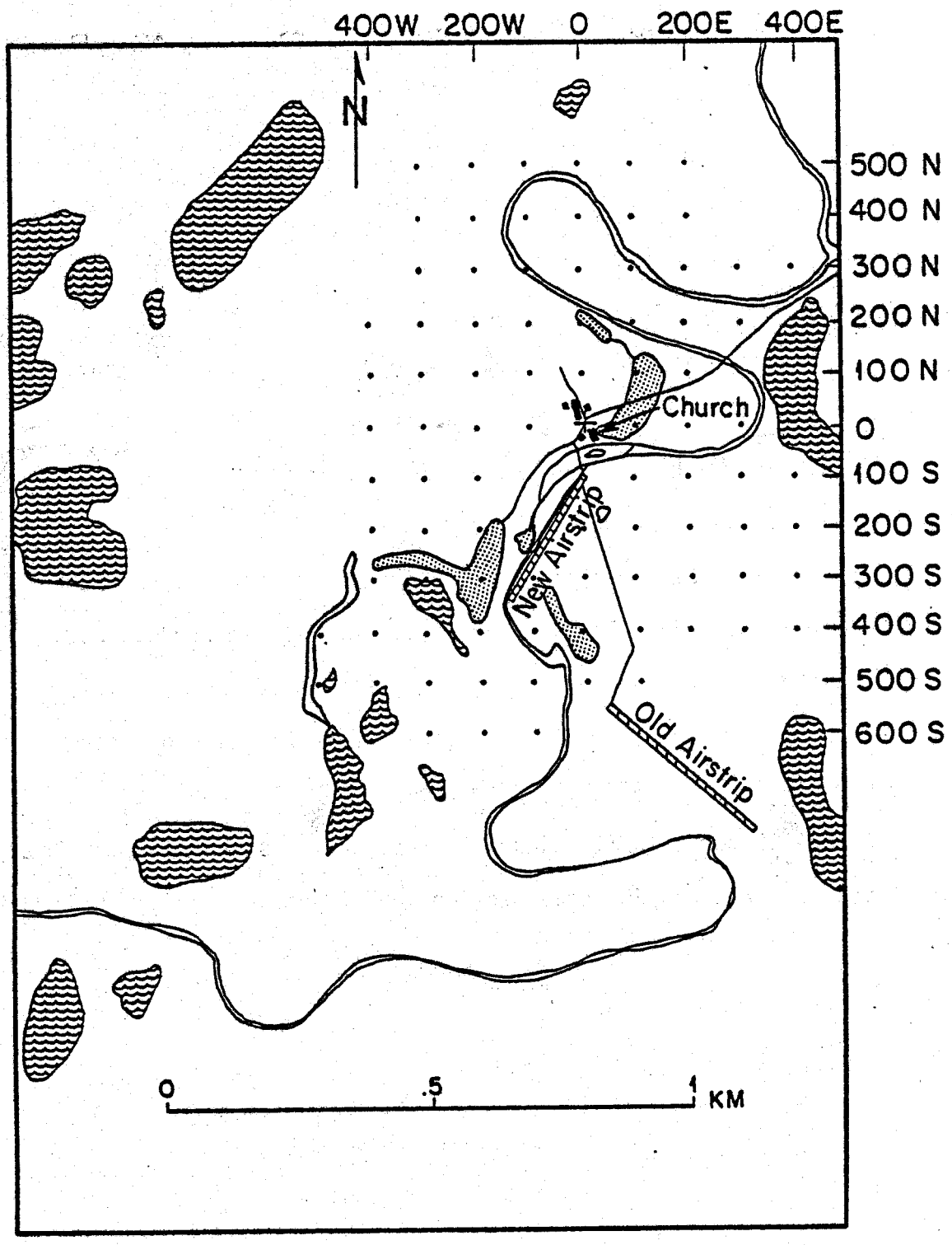

Figure 2. Points on surveyed 100 meter grid used as base for all geophysical surveys and drill hole locations. Stippled areas are agricultural fields. Wave pattern indicates lakes and ponds.

A preliminary report to the Alaska Division of Energy and Power Development (A.D.E.P.D.) with analysis of field data and drilling recommendations was completed in late August, 1979 (Forbes, et al., 1979). Based on the recommendations of the report, the A.D.E.P.D. contracted for two 150-ft test drill holes which were drilled in November, 1979, with geologic supervision and logging by the A.D.G.G.S.

The present report contains a more extensive analysis of the results of the geological and geophysical surveys than was presented in the preliminary report. It also provides a preliminary discussion of the recent initial exploratory drilling results and recommendations for phase-two geophysical surveys, hydrologic studies, exploratory drilling and geochemical studies. All geophysical surveys and drill hole locations discussed in subsequent sections of this report are referenced to the 100-meter-spacing, surveyed grid shown in Figure 2.

The Geophysical Institute part of the Pilgrim Springs study was supported by funding from the U.S. Department of Energy, Division of Geothermal Energy ($97,000); State of Alaska Division of Energy and Power Development ($56,000); Comprehensive Employment Training Act ($20,000); and National Science Foundation, Division of Polar Programs, Polar Earth Sciences Section, NSF Grant DPP77-20462 ($15,000).

REFERENCES

Forbes, R. B., L. Gedney, D. VanWormer and J. Hook, (1975) A geophysical reconnaissance of Pilgrim Springs, Alaska; Technical report, Geophysical Institute, University of Alaska.

Forbes, R. B., E. M. Wescott, D. L. Turner, J. Kienle, T. Osterkamp, D.B. Hawkins, J. T. Kline, S. Swanson, R. D. Reger and W. Harrison, 1979, A geological and geophysical assessment of the geothermal potential of Pilgrim Springs, Alaska, Geophysical Institute, University of Alaska and Alaska Division of Geological and Geophysical Surveys Preliminary Rept., 39 pp., 1 plate.

Miller, Thomas P., Ivan Barnes and William W. Patton, Jr., (1975) Geologic setting and chemical characteristics of hot springs in west-central Alaska; J. Research U.S. Geological Survey, V. 3, No. 2, March-April 1975, p. 149-162.

Waring, G. A., (1917) Mineral springs of Alaska; U.S. Geological Survey Water Supply Paper 492.

ACKNOWLEDGEMENTS

We are deeply indebted to the C.J. Phillips and Louis Green families of Nome, Alaska for their continued cooperation and support throughout the Pilgrim Springs project. This report was typed and collated by Penny Toston. Figures were drafted by James Burton, Debbie Coccia, Danny Thompson, and Brian Blevins. A considerable amount of drafting and typing were done outside of normal working hours and we wish to thank our drafting department and typist for their dedication and fine work.

BEDROCK GEOLOGY OF THE PILGRIM SPRINGS GEOTHERMAL AREA, ALASKA

Samuel E. Swanson, Donald L. Turner,
Robert B. Forbes and Danita Maynard

INTRODUCTION

Pilgrim Springs is located in the Pilgrim River Valley, about 75 km north of Nome, Alaska. The valley is about 6.5 km wide, and bounded on the north by Marys Mountain and Hen and Chickens Mountain, and to the south by the Kigluaik Mountains. Helicopter-supported mapping has produced a 1:63,360-scale geologic map of the area (Plate I, in pocket). The mountains are composed of Precambrian upper amphibolite facies metamorphic rocks, cut by discordant granitic intrusions of probable Mesozoic age. Locally some of the metamorphic rocks show the effects of retrograde metamorphism to upper greenschist facies. The metamorphic sequence includes pelitic gneisses, synkinematic gneissic granites, calc-magnesian schists, and metaquartzites. The metamorphic terrane is highly deformed with east-west trending isoclinal-overturned-to-recumbent folds.

The Kigluaik Mountains are bounded on the north by a prominent range front fault, the Kigluaik Fault, which cuts glacial moraines and is inferred to be still active. The valley floor is downthrown to the north. The actual displacement is unknown, but geophysical surveys indicate a downthrow of at least 200 meters (Kienle, et al., this report). The Pilgrim River Valley appears to be a fault-bounded tectonic depression filled by a great thickness of relatively unconsolidated sedimentary fill, including alluvial sediments, glacial outwash, terrace deposits and possible Tertiary sediments at depth. The valley is an eastern extension of the Imuruk Basin, and is similar to the Kuzitrin basin to the northeast which contains a considerable thickness of sedimentary fill, including Tertiary gravels.

Several north-south trending faults with large displacements were mapped in the Kigluaik Mountains south of Pilgrim Springs. It is likely that these faults may extend through the downdropped crystalline basement under the Pilgrim River Valley.

PREVIOUS WORK

The area surrounding Pilgrim Springs (Bendeleben A-6 and Teller A-1 quadrangles) has been mapped previously by C.L. Sainsbury (1969a, 1972, 1974, 1975). This earlier work provided a useful geologic background for our subsequent, more detailed mapping and petrologic studies. These studies have resulted in a somewhat different set of designated map units than those used by Sainsbury, as discussed below.

METAMORPHIC AND INTRUSIVE ROCKS OF PROBABLE PRECAMBRIAN AGE

The Pilgrim Springs area contains a heterogeneous assemblage of metamorphic rocks that have been recrystallized under conditions corresponding to the upper amphibolite facies of the Barrovian Facies Series of regional metamorphism. Paragneisses from the core of the Kigluaik Mountains complex southwest of Pilgrim Springs give a Rb-Sr whole rock isochron age of 735 m.y. (late Precambrian). This probably represents a minimum age for metamorphism and the parent rocks are thus at least late Precambrian in age (Bunker and others, 1977). Intrusion of small masses of biotite quartz monzonite and biotite granite in the form of small stocks and pegmatites has had little effect on mineral assemblages in the metamorphic rocks. An

area of retrograde metamorphism (chlorite and epidote-bearing assemblages) is found along the northern border of the Kigluaik Mountains.

Calc-Silicate Rocks

In the northwest portion of the area studied, calc-silicate rocks are the dominate lithology and are mapped as a separate unit. They also occur in minor amounts as thin beds or layers within the pelitic gneisses interlayered with biotite paragneiss. The calc-silicate rocks include diopside-quartz-plagioclase±calcite gneiss, quartz-plagioclase-hornblende± garnet amphibolite, and calcite marble. Other minerals include talc, chlorite, tremolite, scapolite, vesuvianite, and sphene. These lithologies are intimately interlayered, even at the scale of a thin section, reflecting either original bedding or metamorphic differentiation. Retrograde metamorphism has resulted in the partial conversion of diopside to an assemblage of calcite+tremolite in one sample studied, and in the formation of chlorite in three others.

Metaquartzite

The dominate lithology of this map unit is a dark-gray, fine-grained graphitic metaquartzite. Outcrops are not found in the area studied and exposures are limited to angular surface rubble. In the eastern Kigluaik Mountains the fine grain size combined with the abundance of graphite give the rock the appearance of slate.

The metaquartzite contains minor amounts of graphite, muscovite, sillimanite, biotite, and chlorite. Some of the muscovite is being replaced by sillimanite, resulting in fibrous patches of white mica and sillimanite 1-3 mm across that are apparent in hand specimen. Chlorite appears to be a retrograde phase associated with biotite.

Due to a lack of outcrop, contact relations between the metaquartzite unit and other units could not be determined. However, the distribution of the unit (Plate I) suggests it is conformable with the paragneiss. In the eastern portion of the map area, small amounts of metaquartzite are found interlayered with the paragneiss, again suggesting a conformable relationship between the units. Considering the map pattern of this unit (Plate I) it is possible that there may be more than one metaquartzite unit in the area.

Gneissic Rocks

Gneissic rocks include biotite-quartz-plagioclase paragneiss and gneissic biotite granite. The two lithologies are easily distinguished in the field and they have been mapped as two separate units (Plate I). Contact relations show that the gneissic granite is intrusive into the paragneiss as evidenced by cross-cutting relations and xenoliths of paragneiss included in the granite.

Paragneiss

Biotite-quartz-plagioclase paragneiss is the dominant lithology in the region studied (Plate I). Concentration of biotite into discontinuous bands or lenses gives the rock a banded appearance. Modal amounts of biotite are variable and in some places the rock could be termed a schist. The unit does form moderately abundant outcrops and preferential weathering of the biotite-rich layers accentuates the foliation.

Plagioclase and quartz are generally the most abundant minerals in the paragneiss, although biotite is quite abundant in some samples. Other minerals that are locally important in the paragneiss include garnet, sillimanite, muscovite, staurolite, andalusite, alkali feldspar,

and chlorite. Textural relations indicate that the andalusite and some of the muscovite have been replaced by sillimanite. Alkali feldspars contain coarse perthitic exsolutions in some samples, especially in samples that contain chlorite.

The biotite-quartz-plagioclase paragneiss commonly contains small layers of metaquartzite and calc-silicate rocks and this, together with the apparently conformable contacts, indicates that the paragneiss-metaquartzite-calc-silicate units probably represent a conformable sequence of metasediments. This sequence was intruded by granite (now the gneissic granite) prior to the thermal peak of metamorphism. The andalusite noted in one thin section may represent a relic phase formed during the contact metamorphism associated with the granite intrusion.

Chlorite-Biotite Schist

Mineral assemblages found in this unit are retrograde assemblages containing chlorite in the pelitic rocks and tremolite in the calc-silicates. The unit is restricted to the northern border of the Kigluaik Mountains. The unit probably represents pelitic rocks of the paragneiss unit that have undergone low temperature recrystallization to produce chlorite and tremolite. Relic high temperature phases such as sillimanite or diopside are locally preserved. Only the retrograde metamorphism distinguishes this unit from the paragneiss.

Gneissic Granite

Gneissic granite is widespread in the southwestern portion of the area studied (Plate I) where it forms isolated masses surrounded by the paragneiss and metaquartzite units. The unit has a good foliation defined by biotite and is generally conformable to the regional foliation. Compositional layering, defined by biotite abundance, is common in this unit.

Outcrops of gneissic granite are fairly abundant and in some cases form picturesque tors, such as those found on Hen and Chickens Mountain.

Mineralogically, the granite is dominated by feldspars and quartz with alkali feldspar being more abundant than plagioclase. Biotite is the common mafic mineral, minor hornblende was found in several samples and a blue amphibole (riebeckite?) was found in one sample. Other minerals include sillimanite, garnet, muscovite, and chlorite. Sillimanite is found replacing muscovite in some of the samples; while chlorite is replacing biotite in other samples. Perthitic alkali feldspars are found in some samples that also contain chlorite.

Contact relations show the granite is intrusive into the paragneiss and the metaquartzite. The granite is not in contact with the calc-silicate rocks in the area studied, but it is presumed to be younger than these rocks. The appearance of sillimanite in the granite indicates that these granitic rocks were crystalline prior to the thermal peak of metamorphism.

INTRUSIVE IGNEOUS ROCKS OF PROBABLE MESOZOIC AGE

Intrusions of three distinct lithologies crosscut the regional foliation and have igneous mineral assemblages and textures, indicating that they post-date the regional metamorphism in the area. The intrusions (with the exception of the granite pegmatites) do not form outcrops and it is thus difficult to study contact effects on the intruded metamorphic rocks. The three types of intrusions are: medium-grained, unfoliated, biotite granodiorite with locally abundant sphene; unfolidated, medium-grained biotite quartz monzonite; and dikes of granite pegmatite with tourmaline and garnet. Since none of

these units are in contact with the other, it is impossible to determine relative age relations. It is possible that the granite pegmatite dikes are genetically related to either or both of the other intrusions.

Biotite Granodiorite

A pluton of biotite granodiorite outcrops in the south-central Kigluaik Mountains (Plate I). The granodiorite is unfoliated, medium grained and is characterized by locally abundant sphene. Biotite, in part altered to chlorite, is the most abundant accessory mineral. Plagioclase is more abundant than alkali feldspar and is commonly altered to sericite and clay minerals in the calcium-rich cores. Although contact relations between the granodiorite and the metamorphic rocks are obscured by rubble, the massive character and mineralogy both suggest that intrusion of the pluton post-dates the regional metamorphism.

Biotite Quartz Monzonite/Granodiorite

Rubble crops of this unit are found in the north-eastern part of the area studied (Plate I). The rock is massive and contains alkali feldspar and plagioclase in variable amounts. Biotite and hornblende are the common accessory phases. The rubble crops of this unit are believed to represent post metamorphic intrusions.

Granite Pegmatites

Pegmatite dikes (up to 500 m long and 100 m wide) of granite composition form good outcrops in the area studied. The rocks are typically very coarse-grained and contain alkali feldspar in much greater amounts that plagioclase. Additional accessory minerals include muscovite, garnet, and tourmaline. Biotite was only observed in one or two outcrops. The dikes intrude and cross cut the foliation of all the metamorphic rocks units.

METAMORPHISM

Metamorphic rocks in the Pilgrim Springs area have been regionally metamorphosed under conditions corresponding to the upper amphibolite facies of the Barrovian Facies Series of regional metamorphism. Mineral assemblages in the pelitic rocks are commonly sillimanite+biotite+quartz+plagioclase (±staurolite, ±muscovite, ±garnet). Calc-silicate rocks contain the assemblage diopside+quartz+plagioclase (±hornblende±calcite±sphene±biotite±scapolite). Amphibolites commonly contain quartz+hornblende+plagioclase (±garnet±sphene). Within the paragneiss of the Kigluaik Mountains are layers of granitic rock suggesting partial melting of the metamorphic rocks at the peak of the thermal episode. A Rb-Sr whole-rock isochron age of 735 m.y. has been determined for paragneisses of the Kigluaik Mountains by Bunker, et al. (1977). This age probably corresponds to the time of post-metamorphic cooling and the protolith is therefore older than 735 m.y.

All three polymorphs of Al_2SiO_5 are found in the pelitic rocks of the Kigluaik Mountains. Sillimanite is the dominant form and is widespread throughout the area. It occurs in mica-rich layers as slender needles and prisms up to 15 mm in length. Andalusite as anhedral crystals 1-2 mm long is found in a sample from the Kigluaik Mountains 4.5 km east of Pass Creek at an elevation of 580 m. The andalusite is not in equilibrium and is being replaced by sillimanite. Kyanite occurs as euhedral crystals up to 0.5 mm long in association with sillimanite in pelitic gneiss 5.5 km east of Pass Creek at an elevation of 500 m in the Kigluaik Mountains. Some of the kyanite is rimmed by sillimanite. Pressure-temperature conditions during the regional metamorphism were clearly in the stability field of sillimanite. However,

the pressure-temperature path followed prior to the peak of metamorphism must have come close to the aluminosilicate triple point (6Kb, 600°C) as evidenced by the occurrence of all three polymorphs within a relatively small geographic area.

Due to the uniformly high grade of metamorphism in the Pilgrim Springs area, it has not been possible to map isograds. However, the distribution of muscovite does form a pattern within the area studied, a pattern that is probably related to metamorphic grade. Muscovite is found as a stable phase in pelitic rocks of the eastern hills and the southeastern Kigluaik Mountains. In the central Kigluaik Mountains, muscovite is found being replaced by sillimanite. Muscovite is not found in the western range front of the Kigluaik Mountains, Marys Mountain, Hen and Chicken Mountain, or in the extreme southern portion of the study area. Apparently the pressure-temperature conditions in these areas exceeded the upper stability limit of muscovite+quartz during metamorphism.

Evidence for retrograde metamorphism in the Pilgrim Springs area is found in the contact zones of igneous intrusions and along the northern border of the Kigluaik Mountains. Pelitic and calc-silicate gneisses form a small pendant in the granitic rocks of Hen and Chickens Mountain. The metamorphic rock has been intruded by the granite and the granite contains hornblende near the contact with the metamorphic rocks. Mineral assemblages in the pelitic rocks are characterized by epidote+chlorite+biotite+plagioclase+quartz, while the calc-silicate rocks contain clinozoisite+tremolite+biotite+diopside+ plagioclase+quartz. Chlorite and epidote are replacing biotite in the pelitic rocks and tremolite is replacing diopside in the calc-silicate rocks. Extensive chloritization of biotite in the assemblage sphene+biotite+ diopside+quartz+plagioclase is also found in the contact zone of the plutons

in the eastern hills. A rock unit composed of retrograded calc-silicate and pelitic rocks occurs along the northern margin of the central and western Kigluaik Mountains. Calc-silicate rocks contain the assemblage clinozoisite+ tremolite+biotite+quartz+plagioclase and the pelitic rocks are characterized by biotite+plagioclase (largely altered to muscovite)+ quartz. Some relic sillimanite is found in the pelitic rocks, but only as inclusions in biotite. The distributions of these relatively low grade rocks near the Kigluaik Fault suggests this retrograde metamorphism might be related to movement along the fault, perhaps caused by the movement of hot fluids along the fracture system.

STRUCTURE

Structural relations discussed here are based on observations made principally in the metamorphic rocks. The igneous rocks, with the exception of the gneissic granite, are unfoliated and generally structureless. Where relic bedding is found, the strike is westerly and dips are moderate to either the north or south. Large-scale folding was not recognized during the present study. However, small-scale, east-west-trending, isoclinal-overturned-to-recumbent folds suggest a complex deformational history for the metamorphic rocks. Jointing is common in the basement rocks and is especially well developed in the intrusive igneous rocks. These joints control the formation of the distinctive tors developed on the gneissic granite of Hen and Chickens Mountain and the granite pegmatites of the eastern hills. Faulting in the area is characterized by high-angle faults with a significant component of vertical movement. Only one possible low-angle fault was identified in the current study.

Faults

High-angle dip-slip faults are common in the Kigluaik Mountains, south of Pilgrim Springs (Plate I). Two sets of faults are found, one with a east-west strike and another with a predominantely north-south orientation. This orthogonal fault system, together with the east-west trending pattern of contacts between rock units, produces a checkerboard pattern of rock units, especially well-developed in the southwestern portion of the map area (Plate I). The offset of the steep lithologic contacts together with the trace of the faults shows the high-angle character of these features. An east-west system of faults forms the northern border of the Kigluaik Mountains and is called the Kigluaik Fault. Two distinct "steps" in the range-front are found in the map area and these appear to correspond to northweard steps in the Kigluaik Fault as the fault is traced from west to east. The Kigluaik Fault is downthrown on the north side, forming the graben of the Pilgrim River Valley. The throw of the Kigluaik Fault is at least 200 m, corresponding to the minimum depth of valley fill determined by geophysical studies. The fault offsets moraines along the base of the Kigluaik Mountains at least 10 m and is thus relatively young. Seismic activity in the area of the Pilgrim River Valley shows currently active normal faulting; thus suggesting the Kigluaik Fault is still active (Biswas, et al., 1980).

Many of the canyons found on the north flank of the Kigluaik Mountains are apparently controlled by north-south-trending faults (Plate I). A similar vertical fault was also mapped on Marys Mountain. Some faults in the north-south-trending system may have a significant strike-slip component as evidenced by the offset of lithologic units and the apparent offset of the

Kigluaik Fault to form "steps" in the range front. It has not been possible to measure the amounts of displacement along these faults. The trace of one of these faults can be followed across the Pilgrim River Valley just west of Pilgrim Springs, where the fault apparently cuts Quaternary terrace deposits (Plate I). This fault will be discussed in more detail in the following section (Kline, et al., this report).

Only three faults were mapped that do not correspond to the previously discussed north-south or east-west fault systems. North of Hen and Chickens Mountain there are two faults with a northeasterly trend and undetermined displacements. These faults show the same trend as some of the near-surface thermal anomalies at Pilgrim Springs. In addition, the possibly fault-controlled alignment of Pilgrim Springs with the newly-discovered small thermal area just south of Hen and Chickens Mountain (Kline, et al., this report) also defines a similar northeasterly trend, as does the major axis of the thaw ellipse at Pilgrim Springs. The age, displacement, and significance of this northeasterly faulting is undetermined. The third set of faults on the east end of Marys Mountain appears to have a relatively small dip and may be related to an extensive series of thrust faults found on the Seward Peninsula as described by Sainsbury (1969b).

It is likely that the north-south-trending faults may extend through the downdropped crystalline basement under the Pilgrim River Valley. One or more of these faults could provide a deep conduit for upward migration of hot water to Pilgrim Springs. The pervasive joints and fractures in the crystalline rocks of the mountains north and south of

Pilgrim Springs could possibly provide an entrance for meteoric water to enter the geothermal system. Deep circulation could allow this water to be heated and later rise along one or more fault-controlled conduit systems by thermal convection.

However, the mountains to the north and south are probably part of the pervasive permafrost terrain surrounding the Pilgrim Springs thaw ellipse. If this is true, meteoric water would freeze at shallow depths after entering bedrock fractures and could not penetrate to sufficient depths to enter the geothermal system. At present, the permafrost thickness under these mountains is unknown. An alternate water balance model for the geothermal system is discussed in a subsequent section by Osterkamp, et al.

REFERENCES

Biswas, N. N., L. Gedney and J. Agnew, 1980, Seismicity of western Alaska, Bull. Seismol. Soc. Am. (in press).

Bunder, C. M., Hedge, C. E., and Sainsbury, C. L., 1977, Radiometric concentrations and preliminary radiometric ages of rocks of the Kigluaik Mountains, Seward Peninsula, Alaska: U.S.G.S. Open-File Report 77-735, 36 pp.

Sainsbury, C. L., R. Kachadoorian, T. Hudson, T. E. Smith, T. R. Richards and W. E. Todd, 1969a, Reconnaissance geologic maps and sample data, Teller A-1, A-2, A-3, B-1, B-2, B-3, C-1, and Bendeleben A-6, B-6, C-6, D-5, D-6 quadrangles, Seward Peninsula, Alaska, U.S. Geol. Survey Open-File Report 377.

Sainsbury, C. L., 1969b, The A.J. Collier thrust belt of the Seward Peninsula, Alaska: Geol. Soc. Am. Bull., v. 80, p. 2595-2596.

Sainsbury, C. L., 1972, Geologic map of the Teller quadrangle, western Seward Peninsula, Alaska: U.S. Geol. Survey Map I-685.

Sainsbury, C. L., 1974, Geologic map of the Bendeleben quadrangle, Seward Peninsula, Alaska: The Mapmakers, Anchorage.

Sainsbury, C. L., 1975, Geology, ore deposits, and mineral potential of the Seward Peninsula, Alaska: U.S. Bur. Mines Open-File Report.

SURFICIAL GEOLOGY AND TEST DRILLING AT PILGRIM SPRINGS, ALASKA

Jeffrey Kline[1], Richard Reger[1], Rena McFarlane[1] and Thomas Williams[1]

SURFICIAL GEOLOGY

Surficial geologic mapping in the Pilgrim Springs area disclosed an interesting and complex Quaternary history in the Pilgrim River valley, which may provide some insights into the age and characteristics of Pilgrim Springs. Changes in regional base level, rates of sedimentation, and climate have combined to produce at least three major episodes of terrace formation since Sangamon time. Evidence that relatively rapid subsidence has recently been occurring in the vicinity of Pilgrim Springs includes: (1) the apparent burial of older terraces by modern alluvium upstream from the springs while terraces downstream from the springs are relatively well preserved, (2) major changes in the course of the Pilgrim River as indicated by abandoned river channels whose former flow direction was significantly different than at present, (3) the relative absence of thaw lakes and thermokarst features in a 5 square mile area upstream from and including the thermally disturbed area, (4) apparent grading of old alluvial and outwash fans to a level higher than the present valley floor, (5) the presence of abrupt scarps at the toes of alluvial and outwash fans derived from the Kigluaik Mountains, (6) mudflows and springs occurring along the outwash scarps, (7) a significant steepening of stream gradient just upstream from the area of maximum apparent subsidence, and (8) the presence of lacustrine or estuarine clay, silt, and a very fine sand beneath 1.5 to 4.5 m of modern floodplain alluvium.

[1]Alaska Division of Geological and Geophysical Surveys

Areal distribution of these features as well as the presence of several faults, including the east-west-trending Kigluaik fault which is inferred to be active, and several north-trending cross faults (Plate I) suggests that Pilgrim Springs may be located near the western edge of an actively subsiding graben whose surface is being continually buried by the accumulation of alluvial sediments. Further evidence which may support or refute this hypothesis will be forthcoming when terrace samples collected for radiocarbon dating are processed and after the environment of deposition of the clays and silts has been more firmly established. Information derived from future exploration and test drilling logs will be invaluable in pulling together the complete history and geometry of the Pilgrim Springs thermal anomaly.

A thermal anomaly located approximately 4 km to the northeast of the main thaw window was discovered by examination of the U-2 aerial photographs, and later verified by thermal probing. This small outlying anomaly lies along the same northeasterly trend as that defined by the direction of elongation of the Pilgrim temperature anomalies and the main thaw window (Plate I).

PRELIMINARY DRILLING RESULTS

Two 150 ft test holes (PS1H and PS2H) were drilled in November, 1979, at grid locations 200 m S, 150 m W and 258 m S, 207 m W, respectively. Test hole locations are shown on Figure 1. Holes were sited based on the recommendations from the shallow ground temperature, shallow ground conductivity and deep resistivity surveys conducted by the Geophysical Institute (Forbes, et al., 1979). In addition, the

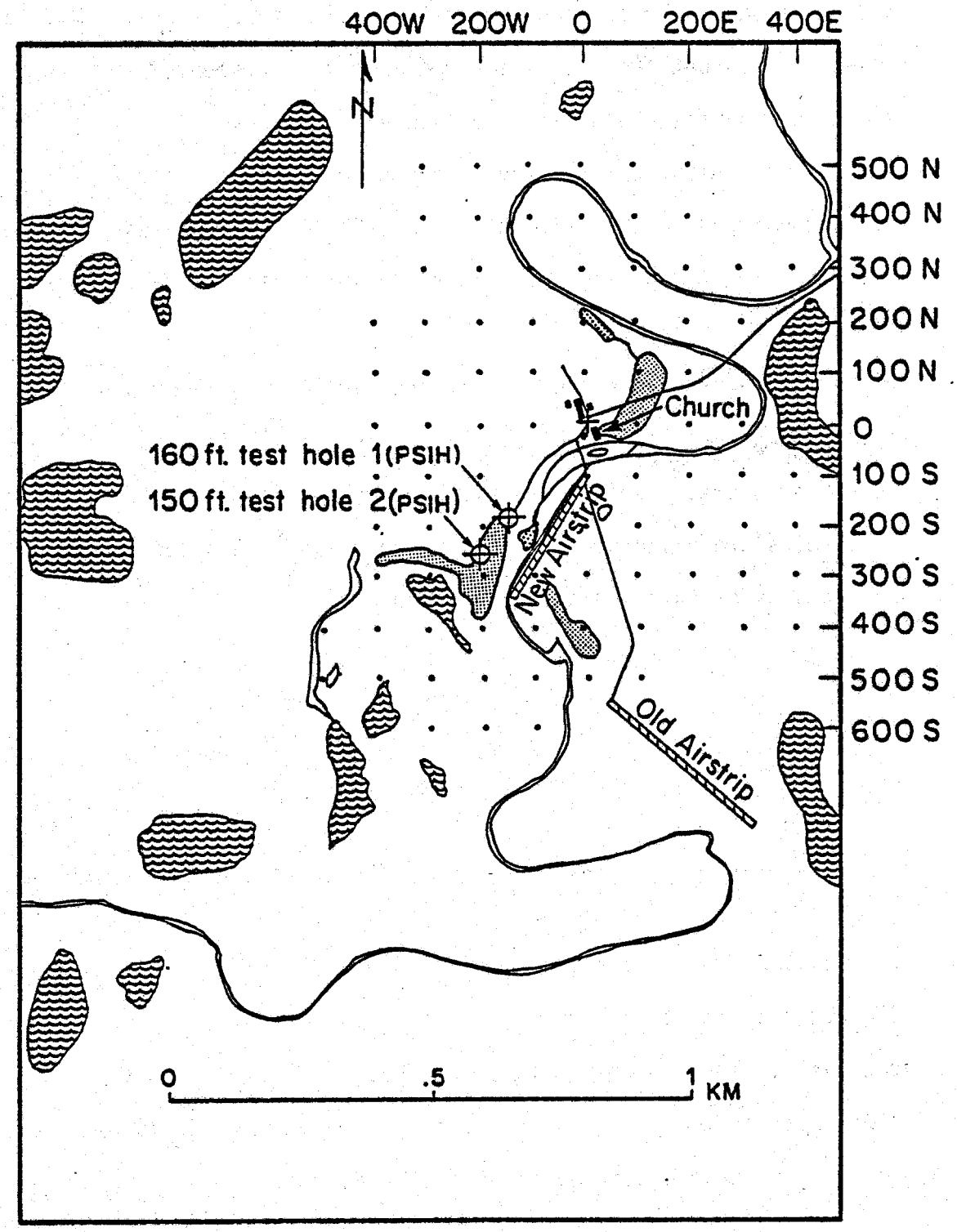

Figure 1. Locations of 1979 test drill holes and 100 meter grid. Stippled areas indicate agricultural fields. Wave pattern indicates lakes and ponds.

Alaska Division of Oil and Gas (A.D.O.G.) required that the initial test well be sited outside the 60°C ground temperature isotherm due to safety considerations. The second test well was allowed by the A.D.O.G. to be sited half way between the first well and the most favorable target site recommended by the Geophysical Institute.

Drilling results were very encouraging. Artesian hot water aquifers were encountered at 21.3-27.4 m and 18.3-27.4 m; flow rates were estimated at 200 and 300-400 gallons per minute, respectively, at a temperature of 90°C.

A more extensive discussion of the surficial geology and preliminary test drilling results will be forthcoming in a future D.G.G.S. open-file report. Preliminary lithologic logs for the two initial test drill holes are given below. Rock descriptions are based on field examinations of cuttings and drive samples.

PS 1 H
Grid Location = 200 m South x 150 m West
Elevation above MSL - 4.4 m

Depth Below Surface (m)	Generalized Hole Log
0-3.0	Medium sand with trace to some silt intercalated with coarse pebble sand and 3-5 cm organic layers or lenses/very low compaction: easily driven.
3.0-6.1	Coarse sand and pea gravel intercalated with thin beds or lenses of fine-to-medium sand and thin (< 1 cm) organic layers and smears. Increase in density over previous interval.
6.1-9.1	Sand with some silt (poorly sorted) intercalated with considerable organic material. Organics, peaty, up to 18 cm thick. Drive sample contains trace to some peat slightly less dense than preceding interval.
9.1-12.2	Moderately-to-well-sorted fine sand with 12% silt, discontinuous organic streaks; 7-fold increase in density over preceding intervals (penetrometer).
12.2-15.2	Fine sand with some silt. Peat streak (discontinuous); density similar to previous interval.
15.2-18.3	Interbedded medium sand and 2 to 4 cm diameter subrounded gravel layers; 5-10 cm peaty organic layers occur this interval; density decrease noted. Penetrometer measurements approximately 1/2 preceding interval, probably due to increased organic content and less dense gravels.
18.3-21.3	Fine-to-medium sand, trace silt, trace organics; density has tripled this interval.
21.3-24.4	Cemented medium sand encountered at 22.3 m below ground surface. Thin-bedded cemented sandstone. Diagenetic, euhedral quartz overgrowths on grains and cubic pyrite. Density very high. Material too hard to take drive sample.

PS 1 H (Cont'd)

Depth Below Surface (m)	Generalized Hole Log
24.4-27.4	Cemented silty sand with some pebble gravel intervals. Drilling rate considerably slower than previous intervals.
27.4-30.5	Cemented fine-to-medium sand; thin-bedded with trace silt; diagenetic euhedral quartz overgrowths on clastic quartz grains and cubic pyrite. Scattered pebble intervals. Density approximately equivalent to previous interval.
30.5-33.5	Dirty sandstone (poorly sorted) and pebble conglomerate intervals.
33.5-36.6	Coarser conglomerate (to 7.6 cm clasts); thin sandstone and siltstone intervals.
36.6-39.6	Coarse gravel conglomerate with sand matrix; drilling hard.
39.6-42.7	Finer sand conglomerate intercalated with silty sandstone intervals; drilling slightly easier.
42.7-45.7	Coarse sandstone with trace to some pebbles. Secondary sulfide mineralization. Drilling rate slowed dramatically at 44.2 m.
45.7-48.8	Medium-to-coarse sandstone with coarse conglomerate interval. Drilling rate very slow.

PS 2 H
Grid location - 258 m South x 207 m West
Elevation above MSL - 3.9 m

0-3.0	Top 30.5 cm sandy silt (oxidized) underlain by 45-60 cm of dark blue silt and clay. Rest of interval silty sand with trace gravel. Organic layer encountered at 90 cm.
3.0-6.1	Fine-to-coarse sand and silt to 5.5 m. Pebble gravel 5.5-6.1 m.
6.1-9.1	Poorly sorted silty fine-to-coarse sand. Gravel intervals to 15.2 cm thick; very soft, easy drilling.

PS 2 H (Cont'd)

Depth Below Surface (m)	Generalized Hole Log
9.1-12.2	Fine sand with trace silt. Dense interval; possible weak cementation; slower drilling.
12.2-15.2	Medium sand with some silt; easier drilling this interval. Less dense material.
15.2-18.3	Medium sand with trace silt. Scattered thin gravel intervals less compacted than previous interval.
18.3-21.3	Entering cemented gravels and sands; cementing discontinuous first 1.5 m of this interval. Cubic pyrite present.
21.3-24.4	Sandy shale and siltstone; possible conglomerate between 23.7-24.4 m.
24.4-27.4	Silty micaeous medium-to-fine sand contains organic fragments; some recognizable plant material.
27.4-30.5	Poorly sorted, poorly consolidated sandstone and siltstone, some minor gravel intervals; less dense than previous interval.
30.5-33.5	Fine-grained-to-very-fine-grained micaceous subarkose, some siltstone intervals (cemented).
33.5-36.6	Granular poorly sorted sandstone. Occasional thin interval of gravel (pebble gravel) conglomerate (cemented) (Soft interval between 36.0 and 37.8 m).
36.6-39.6	Fine-to-medium sandy pebble gravel conglomerate (cemented).
39.6-42.7	Angular fine gravel to coarse sand. Indicative of relatively short transport. Mostly gneissic and slaty rock fragments.
42.7-45.7	Intercalated very fine sandstone and coarse sandstone, cementing weak to moderate. Hydrothermal alteration and diagenetic minerals present, including sulfides. Micas look altered; bottom of hole shows little or no porosity.

REFERENCES

Forbes, R. B., E. M. Wescott, D. L. Turner, J. Kienle, T. Osterkamp, D.B. Hawkins, J. T. Kline, S. Swanson, R. D. Reger and W. Harrison, 1979, A geological and geophysical assessment of the geothermal potential of Pilgrim Springs, Alaska, Geophysical Institute, University of Alaska and Alaska Division of Geological and Geophysical Surveys Preliminary Rept., 39 pp., 1 plate.

LOCAL AND REGIONAL GEOTHERMAL GRADIENTS AND RADIOGENIC HEAT PRODUCTION IN CRYSTALLINE BASEMENT ROCKS

Robert B. Forbes

RADIOGENIC HEAT AND GEOTHERMAL GRADIENTS

Regional and local geothermal gradients in the upper part of the earth's crust can be elevated by the addition of radiogenic heat generated by the decay of the unstable isotopes of uranium, thorium and potassium, if these elements are present in abnormally high concentrations.

Studies of thermal spring convection systems must address the question of whether or not the spring waters have acquired their heat by deep descent and return in a crustal section characterized by a normal geothermal gradient, or to shallower depths under conditions of a high geothermal gradient. Unfortunately, chemical geothermometers cannot answer this question, and there are no recognized solution geobarometers to estimate confining pressure at the time of equilibration.

Near Surface Heat Production in Crystalline Rocks

The contribution of radiogenic heat to the thermal regime of near-surface rocks can be calculated, if analyzed uranium, thorium and potassium concentrations can be obtained from a representative sample grid. Heat production may be calculated from equation (1):

$$H(\mu cal/g\text{-}yr) = 0.73U(ppm) + 0.20Th(ppm) + 0.27K(\%) \qquad (1)$$

H is independent of rock density, but it can be converted to volumetric heat-generation units (HGU), by equation (2):

HGU: $(10^{-13}\ cal/cm^3\ sec = 0.418\ w/m^3) = \frac{H \times \rho}{3.156}$ (2)

where ρ is the rock density.

Sample Location and Distribution

Figure 1 shows the locations of rock samples analyzed for uranium and thorium. As shown on the sample location map, an attempt was made to sample the most representative rock units which crop out in the highlands surrounding the Pilgrim River Valley.

As discussed in the section by Swanson, et al. (this report), the crystalline basement rocks in the area have been subdivided into three groups, including:

(1) High pressure/low temperature metamorphic rocks of the Precambrian "Nome Group" terrane.

(2) Gneiss complexes, including amphibolite and granulite facies terranes, of the Kigluaik and Bendeleben Mountains.

(3) Discordant granitic (granite-quartz monzonite-granodiorite) plutons with Cretaceous and early Tertiary K-Ar cooling ages.

Rocks from each of these groups occur in the highlands adjacent to Pilgrim Springs, but in this area the rocks of Group (1) have been upgraded by the thermal perturbation accompanying the emplacement and recrystallization of the gneiss complexes and the intrusion of the granitic plutons.

Uranium-Thorium Concentration and Heat Production Calculations

Table 1 lists uranium and thorium analytical data for the 17 rock samples discussed above. As shown in Table 2 the average concentration of uranium and thorium for all 17 samples far exceeds that of "average

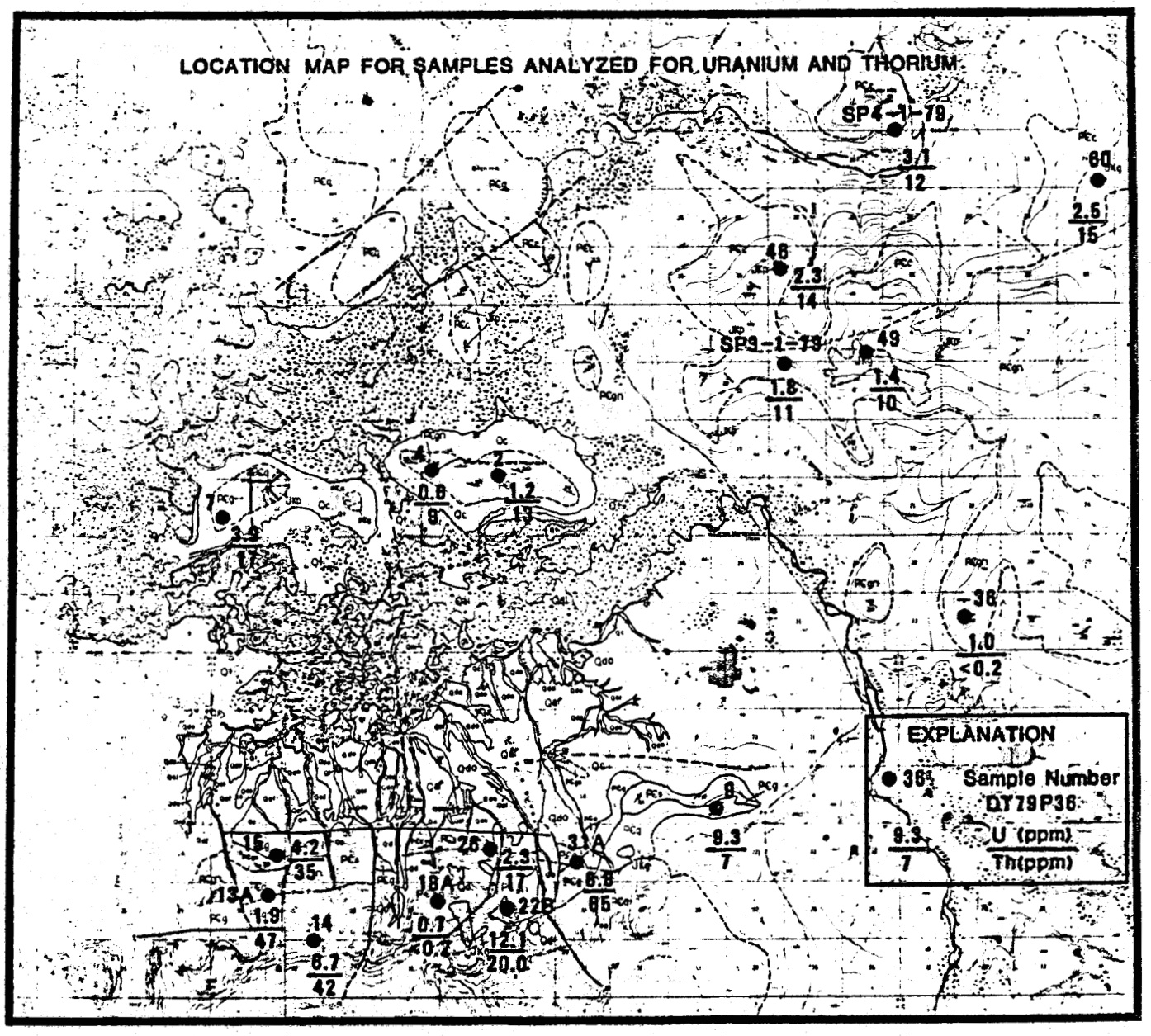

Figure 1. Location map for samples analyzed for uranium and thorium. Base reduced from Plate I (geologic map).

TABLE 1

URANIUM-THORIUM CONCENTRATIONS IN METAMORPHIC AND INTRUSIVE IGNEOUS ROCKS IN THE PILGRIM SPRINGS AREA

Sample No.	Rock Type	Uranium (ppm)	Thorium (ppm)	Th/U
DT-79-P-2	biotite-granodiorite gneiss	1.2	13	10.8
DT-79-P-4	diopside-bearing amphibolite	0.6	9	15
DT-79-P-7	biotite-sillimanite gneiss	3.9	17	4.4
DT-79-P-	biotite-muscovite granite	9.3	7	0.75
DT-79-P-13	biotite-granite gneiss	1.9	47	24.7
DT-79-P-14	biotite-granodiorite	6.7	42	6.3
DT-79-P-15	biotite-granite	4.2	35	8.3
DT-79-P-18A	garnetiferous granite	0.7	n.d.	
DT-79-P-22B	biotite-granite	12.1	20	1.7
DT-79-P-26	biotite gneiss	2.3	17	7.4
DT-79-P-31A	altered aplite (zeolitized?)	6.8	65	9.6
DT-79-)-36	biotite-granodiorite gneiss	1.0	n.d.	
DT-79-P-46	diopside-scapolite gneiss	2.3	14	6.1
DT-79-P-49	biotite-quartz monzonite	1.4	10	7.1
DT-79-P-60	hornblende-granodiorite	2.5	15	6
SP-3-1-79	garnet-biotite-actinolite paragneiss	1.8	11	6.1
SP-4-1-79	diopside-phlogopite gneiss	3.1	12	3.9
	Average	3.64	22.27	6.12

TABLE 2

AVERAGE ABUNDANCES OF URANIUM AND THORIUM IN VARIOUS ROCK TYPES

Rock Type	U (ppm)	Th (ppm)	Th/U	Reference
Crustal	1.7	9.6	5.65	Taylor (1964)
Granite	4.75	18.5	3.89	Wasserburg, et al. (1964)
Intermediate (qtz diorite)	2.0	7.4	3.70	Tilton & Reed (1963)
Basalt	0.6	2.7	4.50	Shimazu (1966)
Eclogite	0.043	0.16	3.72	Tilton & Reed (1963)
Peridotite	0.016	0.06	3.75	Shimazu (1966)

crust" (Taylor, 1964), and is rather close to the concentrations expected in an "average granite" (Wasserburg, et al., 1964), which is slightly enriched in thorium. Several of the analyzed rocks are clearly enriched in thorium vs. uranium, as compared to average Th/U ratios listed in Table 2.

It is interesting to compare the average uranium and thorium concentrations to those that we have recently obtained for other Alaskan crystalline terranes and complexes. Table 3 shows that the average uranium-thorium content of the rocks adjacent to Pilgrim Springs is similar to that of the surrounding Kuzitrin District and to the Granite Mountain complex, but appreciably higher than other Alaskan metamorphic terranes analyzed to date.

The average U and Th values in Table 1 have been used along with an estimated average K content of 2.1 wt%, and the average density of granite (2.67) to calculate the approximate near-surface radiogenic heat production in the crystalline basement underlying Pilgrim Springs.

$$H = (3.64)\ (0.73) + (22.27)\ (0.20) + (2.1)\ (0.27) = 7.68 \qquad (3)$$

$$\frac{H(7.68) \times \rho(2.67)}{3.156} = \underline{6.50\ \text{HGU}} \qquad (4)$$

LOCAL AND REGIONAL GEOTHERMAL GRADIENTS

There are few heat flow or geothermal gradient measurements in most areas of Alaska, including the Seward Peninsula. To date, no test holes of suitable depth have been drilled at the Pilgrim Springs site,

TABLE 3

AVERAGE URANIUM AND THORIUM CONCENTRATIONS IN ALASKAN-CANADIAN CRYSTALLINE TERRANES

Terrane	Type	U(ppm)	Th(ppm)	No. of Samples	References
Copper River Basin	Regional greenschist facies and post-kinematic granites	0.76	3.77	15	Eakins, Jones & Forbes (1977)
Copper River Basin	Regional greenschist facies, and post-kinematic granites	0.62	3.16	66	Forbes, et al. (1977)
Chitina River Valley	Regional greenschist and blueschist facies, intruded by post-kinematic granites	1.23	3.14	37	Eakins, Jones & Forbes (1977)
Chitina Terrane	Blueschist facies, intruded by post-kinematic granites	0.55	1.62	21	Forbes (unpublished)
Kennektok Terra	Gneiss dome complex, with core including retrograded granulite facies rocks	0.47	3.38	21	Forbes (unpublished)
Kluane Terrane	Regional Barrovian terrane with synkinematic granites & migmatitic gneisses	1.80	2.70	21	Forbes (unpublished)
Lake Clark	Amphibolite facies terrane intruded by post-kinematic granites	2.94	4.14	7	Forbes (unpublished)
Wales Group	Regional greenschist facies + synkinematic belt with migmatitic gneisses	1.50	9.85	40	Forbes (unpublished)
Eielson Deep Test Hole; Yukon-Tanana Complex	Regional Barrovian terrane, with post-kinematic granites	2.06	10.93	25	Bunker, Bush & Forbes (1973)
Ruby Ridge, Brooks	Regional blueschist terrane, with post-kinematic granites & gneiss domes	2.42	13.36	15	Forbes (unpublished)
Kuzitrin District, Nome Group	Regional blueschist terrane, with post-kinematic granites & gneiss domes	4.69	19.03	29	Forbes (this study)
Pilgrim Springs Area, Kuzitrin District	Regional blueschist terrane, with post-kinematic granites & gneiss domes	3.64	22.27	17	Forbes (this study)
Granite Mountain	Zoned alkaline granitic complex	3.7	25.60	28	Jones & Forbes (1977)
Darby Mountains	Regional metamorphic belt, with post-kinematic granites	5.1	32.70	26	Jones & Forbes (1977)
Zane Hills	Zoned alkaline granitic complex	6.7	27.60	32	Jones & Forbes (1977)
Selawik Hills	Zoned alkaline granitic complex	10.9	46.10	11	Jones & Forbes (1977)
Bokan Mountain, Prince of Wales Island	Zoned peralkaline granitic complex	11.46	37.50	12	Forbes (this study)

or in the adjacent area for geothermal gradient and heat flow measurements. The closest heat flow measurement yet taken was obtained by the U.S. Geological Survey from a diamond drill hole located on the Lost River mineral claims north of Teller (approximately 75 miles northwest of Pilgrim Springs). Preliminary measurements indicate an abnormal geothermal gradient that may be very high. The measurement may be influenced by a nearby mine; but even with the mine effect taken into consideration the hole gives a heat flow value of > 80 mW/m^2.

Previous work by Sainsbury (1964, 1969) has shown that the Lost River tin and beryllium deposits are associated with biotite granite, which is exposed in subsurface workings. This granite is highly uraniferous, and similar to other granites in the area including the Cape Mountain, Brooks Mountain and Ear Mountain plutons. Local uranium-thorium data indicate that the abnormally high gradient could be due in part to a significant increment of radiogenic heat production. Additionally, a large Quaternary alkali basalt eruptive field is located about 30 miles east of the Lost River claims, and if these vents are a western extension of rift volcanism similar to that of the Imuruk volcanic field, a strong case could also be presented for a rift-related geothermal anomaly (see Kienle and Lockhart, this report).

Test Wells in the Baldwin Peninsula-Cape Espenberg Areas

Under the provisions of a development agreement with the NANA Regional Corporation, the Standard Oil Company of California drilled two wells in the Kotzebue area during the winter of 1974-1975 (Figure 2). Both of the wells were "dry holes", as no indications of gas or oil were detected in either well. Both wells are of interest, however, as they have provided

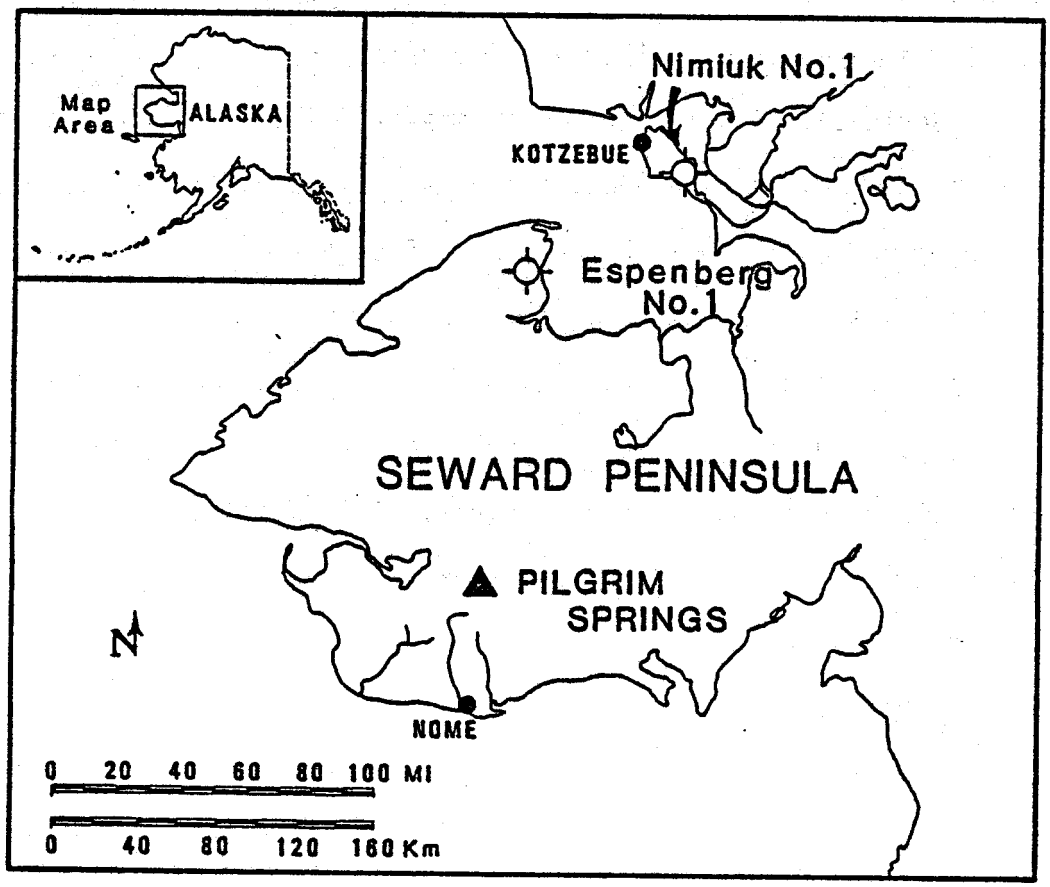

Figure 2. Map showing the location of the Nimiuk Pt. #1 and Cape Espenberg #1 wells.

new information on the subsurface geology of the area, including the presence of a rather thick section of coal-bearing Tertiary rocks which contains salt-water-bearing aquifers and a geothermal gradient which is above normal.

The Nimiuk Pt. #1 Well

The Nimiuk well reached a total depth of 1924 m, with a bottom hole temperature of 72°C. Crystalline basement rocks were penetrated at approximately 1817 m, including calc-schists and phyllites. The schists are overlain by a basal basalt unit which is about 100 m thick. The Tertiary section is dominated by sandstones with subordinate conglomerates, siltstones, and claystones. A thin bed of low-grade coal was intersected at 829 m. Conglomerate beds increase in frequency with depth in the section. Based on the bottom hole temperature, the estimated geothermal gradient may be as high as 40°C/km.

A formation test was conducted on the sandstone and conglomerates in the 1145-1078 m interval. No oil or gas was produced, but a column of clear salt water, muddy salt water and drilling fluid rose 668 m in the hole (top 363 m = drilling fluid; next 251 m = muddy salt water; bottom 54 m = clear salt water). The test conclusively showed that the zone was producing salt water. At this depth, the temperature was 42°C. This was the only test which was run on this well. Other sands and conglomerates at greater depths may also be "wet" and potential producers of hot salt water. A geologic section for the Nimiuk Pt. #1 well is shown as Figure 3.

The Cape Espenberg #1 Well

The Espenberg well reached a total depth of 2553 m, (Figure 4) with a bottom hole temperature of 72°C. Crystalline basement rocks

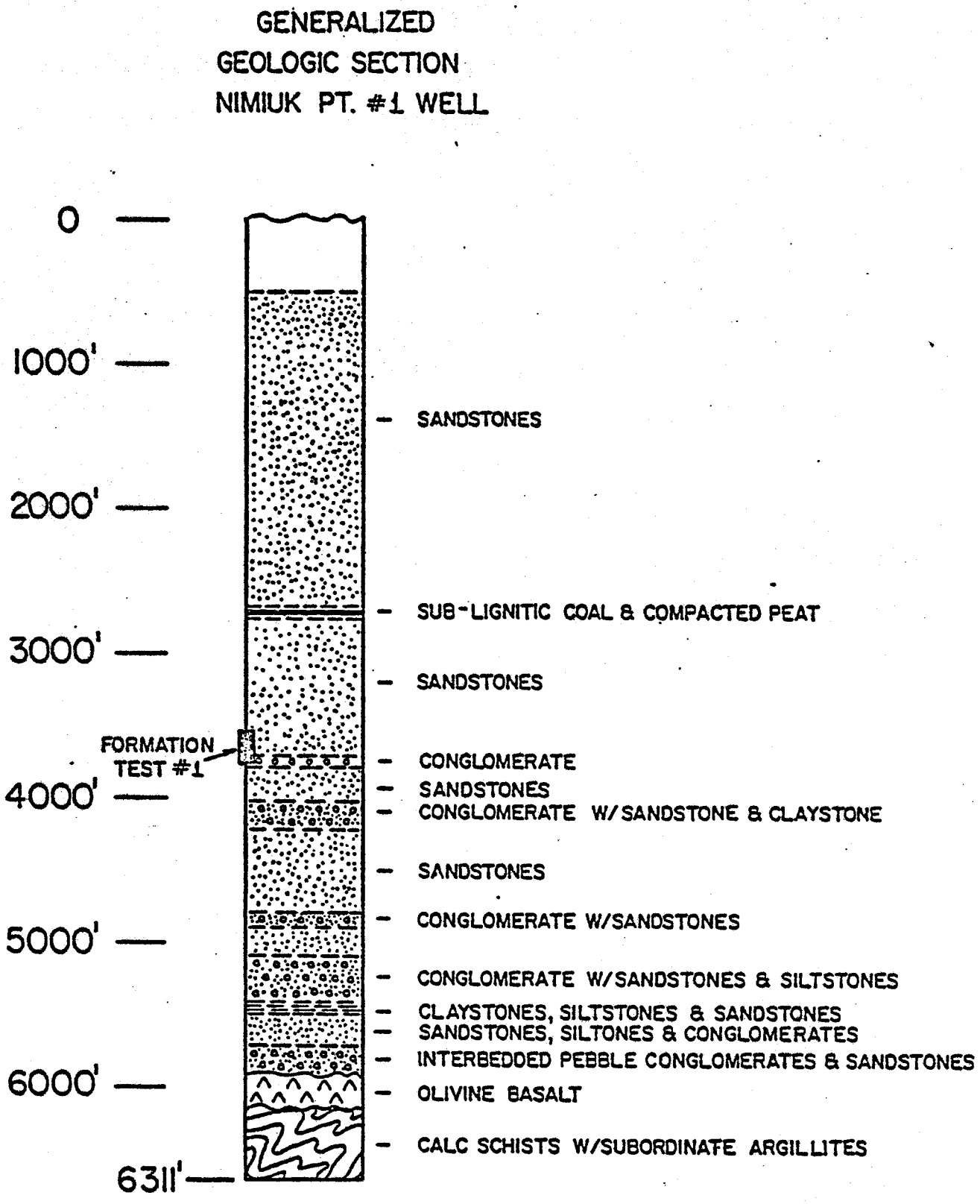

Figure 3. Generalized geologic section, Nimiuk Pt. #1 well.

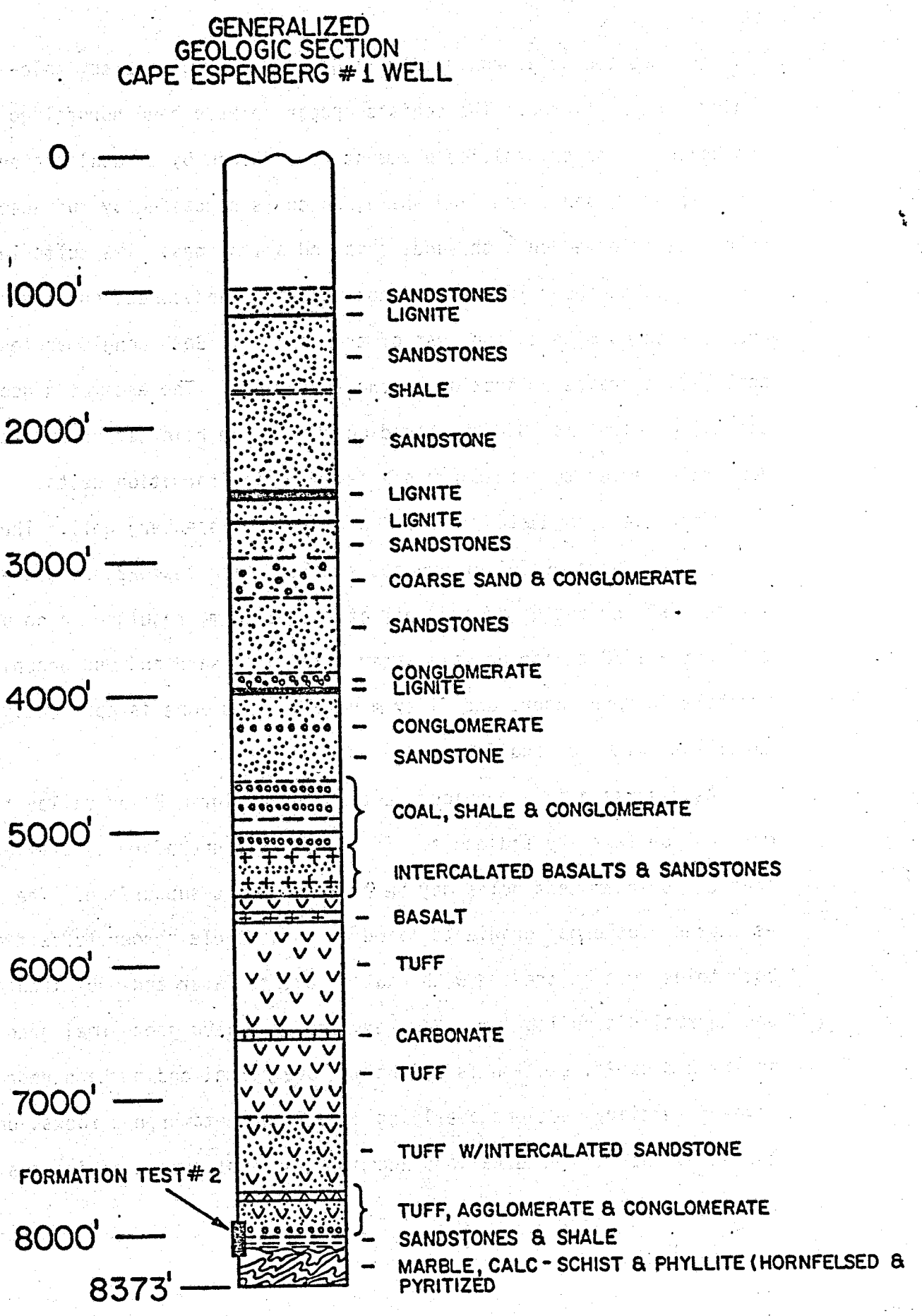

Figure 4. Generalized geologic section, Cape Espenberg #1 well.

were intersected at approximately 2470 m, including marbles, calc-schists and phyllites. The schists appear to have been hornfelsed by intrusives. The crystalline basement is overlain by a basal sequence of conglomerates, sandstones and shale, which is succeeded by tuffaceous volcanics interbedded with sandstones and siltstones. The tuffs leave the section at about 1667 m, and coal-bearing sandstones, conglomerates and siltstones make up the rest of the section. Both conglomerates and coal beds decrease up section in the drill hole. The estimated geothermal gradient is 28°C/km, based on the bottom hole temperature and down hole temperature measurements taken during formation tests.

Tests were conducted on four zones in the Espenberg well. Three were either unsuccessful or dry tests. Formation test #2, conducted on a zone near the bottom of the well at 2413-2478 m, resulted in no oil or gas, but a 2260 m rise of salt water mixed with sand and mud occupied the hole in three hours and fifty minutes. This zone is apparently an excellent saltwater aquifer.

As discussed in a previous section, the Pilgrim River valley fill may include Tertiary sediments. If so, a basal unconformity similar to that cut by both test holes may be present in the subsurface. The estimated geothermal gradients based on bottom hole temperatures from both holes must be treated with caution due to water and mud circulation and thermal disequilibrium. However, the estimated geothermal gradient in the Nimiuk Pt. section is slightly above normal and perhaps representative of Tertiary sections overlying Nome Group metamorphic rocks, undisturbed by thermal perturbations accompanying emplacement of igneous bodies.

SUMMARY

The existence of a large thaw window in permafrost indicates that the underlying basement rocks should be thermally perturbed around the conduit system. However, we have no way to estimate the magnitude of this perturbation, nor do we have any heat flow data for the unperturbed basement rocks, which underlie the valley fill. The available data from the Seward Peninsula and nearby areas indicate thermal gradients in crystalline basement on the order of 20-30°C/km. In areas of low thermal conductivity such as sediment-filled valleys, thermal gradients of this order could produce thermal gradients of 40°C/km in permafrost zones and up to 50-60°C/km in unfrozen, highly porous sediments.

A background heat flow value of 1.8-2.0 HFU (80 mW/m^2) would be a reasonable estimate for the Pilgrim Springs area. In the valley fill sediments at Pilgrim Springs, the background thermal gradient might be as high as 50°C/km. An estimate of 200 m of sediments above the basement would suggest an 8-9°C temperature differential between the surface and basement. Since the mean annual surface temperature may be as low as -4 to -5°C (Nome's mean annual surface temperature is -3.5°C), the assumed thermal gradient would give a permafrost thickness of approximately 125 m. Certainly the bottom 50 m of sediments should be ice free, presumably allowing fluid flow beneath areas of permafrost outside the thaw ellipse.

It is conceivable that the thermal waters of Pilgrim Springs can be explained by the deep circulation of ground water. The estimated radiogenic heat generation (6.5 HGU), even if absorbed totally by circulating groundwater, would only contribute a 2 or 3°C increment assuming a velocity of 5-6 cm/year and a 10^5 year travel time. It is not clear,

given the present data, that a buried magma body needs to be postulated to explain the hot spring. If however, a reservoir temperature of greater than 150°C is found during future drilling and/or unequivocal chemical geothermometry studies, other explanations such as a rift-associated, buried magma body or circulation along deeper faults will be required (see Kienle and Lockhart, this report).

ACKNOWLEDGEMENTS

Mr. L. A. Lawver of the U.S.G.S. Office of Earthquake Studies participated in the field work and has contributed to the heat flow section of this paper. His contributions are gratefully acknowledged.

REFERENCES

Sainsbury, C. L., 1964, Geology of the Lost River mine area, Alaska: U.S. Geol. Survey Bull. 1129, 80 pp.

Sainsbury, C. L., 1969, Geology and ore deposits of the central York Mountains, Seward Peninsula, Alaska: U.S. Geol. Survey Bull. 1287, 101 pp.

Sainsbury, C. L., 1972, Geologic map of the Teller quadrangle, western Seward Peninsula, Alaska: U.S. Geol. Survey Map I-685.

Taylor, S. R., 1964, Trace element abundances and the chondritic earth model, Geochim. et. Cosmochim. Acta, Vol. 28, p. 1989-1998.

Wasserburg, J. G., McDonald, H. F. and Fowler, W. A., 1964, Relative contributions of U, Th, and K to heat production in the earth, Science, Vol. 143, p. 465-467.

GEOCHEMISTRY OF PILGRIM SPRINGS THERMAL WATERS

Roman Motyka[1], Robert Forbes and Mary Moorman[1]

INTRODUCTION

Chemical analyses of thermal waters obtained from Pilgrim Springs and from the two shallow test wells are nearing completion within the ADGGS geochemical laboratory. The preliminary results of these analyses, subject to confirmation, are provided in Table 1. An analysis of waters from Serpentine Hot Springs, located 75 km north of Pilgrim Springs, is also included for comparison. ADGGS water analysis procedures are currently undergoing a process of standardization to conform to USGS established methods. The USGS Branch of Field Geochemistry and Petrology, Menlo Park, CA, is performing duplicate analyses on these samples and is serving as a reference lab for the initial stages of the ADGGS water analysis program. The final results will be presented in an ADGGS open-file report.

Most analyses performed at ADGGS were done by methods described in Skougstad, et al., (1979). Water samples were filtered and treated in the field following procedures described in Presser and Barnes (1974). Bicarbonate and pH were determined in the field for Pilgrim Springs and Serpentine Hot Springs, using methods described by Barnes (1964). Lack of time and equipment prevented field determination of bicarbonate at the two test wells. Water samples from the two wells were obtained at the wellhead. Several hours of flushing the drill hole by natural artesian flow of subsurface thermal waters preceded sample acquisition.

[1]Alaska Division of Geological and Geophysical Surveys (ADGGS)

TABLE 1

PRELIMINARY ANALYSES AND OTHER CHARACTERISTICS OF THERMAL WATERS FROM PILGRIM SPRINGS AND SERPENTINE HOT SPRINGS
(All chemical analyses in parts per million)

	Pilgrim Springs	Pilgrim Well #1[1]	Pilgrim Well #2[1]	Serpentine
SiO_2	74	75	156	95
Al	Inc	Inc	Inc	Inc
Fe	Inc	Inc	Inc	Inc
Ca	381	518	516	92
Mg	1.0	0.9	0.9	0.4
Na	1412	1828	1820	1026
K	55	75	75	44
Li	3.0	3.9	3.9	4.8
HCO_3	32	n.d.	n.d.	60
CO_3	n.d.	n.d.	n.d.	n.d.
SO_4	13	16	15	1
Cl	3250	5000	5000	2000
F	3.8	4.8	4.8	6.0
Br	Inc	Inc	Inc	Inc
B	Inc	Inc	Inc	Inc
pH	7.1	6.4	6.4	7.9
Temperature, °C	81	90.5	90	75
Flow rate, liters/min	250	800[2]	1600[2]	450
Specific conductance micromhos/cm	10,000	10,000	10,000	5300
Date sampled	6/22/79	11/7/79	11/19/79	6/23/79

[1]Water sample obtained from well-head flow under artesian pressure from 50 m deep well. Water is believed to originate in aquifer at 20 m depth.

[2]Well-head flow rate.

Based on evidence accumulated at the drilling sites, the thermal waters emerging from the test wells appeared to be coming from an aquifer at a depth of approximately 20-30 meters.

WATER CHEMISTRY

Comparison of the preliminary chemical analysis of 1979 Pilgrim Springs water to an earlier USGS analysis on waters obtained in 1973 (Table 2; Miller, et al., 1975) suggests a marked decline has occurred in several of the ionic constituents of the thermal springs. The differences, however, could be attributable to dilution effects caused by an abnormally high precipitation in the Pilgrim Springs area just prior to sample acquisition. Meteoric surface waters infiltrating into a shallow subsurface reservoir directly feeding the spring may not have had sufficient time to chemically equilibrate to the subsurface conditions before emerging at the spring site.

The well sites are located in a thermal area which is distinctly different from the thermal area containing the surface springs (Figure 1, Kline, et al., this report). The difference in location could account for some of the differences in chemistry between the wells and the surface springs. The wells themselves are very close to each other, being separated by ~ 100 meters and the marked similarity in chemical composition suggests a common aquifer supplying both wells. One striking difference, however, is in silica content of the water taken from well #2 which has twice the silica concentration of waters from well #1. The cause of this difference is puzzling. Suggested explanations for this difference are discussed below.

TABLE 2

USGS CHEMICAL ANALYSIS, PILGRIM SPRINGS AND SERPENTINE SPRINGS
SEAWATER ANALYSIS FOR COMPARISON
(Values in parts per million)

	Pilgrim Springs (Miller, et al., 1975)	Serpentine Springs (Miller et al., 1975)	Seawater (Krauskopf, 1967)	Seawater (5:1 dilution)
SiO_2	100	100	3	--
Al	0.04	0.08	--	--
Fe	n.d.	n.d.	--	--
Ca	530	47	400	66
Mg	1.4	0.48	1,272	211
Na	1450	730	10,556	1752
K	61	40	380	63
Li	4	4.7	--	--
NH_3	n.d.	n.d.	--	--
HCO_3	30.1	64.5	140	23
CO_3	n.d.	n.d.	--	--
SO_4	24	29	2,690	716
Cl	3346	1480	18,980	3151
F	4.7	6.4	--	--
Br	n.d.	n.d.	65	10.8
B	--	--	--	--
Sr	--	--	8	--
T(°C)	82	77		
pH	6.75	7.91		

TABLE 3

CHEMICAL COMPOSITIONS OF SELECTED EXAMPLES OF ALKALI CHLORIDE THERMAL WATERS
(All chemical analyses are in parts per million)

	Pavzhetsk, Kamchatka, USSR (Ellis & Mahon, 1977)	Spring 80, El Tatiu, Chile (Ellis & Mahon, 1977)	Spring 190, Wairakei, New Zealand (Ellis & Mahon, 1964)	Region III, Hakune Volcano, Japan (Oki & Hirano, 1970)	Growler Spring, Near Lassen Pk., Calif. (White, 1963)
SiO_2	160	174	245	--	233
Al	--	--	--	0.12	--
Fe	0.0	--	--	0.105	0.2
Ca	64	252	20	114	79
Mg	10	1.3	0.05	0.0	0.8
Na	1010	3200	950	1490	1400
K	88	165	62	154	196
Li	--	34	10	2.4	9.2
HCO_3	--	44	--	29.7	52
CO_3	--	--	--	--	0
SO_4	83	50	56	81.5	79
Cl	1684	5878	1596	2568	2430
F	0.8	--	5.8	--	1.5
Br	3.2	--	--	--	0.8
B	39	139	82	3.6	88
pH	8.4	6.93	7.5	7.7	7.8
T°C	100	84	--	91.5	95.4

Under classification schemes advanced by White (1957) and Ellis and Mahon (1964), the thermal waters of Pilgrim Springs belong to the alkali chloride category. These thermal waters are typified by high concentrations of Na, K, and Cl with pH ranging from slightly acid to slightly alkaline (pH 5-9). Chlorine/sulfate and chlorine/bicarbonate are usually high and the main dissolved gasses are carbon dioxide and hydrogen sulfide. Na/Cl ratios are commonly below 1.

Selected examples of alkali chloride thermal waters having compositions similar to Pilgrim Springs are given in Table 3. There are some significant differences. Potassium and magnesium concentrations are comparatively lower in Pilgrim Springs waters, and calcium is higher. The Na/Cl ratios however are similar.

The source and cause of the high salinity of Pilgrim waters is still not well understood. Based on similarity of Na/Cl ratio to sea water Waring (1917) and Miller, et al. (1975) have considered a possible seawater origin for Pilgrim Springs waters, but the low magnesium and sulfate content seems to argue against such an origin. Further, oxygen isotope and deuterium analysis of these waters indicated an origin involving deeply circulating meteoritic water, and extensive deep seated water-rock reactions (Miller, et al., 1975). Alkali chloride waters are commonly associated with areas of recent volcanism. Although the closest Quaternary volcanic field to the Pilgrim Springs lies 60 km to the NE, a volcanic association cannot be discounted.

GEOTHERMOMETRY

Silica and Na-K-Ca geothermometers have proved valuable in estimating subsurface reservoir temperatures (e.g., Fournier and Rowe, 1966;

Fournier and Truesdell, 1973). Using the preliminary chemical analyses these thermometers have been applied to the Pilgrim and Serpentine thermal waters (Table 4). The Na-K-Ca thermometer is based on ratios of element concentrations and is therefore less susceptible to dilution effects. Similar Na-K-Ca temperatures (144-148°C) were obtained for all four analyses of Pilgrim waters. Interpretation of the Na-K-Ca geothermometer, however, is confused somewhat by the uncertainty of the cause of the highly saline waters at Pilgrim.

The quartz-conductive thermometer for well #2 gives the highest estimate of subsurface temperature (164°C). The quartz-conductive temperature for well #1 and the springs is considerably lower. The chalcedony thermometer however is in fairly good agreement with measured water temperatures for the spring water and well #1. Shallow subsurface silica cementation along with diagenetic pyrite was noted in the drill cuttings from the wells. This suggests a possible explanation for the low silica values for either well #1 or both well #1 and the springs. Thermal waters coming from deeper in the system may well up and then reside in the shallower 90° aquifer where, if residence time is long enough, the waters may partially or totally re-equilibrate.

DISSOLVED GASES

Although sulphurous odors can be occasionally detected at upwelling points, the spring waters are not depositing obvious sulphur-bearing mineral phases in surface pools, unless the bottom sediments contain undetected precipitates. The well site geologist (J. Kline) reported

TABLE 4

PILGRIM SPRINGS AND SERPENTINE HOT SPRINGS SUBSURFACE TEMPERATURES IN °C, CALCULATED FROM APPROPRIATE GEOTHERMOMETERS. Temperature of springs and well waters included for comparison

	Water	Chalcedony	Qz-Conductive	Na-K-Ca
Pilgrim Springs[1]	82	110	137	146
Pilgrim Springs[2]	81	93	122	144
Pilgrim Well #1	[3]90.5	93	122	148
Pilgrim Well #2	[3]90	140	164	148
Serpentine	75	108	135	154

[1]Miller, et al., 1975.
[2]ADGGS, this report.
[3]Uniform down-hole temperature measured from 0 to 50 m depth while well flowing at maximum artesian pressure.

that vigorous degassing, accompanied by a strong sulfurous odor and a positive indication with a field hydrogen sulfide detector, occurred at the well during drilling and flow tests. Based on the occurrence of carbon dioxide in test wells at other geothermal fields, it is probable that a carbon dioxide component was also present in the gas which was released during the test.

DISCUSSION

The cause of the difference in silica values between the two closely spaced wells is problematic. Procedures followed in obtaining the well samples are being reviewed in order to eliminate any possibility that inadvertent contamination may have influenced the analysis.

Based on other evidence presented in this report by Osterkamp, et al., it appears that the thermal area in which the wells are located may be composed of a series of shallow subsurface convection cells. It is possible that the wells, although encountering the same aquifer, may have penetrated different cells. If the residence time of thermal waters rising from deeper sources is significantly longer in the cell encountered by well #1, then silica may have precipitated from the waters with re-equilibration to conditions in the shallow aquifer.

Based on the Na-K-Ca thermometry and assuming that the silica concentration determined for well #2 is representative of the deeper system, the chemical data indicate the existence of a deeper, hydrothermal reservoir with a temperature of at least 145-150°C. The presence of a silica cement plus accompanying pyrite deposition at 40-50 m suggests that actual reservoir temperatures may be considerably higher than those derived from the chemistry of samples acquired to date. Whether temperatures are actually higher and whether a multiple reservoir system exists cannot be deciphered without further test holes and geochemical analyses. Further work should include application of chloride-enthalpy models, sulfate isotope geothermometry, and additional oxygen isotope analysis.

In view of the high H_2S content of gases released from the test wells and the lack of any definitive evidence connecting the high salinity of Pilgrim waters to seawater, we prefer at this time to ascribe the high salinity to an association with the region's volcanism.

ACKNOWLEDGEMENTS

We wish to thank D. Hawkins and J. Kline for obtaining the thermal water samples used in this analysis, for performing the necessary field treatment on these samples, and for helpful discussions bearing on interpreting the water chemistry.

REFERENCES

Barnes, I., 1964, Field measurement of alkalinity and pH, U.S. Geol. Survey Water-Supply Paper 1535-H, 17 p.

Ellis, A. J., and Mahon, W. A. J., 1964, Natural hydrothermal systems and experimental hot-water/rock interactions, Geochem. et Cosmochim. Acta., Vol. 28, pp. 1323-13557.

Ellis, A. J., and Mahon, W. A. J., 1977, Chemistry and Geothermal Systems, Academic Press, N.Y., 392 pp.

Fournier, R. O., and Rowe, J. J., 1966, Estimation of underground temperatures from the silica content of water from hot springs and steam wells, Am. J. Sci., Vol. 264, p. 685-697.

Fournier, R. O., and Truesdell, A. H., 1973, Empirical Na-K-Ca geothermometer for natural waters, Geochim. et Cosmochim. Acta., Vol. 37, p. 1255-1276.

Krauskopf, K. B., 1967, Introduction to Geochemistry, McGraw-Hill, 721 pp.

Miller, T. P., I. Barnes and W. W. Patton, Jr., 1975, Geologic setting and chemical characteristics of hot springs in west-central Alaska, J. Res. U.S. Geol. Survey, Vol. 3, No. 2, p. 149-162.

Oki, Y. and T. Hirano, 1970, The geothermal system of the Hakone Volcano, Geothermics-special issue 2, Vol. 2, Part 2, p. 1157-1166.

Presser, T. S., and Ivan Barnes, 1974, Special Techniques for determining chemical properties of geothermal water, U.S. Geol. Survey Water-Resources Inv., 22-74, 11 p.

Skougstad, M. W., M. J. Fishman, L.C. Friedman, D. E. Erlmann, and S. S. Duncan, Eds., 1979, Methods for determination of inorganic substances in water and fluvial sediments, U.S. Geol. Survey Techniques Water-Resources Inv., Book 5, Chap. A1, 621 p.

Waring, G. A., 1917, Mineral springs of Alaska, U.S. Geol. Survey Water-Supply Paper 418, 114 p.

White, D. E., 1957, Thermal waters of volcanic origin, Geol. Soc. America Bull., Vol. 68, p. 1637-1658.

White, D. E., 1963, Chemical composition of subsurface waters, U.S. Geol. Survey, pp 440-F, 67 p.

SEISMIC REFRACTION SURVEY OF THE PILGRIM SPRINGS GEOTHERMAL AREA, ALASKA

Juergen Kienle, Andrew Lockhart and Jerry Peace

OBJECTIVES

The seismic refraction program at Pilgrim Springs was designed to obtain subsurface information on the stratigraphy and structure of the valley fill and to outline the configuration of the crystalline basement and possible faults.

BACKGROUND AND PREVIOUS WORK

In September, 1974, Forbes et al. (1974) shot a seismic refraction profile along a N-S line extending from the old landing strip to the mission buildings. The profile was broken up into 3 reversed sections of 223 m, 226 m, and 290 m lengths, cutting the NE-SW-trending thermally disturbed zone obliquely, and transecting an abandoned meander channel of the Pilgrim River. Their data suggested 3 layers beneath the surficial "weathered zone" (which has a velocity of about 455 m/sec):

(1) Fluvial sediments, including sand and silt, with velocities ranging from 874 to 973 m/sec; with variable thickness, but generally less than 30 m thick.

(2) A layer with a broader range of seismic velocities ranging from 1689 to 2036 m/sec, and about 38 to 46 m thick. This layer was interpreted to be glacio-fluvial gravels. Two breaks in the relief of the upper surface of this layer were interpreted as a normal fault, a buried river terrace or cut and fill structure in gravels.

(3) A third layer was poorly defined in the northernmost section beneath the mission buildings, based on a discontinuity at 63 m. The velocity of this layer was 2761 m/sec and was interpreted as possible poorly consolidated Tertiary sediments.

The subsurface velocity structure of the Pilgrim Springs area appeared to be laterally and vertically heterogeneous, as revealed by consistent departures from expected arrival times at individual geophone sites--anomalies that were most likely due to the presence of discontinuous lenses of sand, silt and gravel.

When we began the 1979 refraction seismic program the major questions to be resolved were (1) whether or not the breaks on the top subsurface of layer 2 were due to normal faults as interpreted from the resistivity work by Harding-Lawson (Stefano et al., 1974) or due to river cut-and-fill structures, (2) whether or not crystalline basement is located at relatively shallow depth, and (3) whether we could locate any faults that might control the conduit system of the thermal springs.

METHODS AND INSTRUMENTATION

In mid-July 1979 we shot 9 reversed refraction profiles in the thermally disturbed zone at Pilgrim Springs, shown in Figure 1, with spread lengths of 110 or 165 m, corresponding to a geophone spacing of 10 or 15 m respectively. In addition to the end shots, one supplementary shot was fired at center profile and usually at least two additional shots were fired beyond the two ends at one-half and onespread lengths. In one case, six shots at even increments of the spread length were fired beyond one end of the profile in an attempt to reach basement.

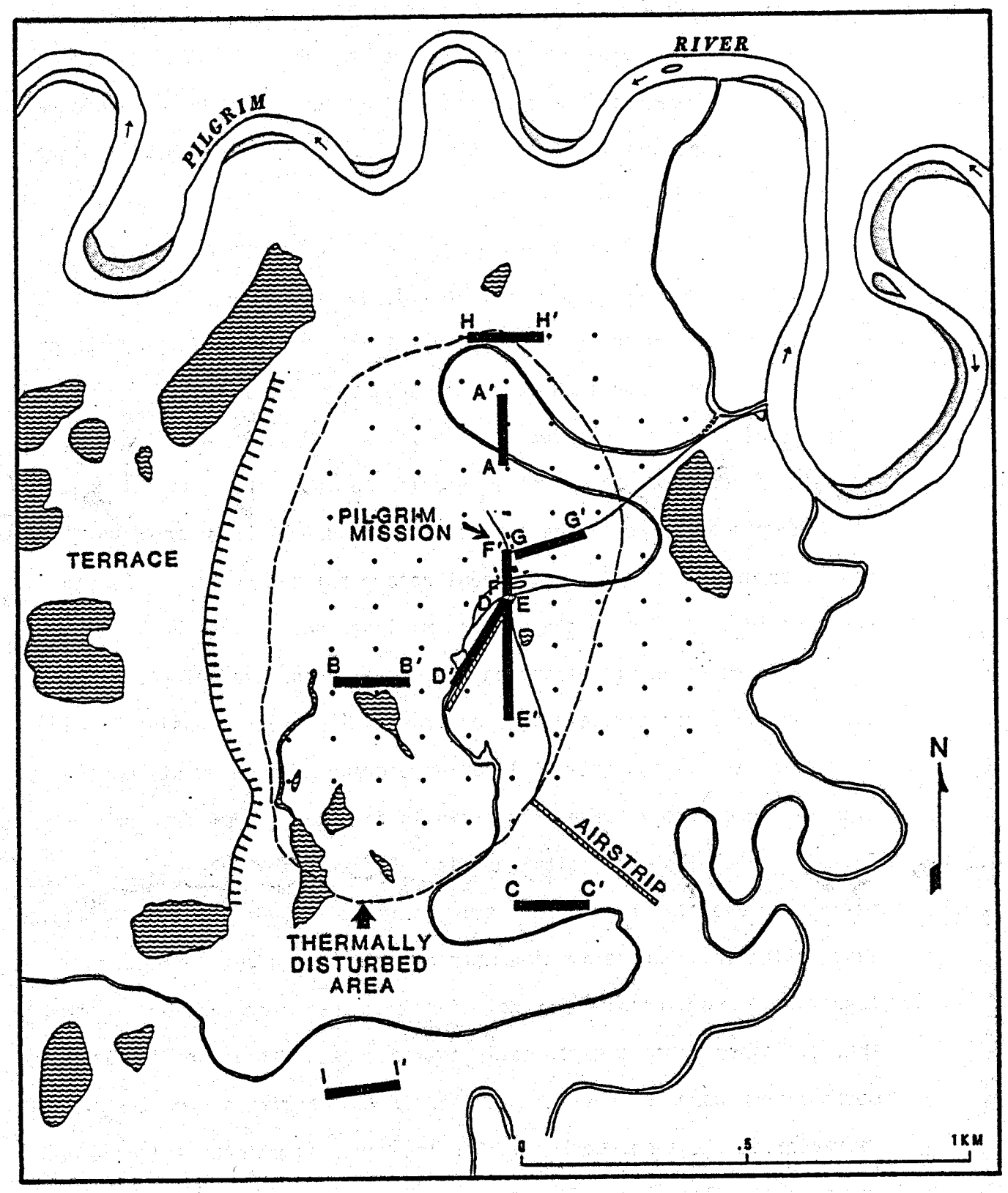

Figure 1. Location of seismic refraction profiles in the thermally disturbed area, labelled A-A', B-B', etc.

We also shot two short (55 and 110 m) reversed refraction profiles outside the Pilgrim area on the metaquartzites of Birch Hill and on gneissose granite on the eastern flank of Hen and Chickens Mountain (PE q and PE g, respectively, Plate I) in order to determine characteristic crystalline basement velocities.

The shot size of nitrocarbonitrate was limited by having to bury the charges using a small, hand-operated, power auger. The signals were recorded on a 12-channel field portable signal enhancement seismograph, Geometrics-Nimbus, Model ES-1210. This seismograph features signal enhancement by stacking repeated signals in a digital memory, allowing the use of repeated shots at one location to improve the signal-to-noise ratio. This tends to increase signal amplitude while random noise is cancelled or limited. The permanent record printed on electrosensitive paper could be scaled to the nearest millisecond.

Interpretation of refraction seismograms consisted of picking and plotting all first arrival times on travel time graphs. Using linear regression analysis, best-fit lines were drawn through points on the travel time graphs representing arrivals from the same refractor. Seismic velocities were calculated and the refractor surfaces were defined by one of three techniques: horizontal layer solutions, dipping layer solutions, and delay time methods which bring out refractor topography. Horizontal layer solutions were used for unreversed data, and for making minimum depth estimates to unseen refractors. Delay time methods were used on reversed profiles showing arrivals from the same refractor at the same geophone. Dipping layer solutions were used on reversed profiles which did not show this 'overlap'.

RESULTS

The seismic refraction profiles and their interpretations are shown in Figures 2 through 11. On the basis of these profiles we have reached two conclusions which relate directly to the geothermal system at Pilgrim Springs:

(A) The Pilgrim River Valley sedimentary fill is much thicker under the springs area than previously suspected; at least 200 meters thick beneath profile D-D'.

(B) There are three seismic refractors in the unfrozen sedimentary fill below the springs.

(1) An upper layer with velocity 600-1000 m/sec and a thickness of 0-25 m.

(2) A second layer with velocity 1200-1800 m/sec at depths of 0-25 m and a thickness of 15-60 m.

(3) A layer of undetermined thickness with velocities of 2100-3300 m/sec, found at various depths greater than 15 m.

Based upon the test well logs (Kline, et al., this report) we suggest that:

(1) Layer 1 consists of wet-to-saturated, fine-grained, fluvial deposits (silts, sands and clays); it is sometimes missing from the section.

(2) Layer 2 consists of a sequence of water-saturated sands, with abundant lenses and thin layers of gravel and finer-grained material.

(3) Layer 3 is characterized by cementation of the sediments and consists of a thick sequence of saturated, moderately-to-well-cemented gravels with some sandy layers.

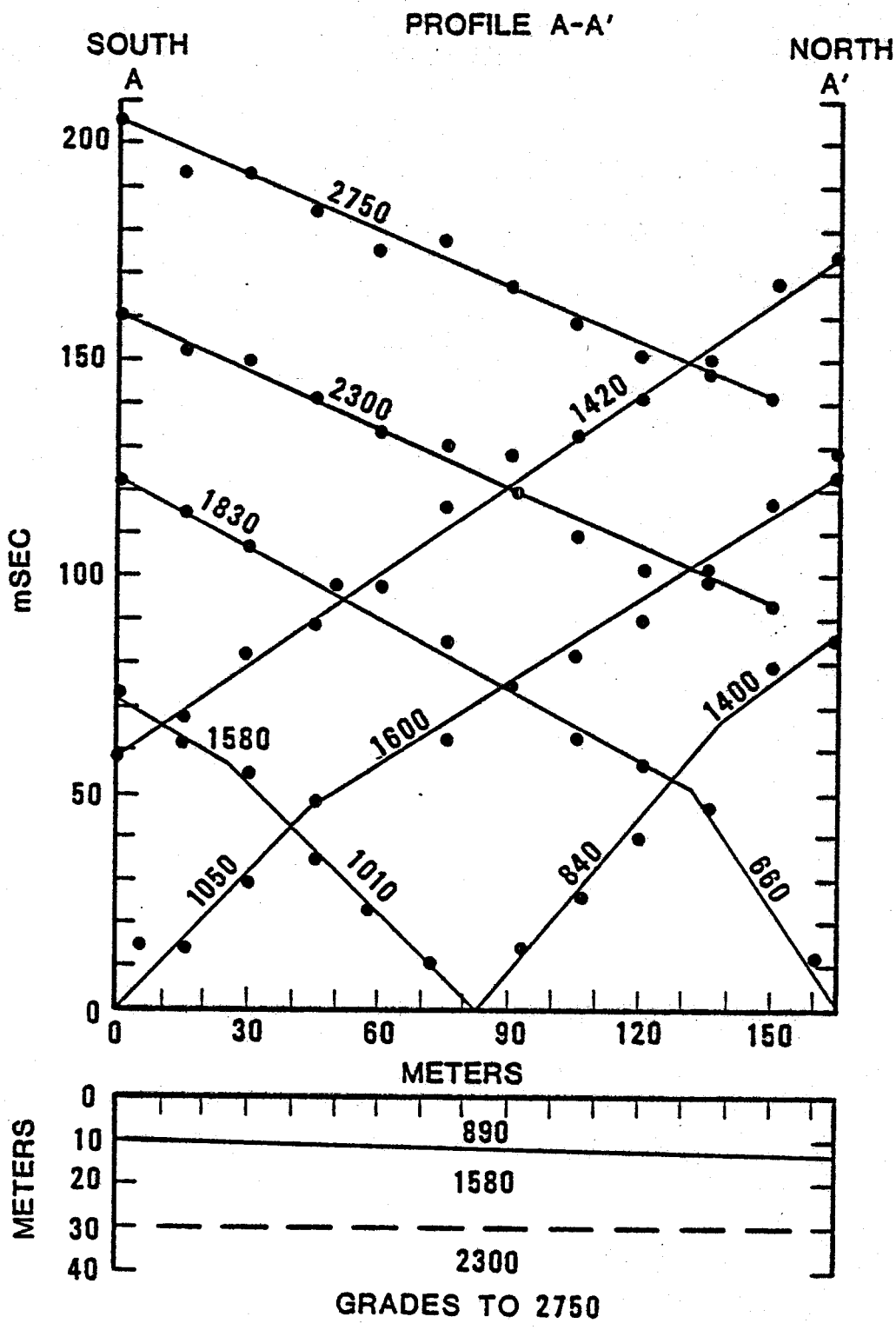

Figure 2. Seismic profile A-A' (in this and the following Figures 3-11 the numbers refer to velocities in m/sec).

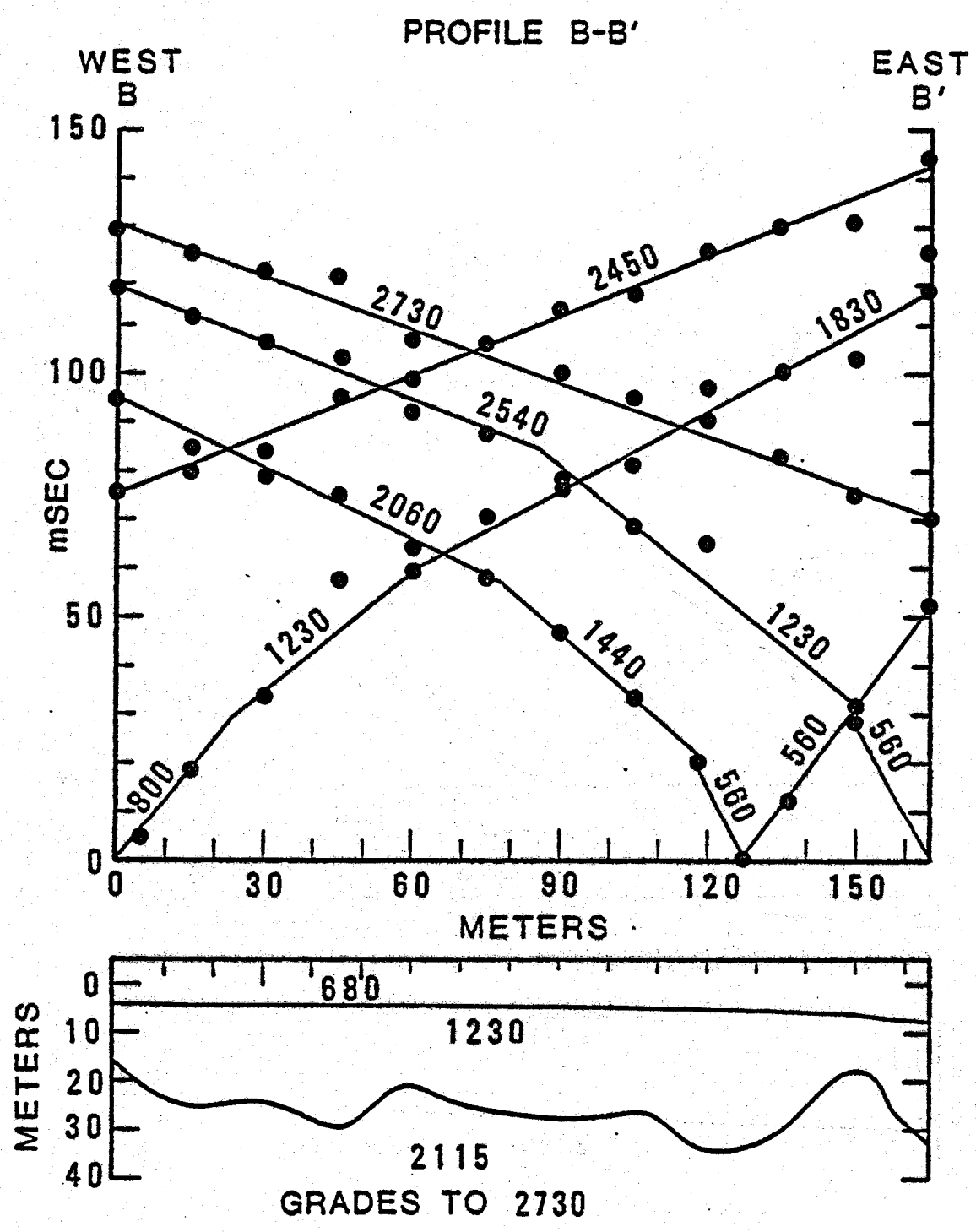

Figure 3. Seismic profile B-B'.

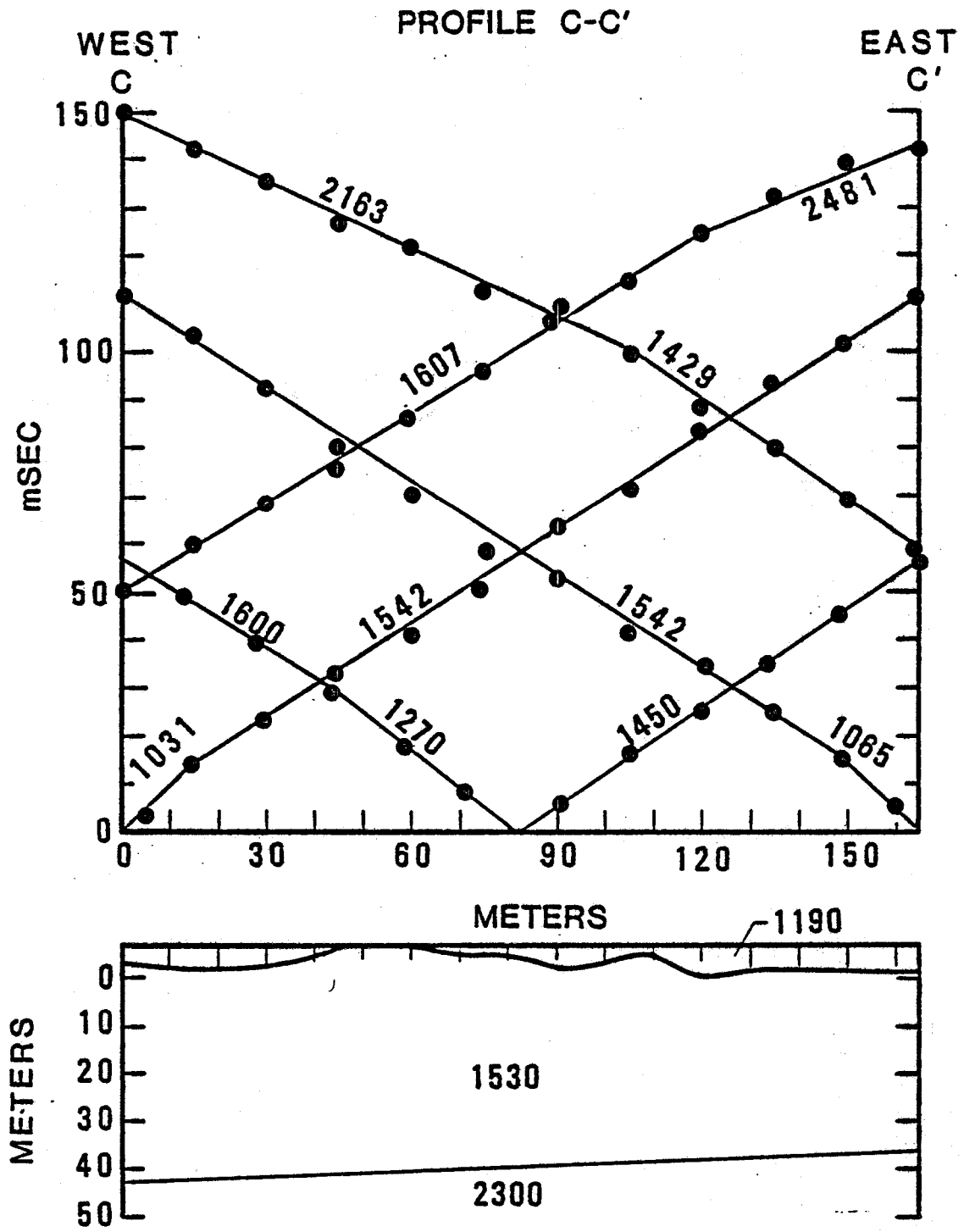

Figure 4. Seismic profile C-C'.

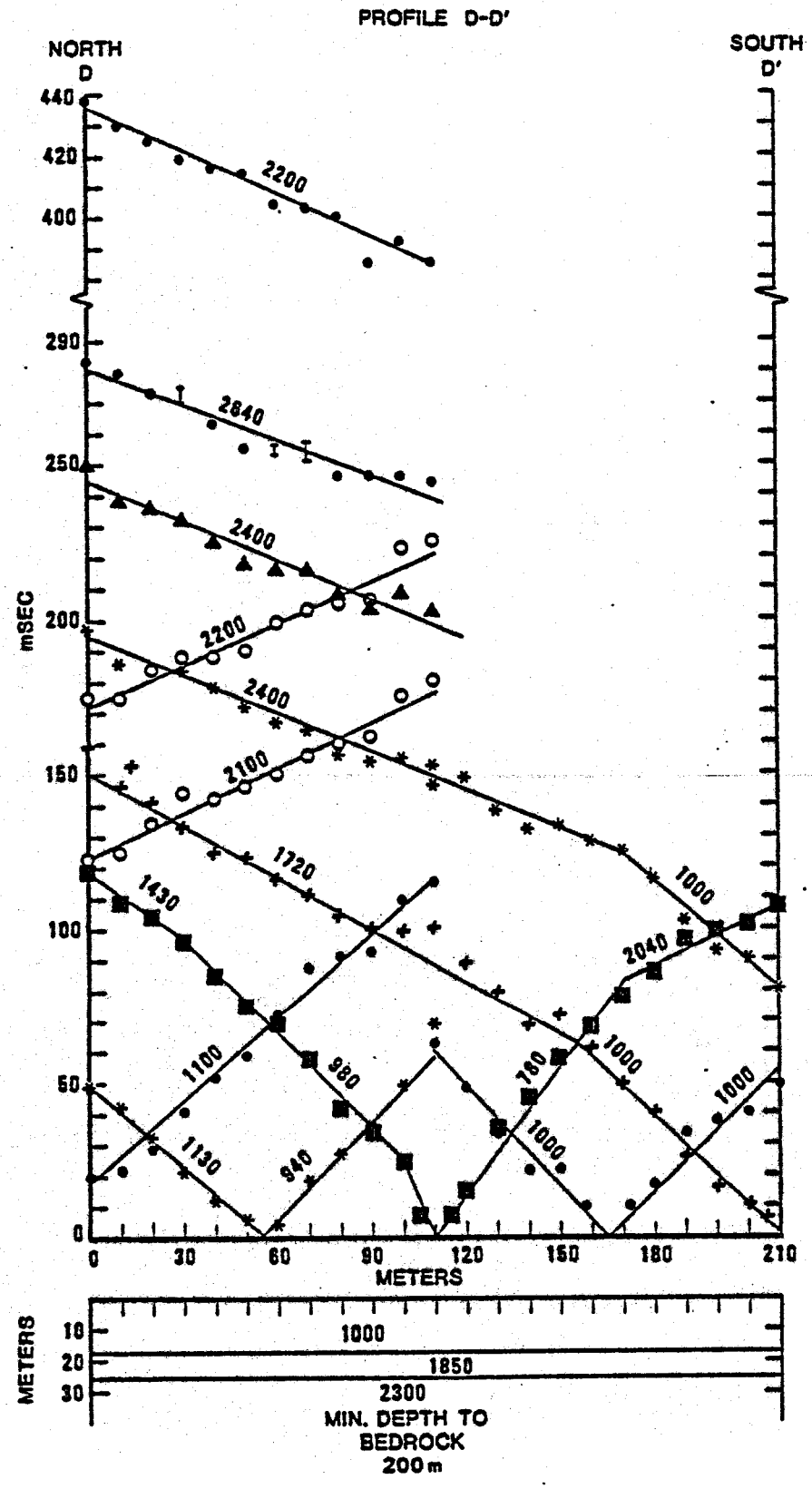

Figure 5. Seismic profile D-D'.

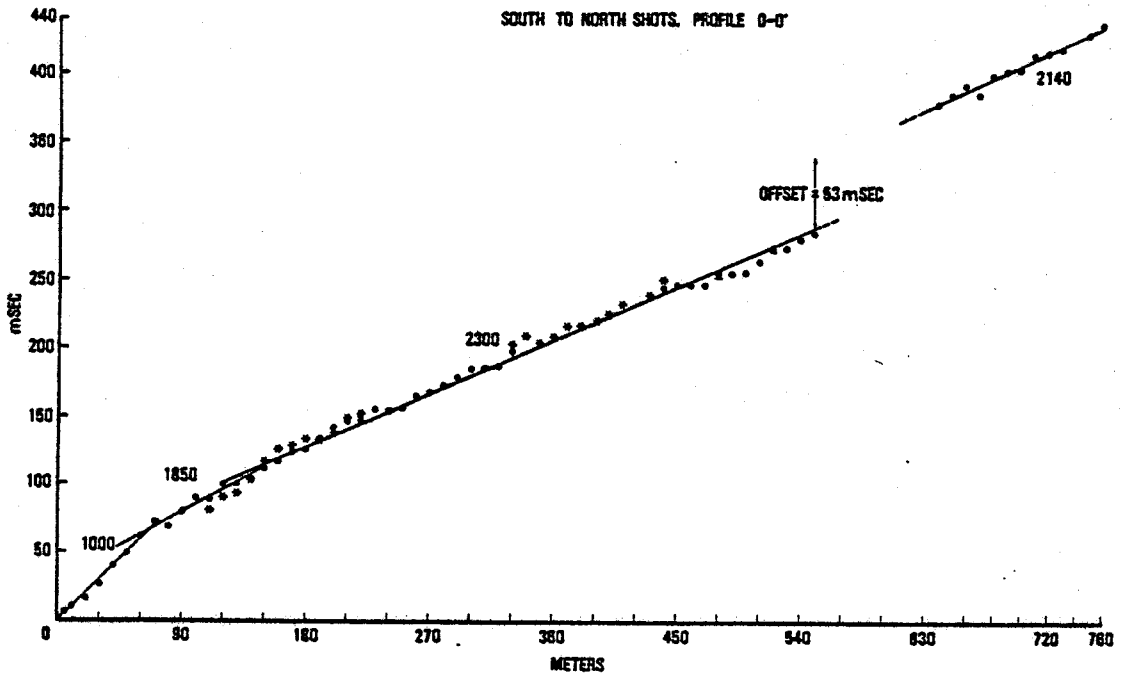

Figure 6. Composite travel-time curve of all south to north shots of seismic profile D-D'.

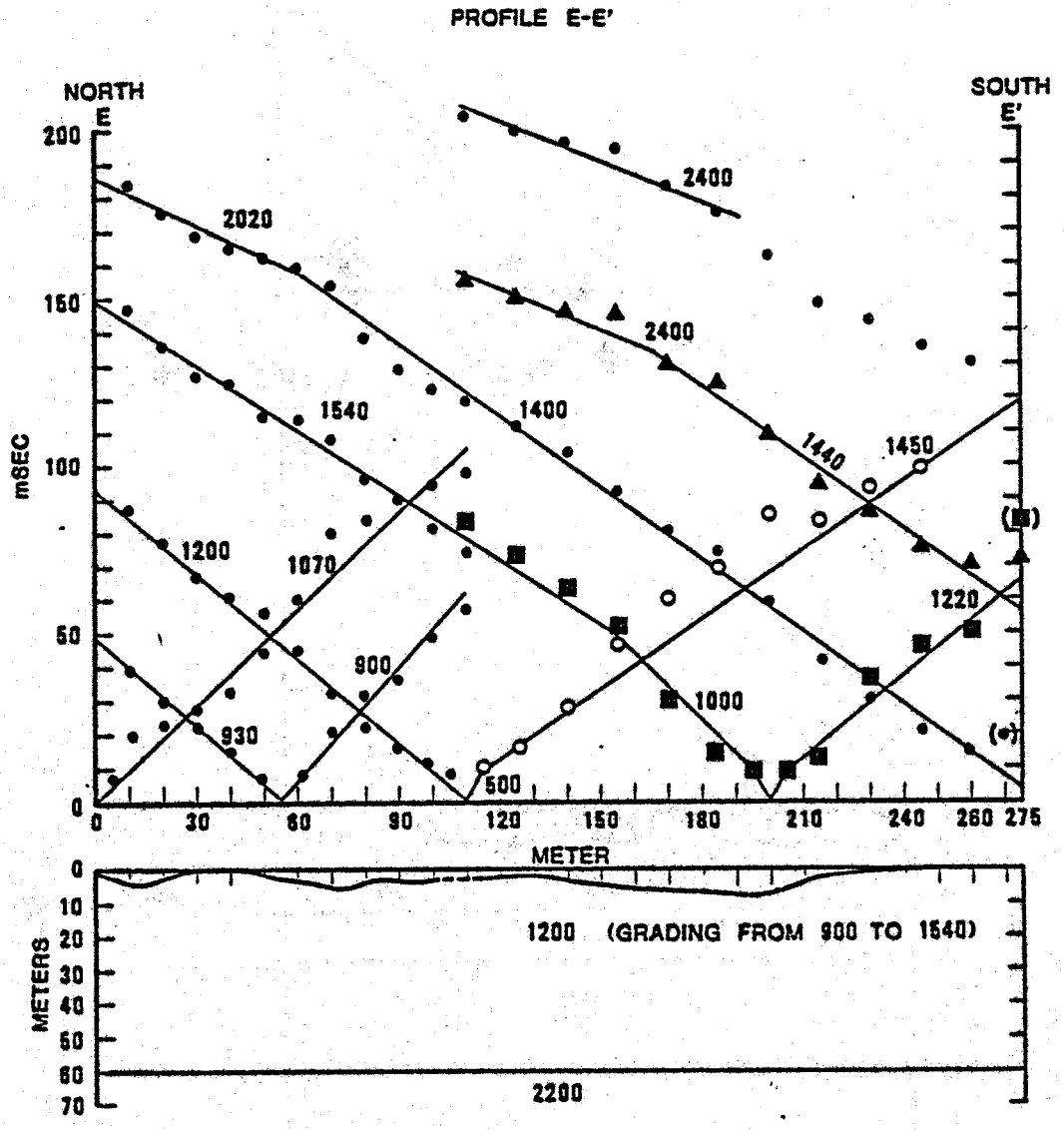

Figure 7. Seismic profile E-E'.

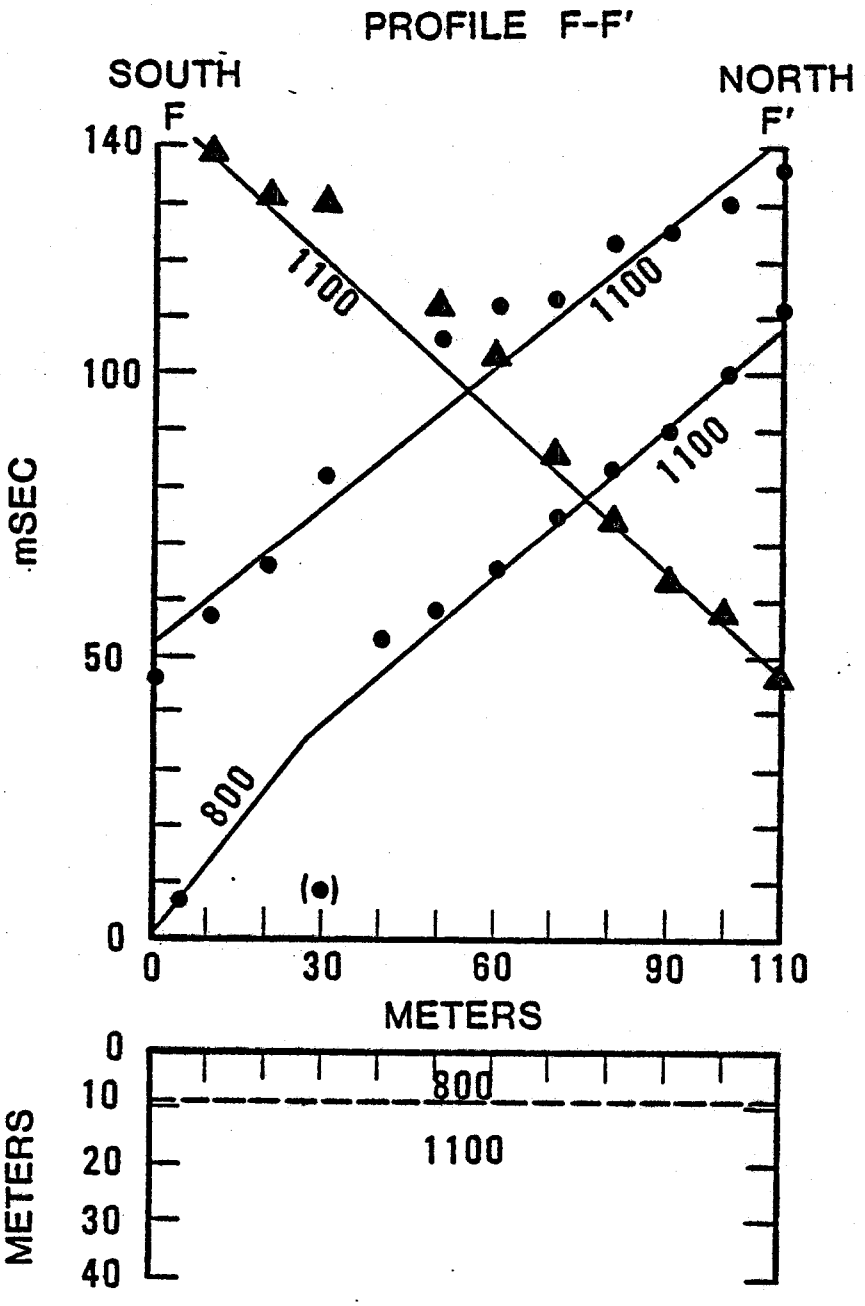

Figure 8. Seismic profile F-F'; the depth to layer 3 with an assumed velocity of 2200 m/sec would be at least 29 m.

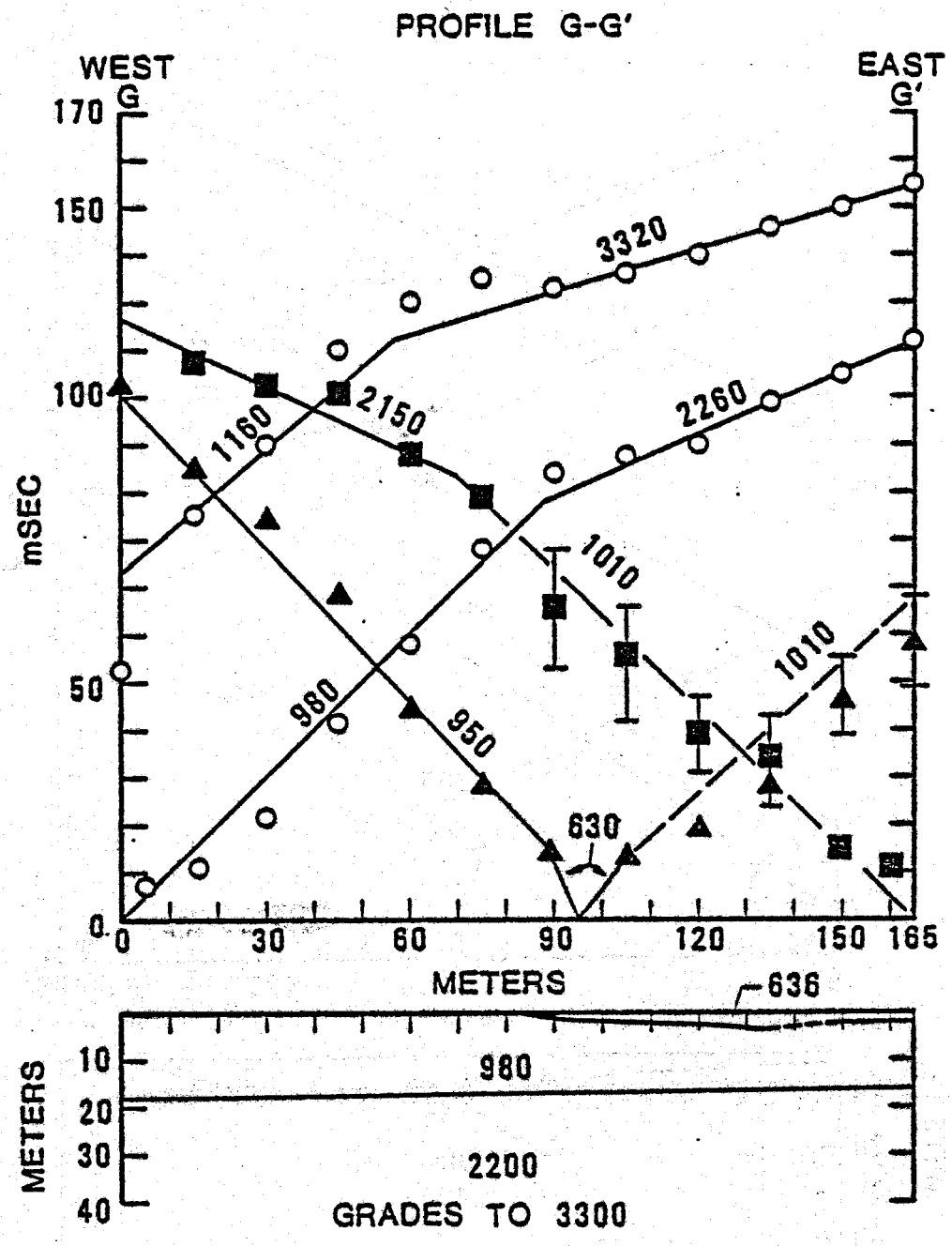

Figure 9. Seismic profile G-G'.

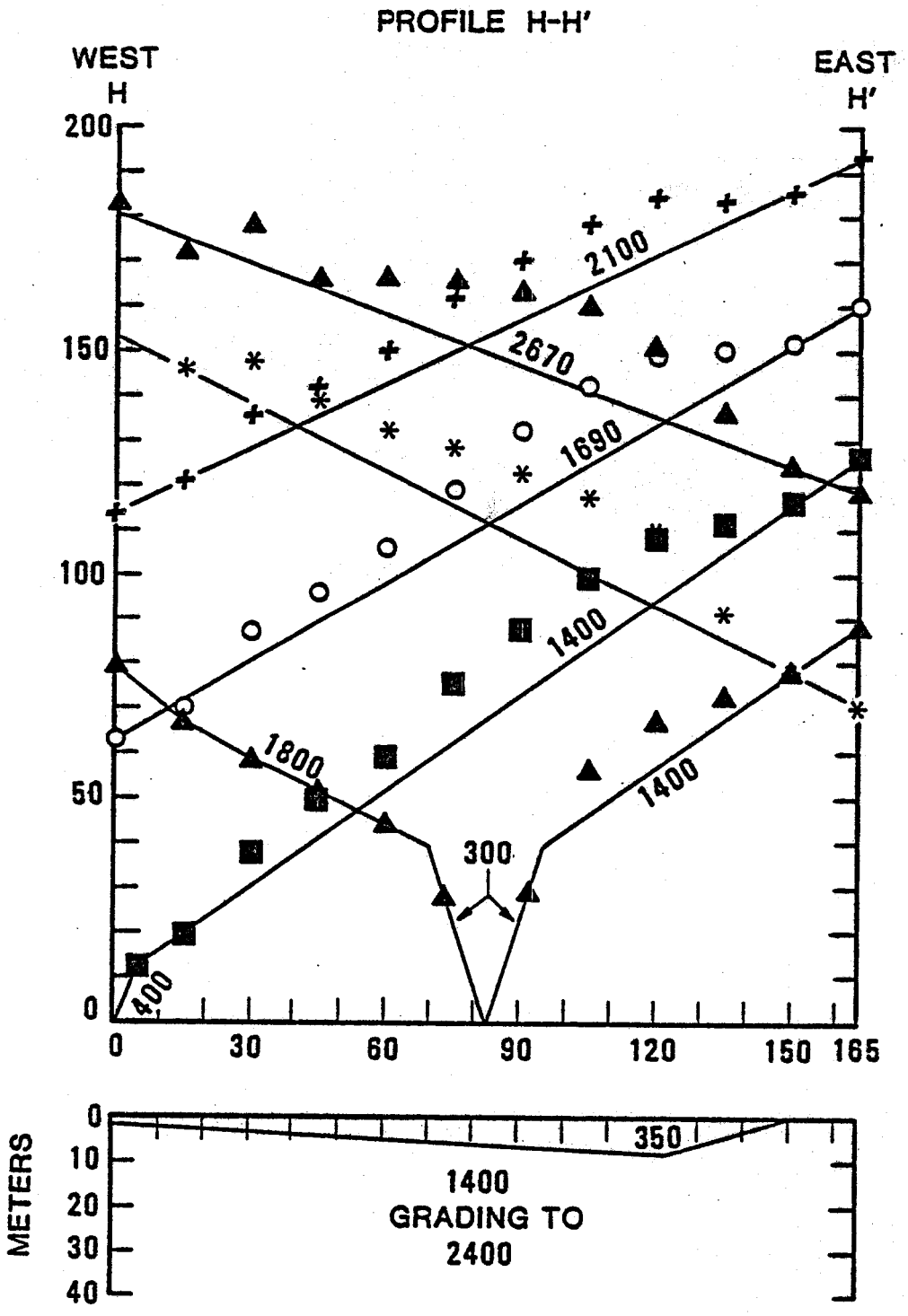

Figure 10. Seismic profile H-H'.

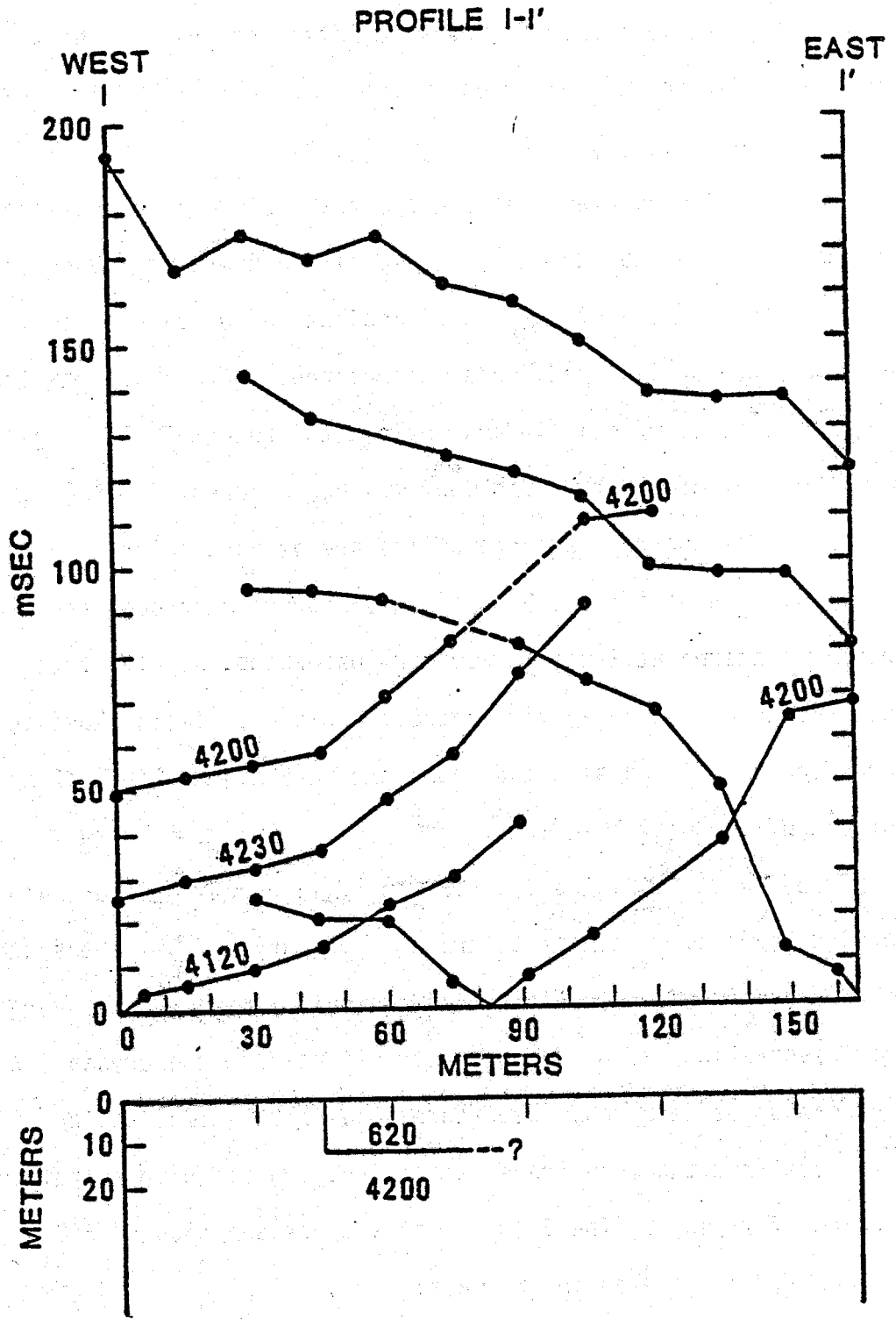

Figure 11. Seismic profile I-I'.

Our results corroborate the preliminary findings of Forbes, et al. (1974) who identified the same three basic units. The travel time data also show substantial scatter of the first arrivals caused by lateral inhomogeneities in the sediments. We interpret these to be cut-and-fill structures related to the depositional history of the Pilgrim River Valley as suggested by Forbes, et al. (1974).

Crystalline basement (metaquartzites ≈ 5000 m/sec; gneissose granites ≈ 5600 m/sec) was not detected in any of the profiles. Long shots up to 760 m beyond the end of array D-D' indicate a velocity of only 2300 m/sec for the deepest sediments encountered. If one assumes that meta-quartzites (5000 m/sec) lie just beyond the reach of the longest shot, a minimum depth of 200 m to basement may be inferred.

Three of the refraction profiles are of particular interest:

Profile B-B' (Figure 3): This is a profile through the thermal anomaly centered at 290 m S, 290 m W (Osterkamp, et al., this report), interpreted by the delay time method. This profile is close to a recommended drilling site and shows the very high relief (10 m) of the surface of the gravel layer 3.

Profile D-D' (Figure 5): This profile represents our main effort to find bedrock. A composite travel-time curve of all the south to north shots is given in Figure 6 showing that even at receiver-shot point separations of over 700 m refractions from the crystalline base-ment cannot be detected. Departures of arrival times at individual receivers from the mean travel time curve suggest high relief on the surface of layer 3. The 53 m sec offset between 550 and 640 m may be reasonably interpreted in two ways:

(1) A large thickness (approx. 70 m) of low-velocity layer 1 material under the last shot point, or:

(2) A depth increase of approximately 80 m to the surface of the layer 3 gravels (assuming layer 1 is 18 m thick).

On the basis of the gravity survey (Kienle and Lockhart, this report) which suggests a downdropped basement to the west of the springs, the second alternative may be more likely. The fact that layer 1 never exceeded 25 m in any of the other profiles also adds support to the second alternative.

Profile I-I' (Figure 11): This profile was shot across a north-south lineament seen on the U-2 photo of the Pilgrim River Valley. This lineament (Plate I) has recently been identified as a Quaternary fault (Kline, et al., this report). In addition, a 100 m dipole-dipole resistivity profile across the lineament suggests a thickness of 100 m of ice-rich permafrost on the west side and only 25 m of less ice-rich permafrost to the east (Wescott, et al., this report).

Because of the presence of high velocity massive ground ice and ice-rich soil, we could not see through to layer 3, in which we hoped to find evidence of faulting. However, several shots suggest an offset (either 12 or 28 m) of the massive ground ice, with the east side down. This is the proper sense of motion for the fault, as discussed in the surficial geology section of the report, but because of the poor quality of the data from this profile, we would be hesitant to use them as solid evidence for the observed fault. Profile I-I' was the only one in which we detected ice.

STRATIGRAPHIC INTERPRETATION

The surficial layer (layer 1-velocity 600-1000 m/sec) appears in places to grade into layer 2 (velocity 1200-1800 m/sec) and in other places (profile C-C', for example) to be entirely absent. Travel time data for both of these layers show remarkable scatter indicating strong lateral variations in velocity and the presence of isolated refractors, typical of a heterogeneous assemblage of materials, often as discrete bodies. Much of the detail of these fine subsurface structures lies beyond the resolution of our wide geophone spacing, designed to find deep refractors. However, the recent surficial geologic studies of the depositional history of the area by J. Kline, et al. (this report), allow us to postulate a depositional sequence which is consistent with the travel time data of our seismic survey.

Today the Pilgrim River is a meandering stream and numerous meander scars demonstrate that it has previously meandered over the thermally disturbed area surrounding Pilgrim Springs. A meandering river leaves a distinctive set of deposits as it sweeps back and forth over a valley. The deposits may be broken down into two major groups (Reineck and Singh, 1975).

(1) Channel deposits: Volumetrically the most important, these are deposits formed mainly from processes in river channels and include:

   (a) channel lag deposits; coarse-grained sediments deposited in the deeper parts of the channel in discontinuous lenticular bodies,

   (b) point bar deposits; large volumes of sand which accumulate on the insides of meander scrolls forming thick, tabular bodies,

(c) channel fill deposits; fine-grained sediments which eventually fill an abandoned meander loop.

(2) Bank and floodplain deposits: Flood deposits composed mainly of fine-grained sediments which spread-out in thin layers over the floodplain, and slightly coarser sediments which tend to pile up on the river banks.

The thickness of an ideal sequence of meander deposits will depend on the size of the river. An estimate for the Pilgrim River might be 1-5 m. In time, a meandering river valley will develop a sedimentary package consisting mainly of point bar sands which contain lenses of channel lag gravels and channel fill deposits covered by a drape of fine-grained flood deposits. If the valley is slowly dropping while maintaining a low river gradient, the resulting fill will be a complex sedimentary package of sands, gravel lenses, filled channels, and layers of fine-grained sediments.

Elsewhere in this report, J. Kline, et al., cite evidence suggesting that the Pilgrim River Valley has been lowered in the vicinity of Pilgrim Springs. This downdropping probably resulted in the heterogeneous sedimentary package discussed above. This model, together with the silica cementation probably caused by hydrothermal activity, could be expected to produce the travel time anomalies detected in our survey.

SUMMARY AND CONCLUSIONS

We have obtained shallow subsurface information on the sedimentary fill of the Pilgrim Springs area. Three basic units have been defined on the basis of seismic velocities, the most important of which is the conglomeratic third layer of possible Tertiary age. This layer is over-

lain by river meander gravels, sands and fines that make up layers 1 and 2. In the area of the first two test drill holes the top 9 m of this layer contains a hot artesian aquifer with estimated flows of 200 and 300-400 gal/min (Figure 1, Kline, et al., this report).

We have also determined that the crystalline basement of the valley floor is much deeper than previously thought, at least 200 m beneath Pilgrim Springs.

REFERENCES

Forbes, R. B., L. Gedney, D. VanWormer and J. Hook, 1975, A geophysical reconnaissance of Pilgrim Springs, Alaska, Technical Report, Geophysical Institute, University of Alaska.

Harding-Lawson Associates, 1973, Resistivity survey of Pilgrim Springs, Alaska, Contract report to Stephano and Associates, Anchorage, Alaska.

Reineck, H. E., and I. B. Singh, 1975, Depositional sedimentary environments, Springer-Verlag, Heidelberg.

GRAVITY SURVEY OF THE PILGRIM SPRINGS GEOTHERMAL AREA, ALASKA

Juergen Kienle and Andrew Lockhart

OBJECTIVES

A reconnaissance gravity survey was undertaken to aid in defining the regional crustal structure and to attempt to estimate the depth to crystalline basement at Pilgrim Springs.

METHODS

During July and October, 1979, 122 gravity stations were occupied covering an area of about 720 square kilometers, including the Pilgrim River Valley near Pilgrim Springs and parts of the Kuzitrin Valley, the northern flank of the Kigluaik Range and the hills north and east of the Pilgrim and Kuzitrin Valleys. Data were also taken along the south flank of the Kigluaik Mountains south to Salmon Lake along the Taylor Road, and a detailed survey followed the course of the Pilgrim River.

The survey was tied by repeated flights and truck trips to the gravity base station NOMA (Barnes, 1968) at the Nome airport. Uncertainties in this tie affect absolute gravity values at Pilgrim Springs by less than 0.8 mgal.

The instrument used was a LaCoste-Romberg gravimeter, model G-248, which is thermostatically maintained at constant temperature. The gravimeter drift was evaluated by repeated ties at the Pilgrim Church secondary base; the drift correction was less than 0.12 mgal/hour under the worst conditions.

The only real limitation of the quality of the gravity survey was the elevation control. Station elevations determined with a Paulin surveying altimeter were corrected by recordings from a base station barograph at Pilgrim Springs and are accurate to ± 4.6 m (± 0.90 mgal). Whenever possible we occupied stations on benchmarks (± 0.9 m, ± 0.18 mgal) or on checked elevations (± 2.3 m, ± 0.45 mgal). The best relative elevation control was obtained along the gradient of the Pilgrim River with stations taken at river level (± 0.9 m, ± 0.18 mgal).

The Bouguer reduction density used for all gravity stations is 2.67 g/cc. This is a standard reduction density for gravity stations on crystalline basement. For the valley stations taken on alluvium, a more accurate reduction density would be 2.00 g/cc. However, because most valley station elevations are less than 10 m, the error caused by using the higher reduction density is less than 0.3 mgal which is insignificant in terms of the magnitudes of the observed anomalies.

Terrain corrections for selected gravity stations have been made in order to estimate the terrain effects on the gravity map shown on Figure 1. Figure 1 is bounded on the south by the east-west trending Kigluaik Mountains which crest at about 915 to 1430 m. These mountains require a positive terrain correction on the Pilgrim River valley stations grading from 1.5 mgal on the southernmost gravity stations to 0.5 mgal near the axis of the Pilgrim River. Terrain corrections for stations along the Pilgrim River show no change in magnitude from east to west. Terrain corrections for stations on Mary's Mountain and Hen and Chickens Mountain range from 1 to 2 mgal as do corrections for stations in the hills to the west of the Pilgrim River and north of the Kuzitrin River.

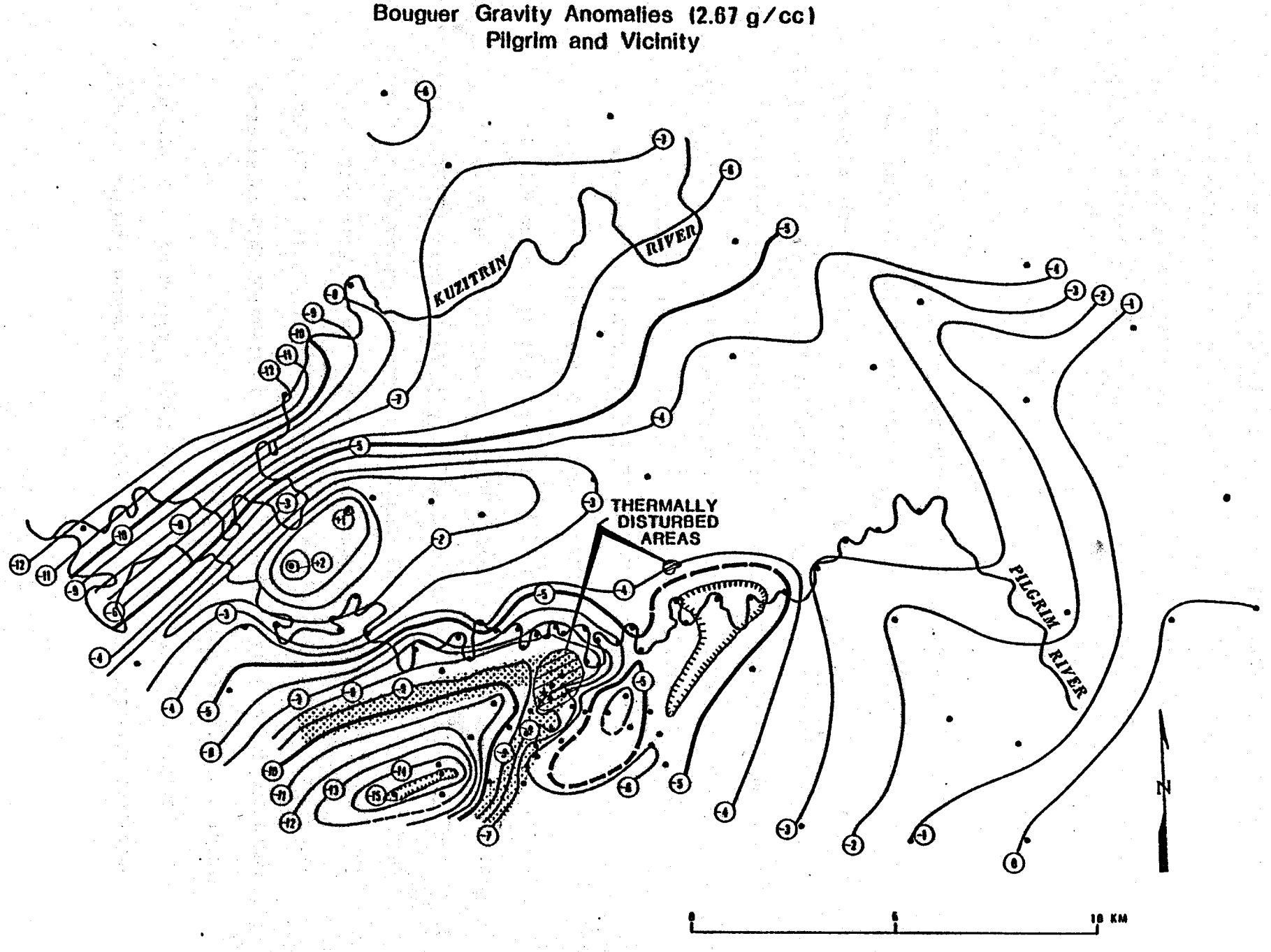

Figure 1. Bouguer 2.67 g/cc gravity anomaly map (mgal), Pilgrim Springs and vicinity. Stippled areas represent possible fault zones.

Adding the terrain corrections would have very little effect on the overall shape and magnitude of the gravity anomalies shown in Figure 1: The gravity low to the southwest of Pilgrim Springs would be slightly reduced, and the dominant northeast-southwest grain of the gravity map would be slightly enhanced.

RESULTS

Figure 1 is a simple (not terrain corrected) 2.67 g/cc Bouguer gravity anomaly map, which reveals surprising complexities near Pilgrim Springs. The old crystalline terrain north and east of Pilgrim Springs is characterized by gentle gravity anomalies that vary between 0 and -7 mgal. The gravity data taken in the Pilgrim River valley and a few stations in the lower Kuzitrin drainage reveal sizeable negative anomalies, implying that in places the low density valley fill is quite thick.

The gravity anomalies in the Pilgrim River Valley between the Taylor Highway bridge and Marys Mountain define 2 distinct regions roughly separated by the 164°55'W meridian passing through Pilgrim Springs. As discussed elsewhere in this report (Kline, et al.) this line also separates regions of distinctly different morphology and surficial geology and is the locus of a mapped Quaternary fault (Plate I). The valley is narrower and the river gradient steeper east of Pilgrim Springs as compared to the much wider valley west of the Springs characterized by a lower river gradient and extensive thaw lakes at the level of the flood plain.

Northeast of the springs, Bouguer gravity values of -2 to -4 mgal suggest a thin sedimentary cover. A small southwest-northeast-trending

low of 3 mgal (-6 mgal contour closure) centered on the Pilgrim River indicates an 80-to-100 m-deep pocket of low density sediments. A narrow gravity high (-4 mgal contour closure) lies immediately southwest with the same southwest-northeast elongation.

The valley floor west of the Springs, characterized by numerous lakes, has low Bouguer gravity that defines a sedimentary trough, again elongated in a southwest-northeast direction. Pilgrim Springs is located at the northeastern corner of this trough. At the springs, crystalline basement may lie at depths of at least 200 m while the deepest part of the trough, characterized by a -15 mgal contour closure, could be as deep as 400 to 500 m. (These rough depth estimates are based on a horizontal slab approximation of the mass anomalies, using a background regional field value of about -2 to -3 mgal and a density contrast of 0.67 g/cc.) If the sedimentary trough is that deep one might expect to encounter older sediments, such as the late Tertiary Kougaruk gravels which outcrop in the Noxapaga valley, 70 km to the northeast of the Pilgrim area. Bouguer gravity values in the Kuzitrin valley north of Marys Mountain are as low as -12 mgal, again indicating a great thickness of low density valley fill and possibly another area occupied by Kougaruk gravels at depth.

The gravity trough southwest of Pilgrim Springs is bound by fairly steep linear gravity gradients along its northern and southeastern margins (Figure 1, stippled trends). We do not have enough data to define the western and southern margins, but an active normal fault offsetting glacial moraines by as much as 10 m has been mapped at the southern margin (Plate I). Both the northern and southeastern margin gravity gradients suggest normal faulting. If this interpretation is correct, the crystalline

basement is dropped by about 200 to 300 m going south across the Pilgrim River and west across the linear gravity gradient that passes through Pilgrim Springs. The springs appear to be located at the northeastern corner of this subsided basement block. The sense of downdropping is opposite to that shown by the surficial geology as discussed elsewhere in this report (Kline, et al.). However, there is no conflict assuming the surficial geology reflects more recent fault motion than that shown by the gravity data.

A more detailed analysis awaits 3-dimensional computer modelling of the anomalies. Nevertheless, the present gravity data are adequate to show that Pilgrim Springs is located at the intersection of 2 strong gravity gradients that suggest a block-faulted basement. These two gradients correspond in a general way to mapped faults on Plate I.

In view of the surprisingly thick sedimentary section suggested by seismic and gravity data for both the lower Pilgrim and Kuzitrin Valleys one might speculate that the low-lying region extending from the Imuruk Basin through the Kuzitrin Valley to the Imuruk Lava fields, which has had active volcanism perhaps as recently as 200 years ago (Hopkins, 1963), represents an incipient northeast-trending rift through the Seward Peninsula. The rift may be as old as the late Tertiary because the Kougaruk gravels occupy the basal portion of the trough at least in the Noxapaga valley. Because no evidence of young plutonism was found when we mapped the area (Swanson, et al., this report), it may be more attractive to associate manifestations of anomalous heat flow (alkali-basaltic volcanism, hot springs) with tensional tectonics and active rifting in the region. Additional evidence for this model comes from a recent seismic study by Biswas, et al. (1980). This

study indicates that the Imuruk Basin and lower Kuzitrin Valley comprise an area of anomalously high seismicity with fault plane solutions indicating active normal faulting typical of modern rift zones.

REFERENCES

Barnes, D. F., 1968, Alaska gravity base station network: U.S. Geol. Survey Open-File Rept. 304, 8 pp. and tables.

Biswas, N. N., L. Gedney and J. Agnew, 1980, Seismicity of Western Alaska, Bull. Seismol. Soc. Am., (in press).

Hopkins, D. M., 1963, Geology of the Imuruk Lake area, Seward Peninsula, Alaska: U.S. Geol. Survey Bull., 1141C, 101 pp.

ELECTRICAL RESISTIVITY SURVEY OF THE PILGRIM SPRINGS GEOTHERMAL AREA, ALASKA

Eugene Wescott, Richard Sydora, Jerry Peace and Andrew Lockhart

THEORY

The high salinity of the hot spring water produces a water resistivity of 1.0 Ω-m. Thus unconsolidated sediments or rocks containing this hot water will have a low resistivity. By Archie's law the resistivity of a rock is approximately; $\rho = \rho_w \phi^{-2}$, where ρ_w is the resistivity of the interstitial water and ϕ is the porosity. The resistivity will also decrease with increasing temperature up to 250°C. Thus we have confidence that the hot water reservoir underlying Pilgrim Springs can be delineated at depth by low resistivities of the order of a few Ω-m.

METHODS

Deep electrical resistivity measurements were made using a Zonge Engineering and Research Organization GDP-12 induced polarization/resistivity receiver system. A Geotronics FT-4 transmitter capable of a 4 ampere square wave signal was used as the signal source. The Zonge system uses a pair of 6100 Intersil microprocessors to process the field data (stacking and averaging), to improve the signal-to-noise ratio and calculate the resistivity and phase shift. The system can be used with 16 different frequencies from 1/125 to 256 Hz to produce a complex resistivity curve, but due to the time available we ran 1/4 Hz as the standard measurement on both Schluberger and dipole-dipole measurements.

PREVIOUS WORK

The first priority of the resistivity work was to extend and interpret the previous resistivity survey done by Harding Lawson Associates (1973). They had run an east-west Schlumberger depth profile, centered near our 5S station (500 m south of the grid origin), and then had extended to the north and to the south by means of the equatorial dipole system. They found an upper layer of about 30 m thickness with a resistivity of 10 Ω-m underlain by material which they interpreted as being crystalline bedrock with 200 Ω-m resistivity. To the north the equatorial dipole points suggested to them a much greater depth to bedrock of near 180 m. Thus their interpretation suggested an east-west fault near the springs down-dropped to the north with an offset of 150 m somewhere to the north of 5S.

1979 SURVEY

Our first survey to check this hypothesis was to run an east-west Schlumberger depth profile at 5N, line S-S' on Figure 1.

The field data and a theoretical computer model curve are shown in Figure 2. Modelling was done using an automatic curve fitting program (Zohdy, 1974a) for guidance and a convolution curve fitting program to fit the curve with greatest possible accuracy (Zohdy, 1974b). The best fit to the data incorporates 9 horizontal layers. There are a series of thin layers from the surface downward, approximating variations in resistivity due to the dry surface soil grading downward to water-saturated sediments. We find a fairly low resistivity layer, 12.1 Ω-m, 3.1 m thick at a depth of 3.9 m, which may be a blue clay layer found near the surface in seismic drill holes. It is underlain by a layer 8.5 m thick of slightly higher

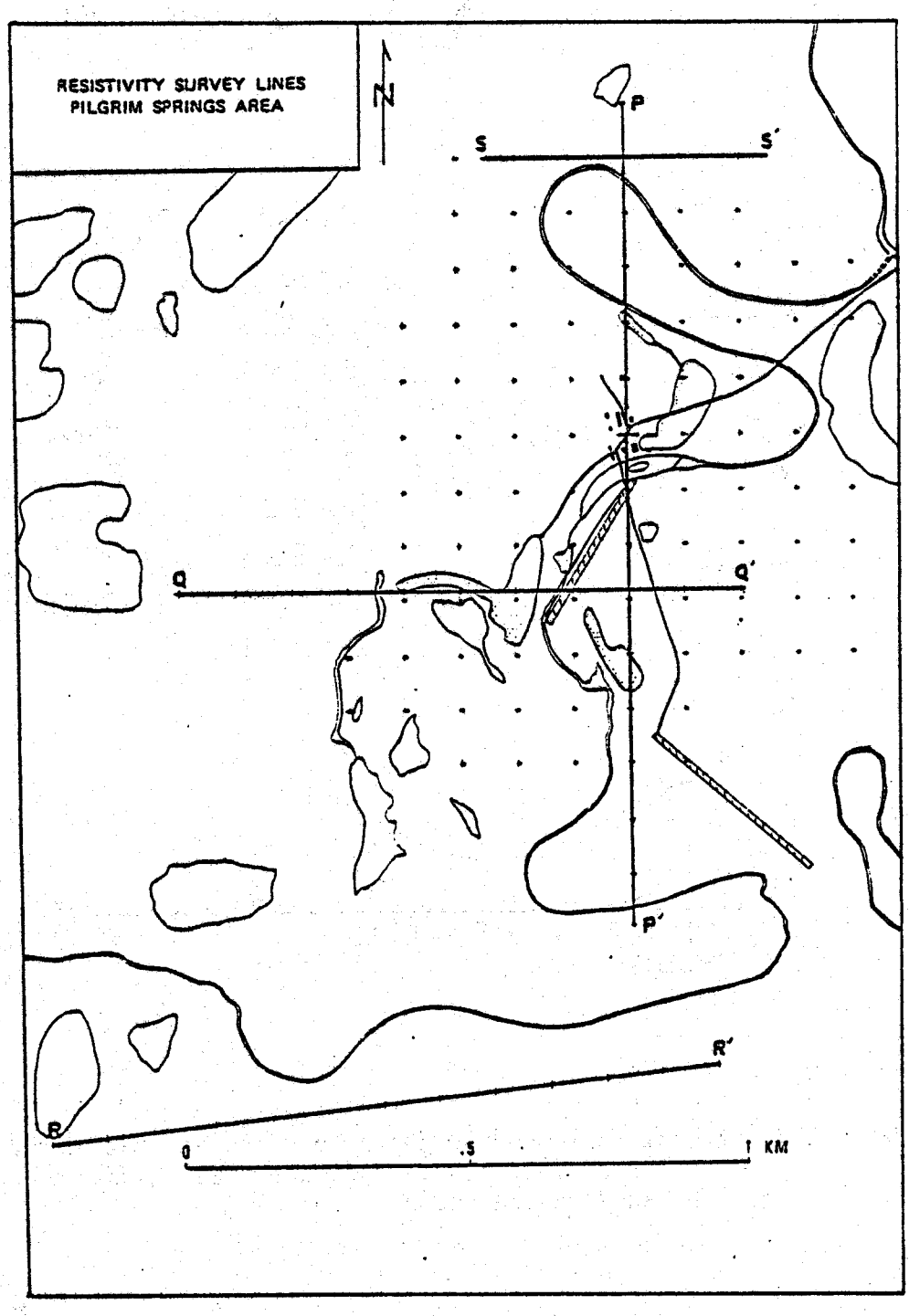

Figure 1. Location of resistivity survey lines. Stippled areas indicate agricultural fields.

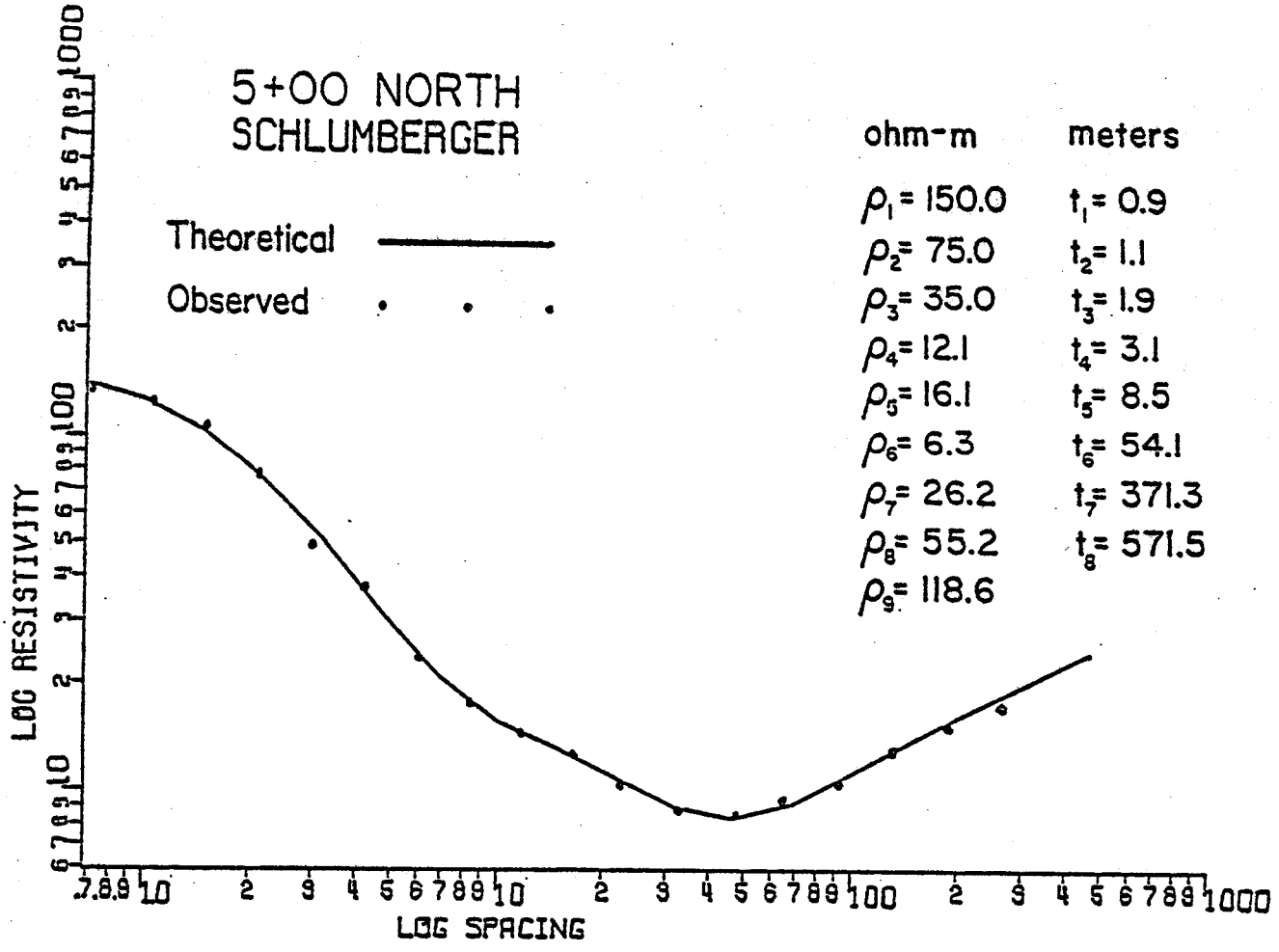

Figure 2. East-west Schlumberger depth sounding at station 5N (500 m north of origin). The model resistivities and bed thicknesses are shown.

resistivity (16.1 Ω-m), which may have a higher sand and silt content. Beneath this layer our model calls for a 54 m thick layer of 6.3 Ω-m. The low resistivity probably indicates a hot water aquifer, with the water somewhat diluted by cold ground water.

Beneath the 54 m thick aquifer the model shows a floor of higher resistivity sediments, presumably of lesser porosity and/or not containing hot water. Owing to seasonal flooding we were only able to extend our current electrode half spacing to 256 m, so the modelled thicknesses and resistivities beyond that depth are not very meaningful. The indicated slope of the resisitivity curve, however, does not suggest that crystalline bedrock was reached.

Further to the north, towards the Pilgrim River, inspection suggests that permafrost is present just below the surface. This is where the Lawson-Harding (1973) equatorial dipoles were located on the northern extension of their Schlumberger sounding. The very high (∿ thousands of Ω-m) resistivity of permafrost constitutes a lateral inhomogeneity which is the most likely explanation for the purported crystalline bedrock at 180 m depth erroneously identified by Harding-Lawson Associates, (1973).

Our next effort was to run a dipole-dipole survey north-south along the baseline, line P-P' on Figure 1. Our pre-survey computer model studies indicated that such a survey would be very sensitive to the type of fault structure proposed by Harding-Lawson Associates (1973). We used 100 m dipoles and generally extended each receiving spread out to n = 5. The diagram below indicates the nature of the dipole-dipole resistivity spread.

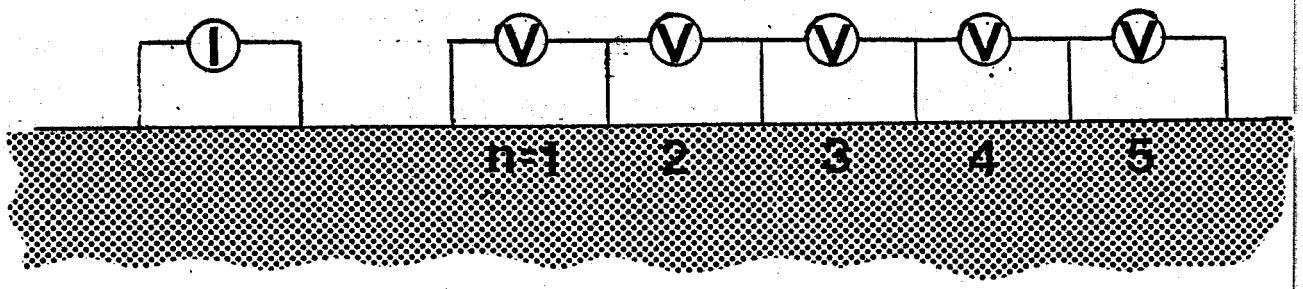

The nominal depth of investigation is 1/2 the distance between the transmitting and receiving dipoles. Thus survey sampled to about 300 m depth, yet features of a few tens of meters could be distinguished.

Figure 3a illustrates the results of this survey presented in pseudo-section, where the resistivity values are plotted at the 45° intersections of lines between the transmitter and receiver locations. Note that several n = 1 values are less than 3, 2.5 and 2.6 Ω-m respectively.

We have made a number of two-dimensional model calculations using the computer code developed by Dey and Morrison, (1975). This modelling program uses a mesh of discrete resistivity values. Owing to the very large size of the array and the cost of computer runs for such a large program, we restricted the array to 113 x 16 elements. This means that the smallest feature we model is a resistivity element 25 x 25 m. With the limitation of this minimum discrete element we have run many models, all of which have shown the same basic structure, that of a low resistivity "pancake" 50 m thick, about 1 km in diameter, and underlain and surrounded by material of resistivity 200 Ω-m.

Figure 3b shows the basic model. The gross features and resistivity values are fairly close to the field values of Figure 3a. The model includes a 25 m layer of 3 Ω-m, underlain by a 25 m thick layer of 1 Ω-m. The south edge of the reservoir is near 5S where the resistivity grades

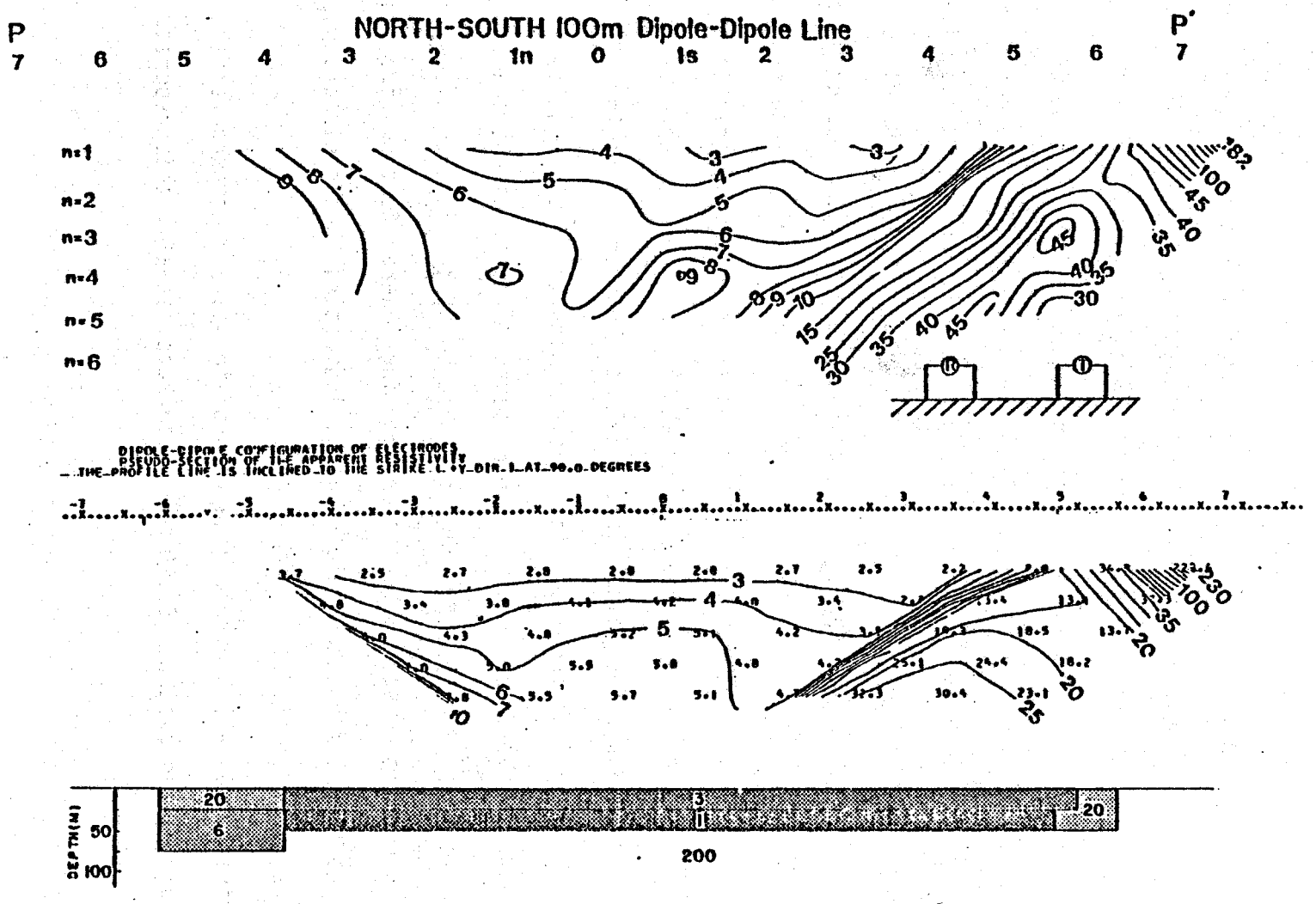

Figure 3a. Field data, N-S 100 m dipole-dipole pseudosection. Station numbers in hundreds of meters (e.g., 1S = 100 m south of origin).

Figure 3b. Two dimensional computer model of the basic shallow reservoir structure underlain by rocks of greater resistivity. All values in Ω-m.

into the background 200 Ω-m. At the north edge near 6N the depth increases to 75 m while the resistivity increases to reflect the Schlumberger results. Thus our basic model agrees with the hypothesies of a shallow reservoir about 50 m thick.

We ran three variations on the basic model to see if we could detect the presence of another hot brine layer at depth. Figure 4b shows the pseudosection for a model with a semi-infinite brine layer of 1 Ω-m, 50 m thick at a depth of 150 m. In Figures 5b we moved the layer up 50 m to a depth of 100 m and in Figure 6b a 25 m layer is modelled at a depth of 75 m. As one can see the gross features of the pseudosections are all similar to the basic model, Figure 3b. The actual numbers vary as do the fit of various features. From the dipole-dipole survey and models we can definitely say that there is a bottom to the shallow (50 m) surface reservoir, but we cannot rule out additional thin reservoir layers at greater depths.

We also ran several inverted cone models in order to represent a rising plume of hot water. A typical cone model is shown in Figure 7b. The general features of the cone model are inconsistent with the field results, and thus argue against the presence of a thermal plume of these dimensions.

Finally, in Figure 8b we show the results of the computer model of the proposed Harding-Lawson fault structure. The general features are significantly different from the field results, indicating that their proposed fault is not present.

We also ran a Schlumberger depth profile near the ground temperature anomaly centered at 290 m S 290 m W (Osterkamp, et al., this report),

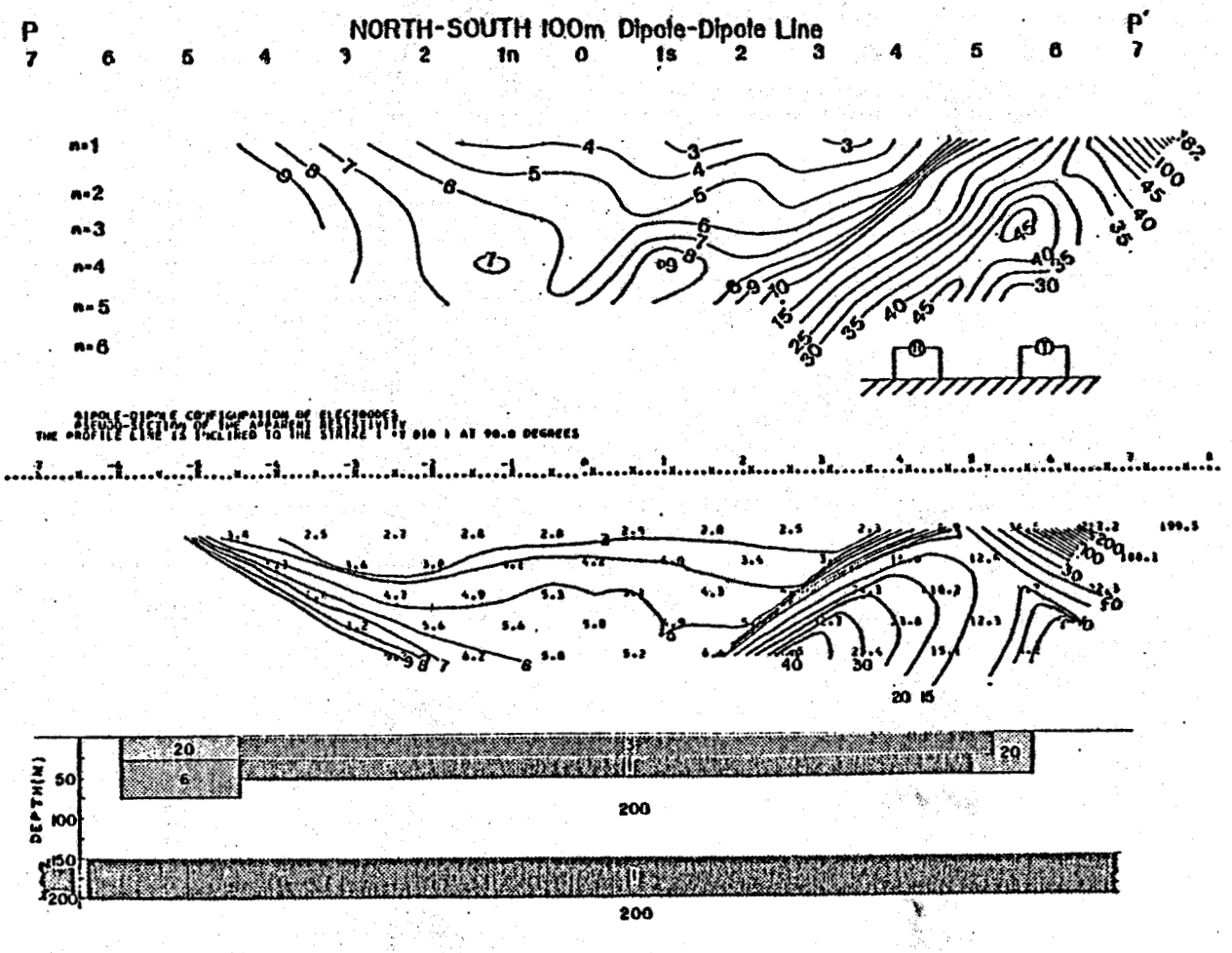

Figure 4a. Field data, N-S 100 m dipole-dipole pseudosection. Station numbers in hundreds of meters (e.g., 1S = 100 m south of origin).

Figure 4b. Two dimensional computer models with a second, deeper hot brine layer at 150 m depth. All values in Ω-m.

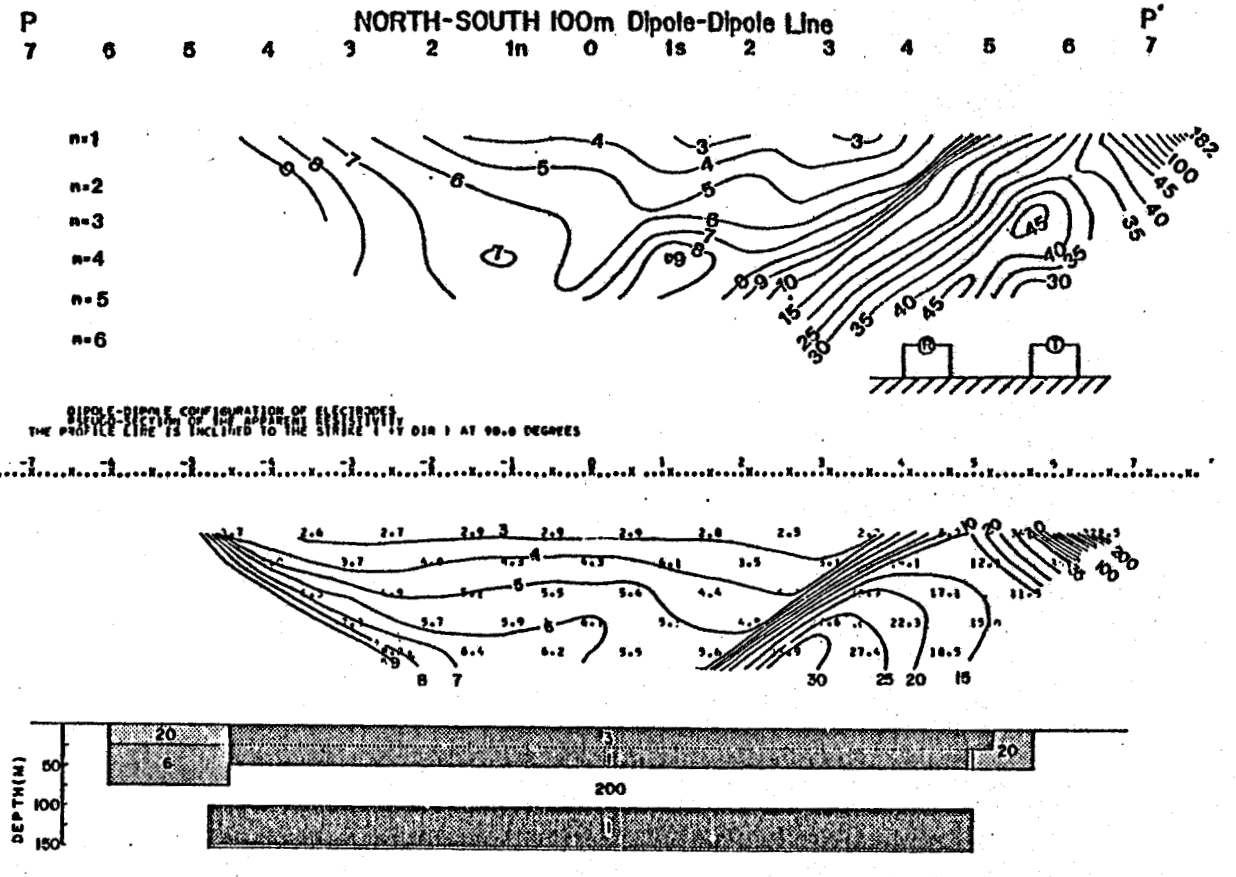

Figure 5a. Field data, N-S 100 m dipole-dipole pseudosection. Station numbers in hundreds of meters (e.g., 1S = 100 m south of origin).

Figure 5b. Two dimensional computer model with a second, deeper hot brine layer at 100 m depth. All values in Ω-m.

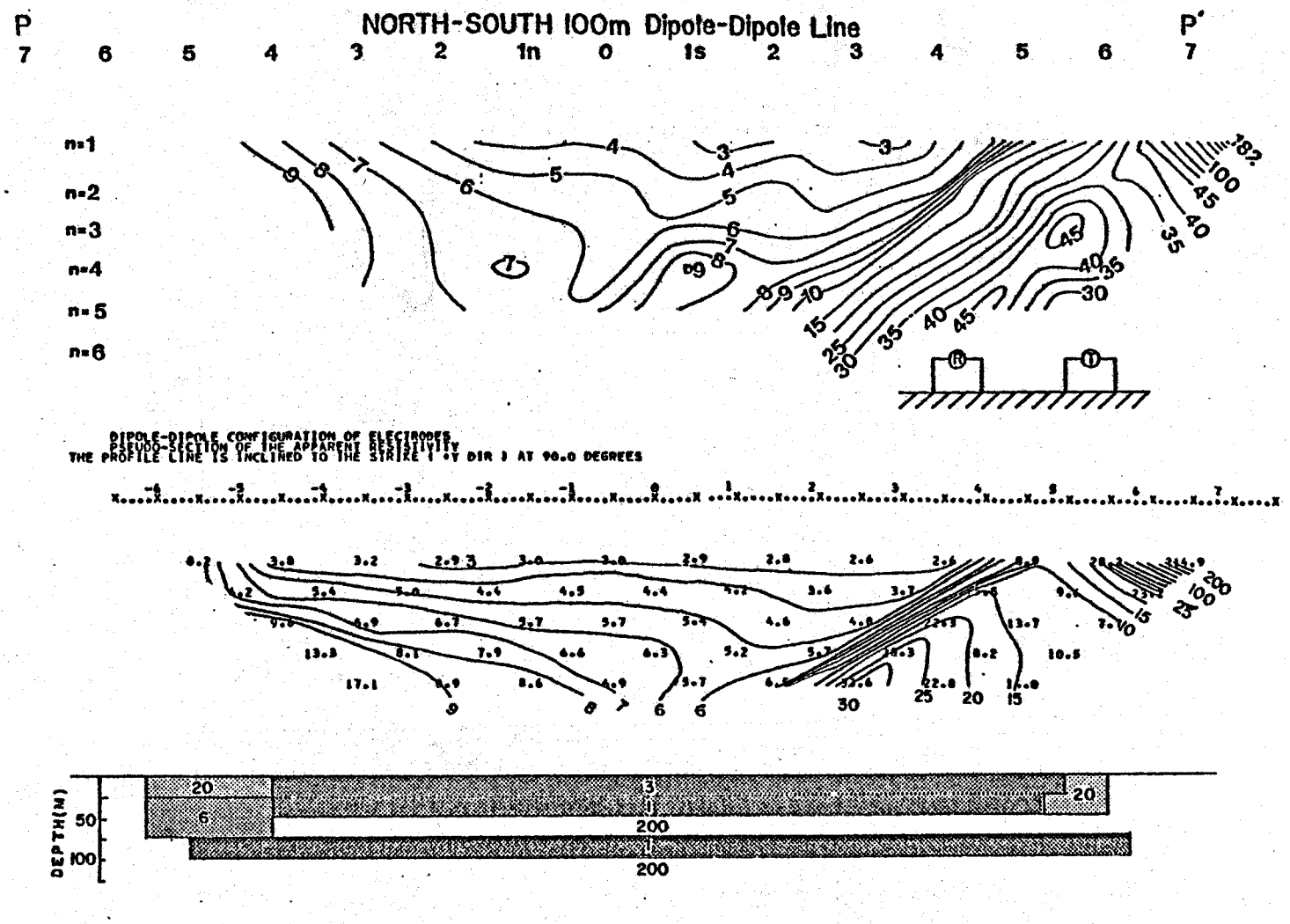

Figure 6a. Field data, N-S 100 m dipole-dipole pseudosection. Station numbers in hundreds of meters (e.g., 1S = 100 m south of origin).

Figure 6b. Two dimensional computer model with second, deeper brine layer of 25 m thickness at 75 m depth. All values in Ω-m.

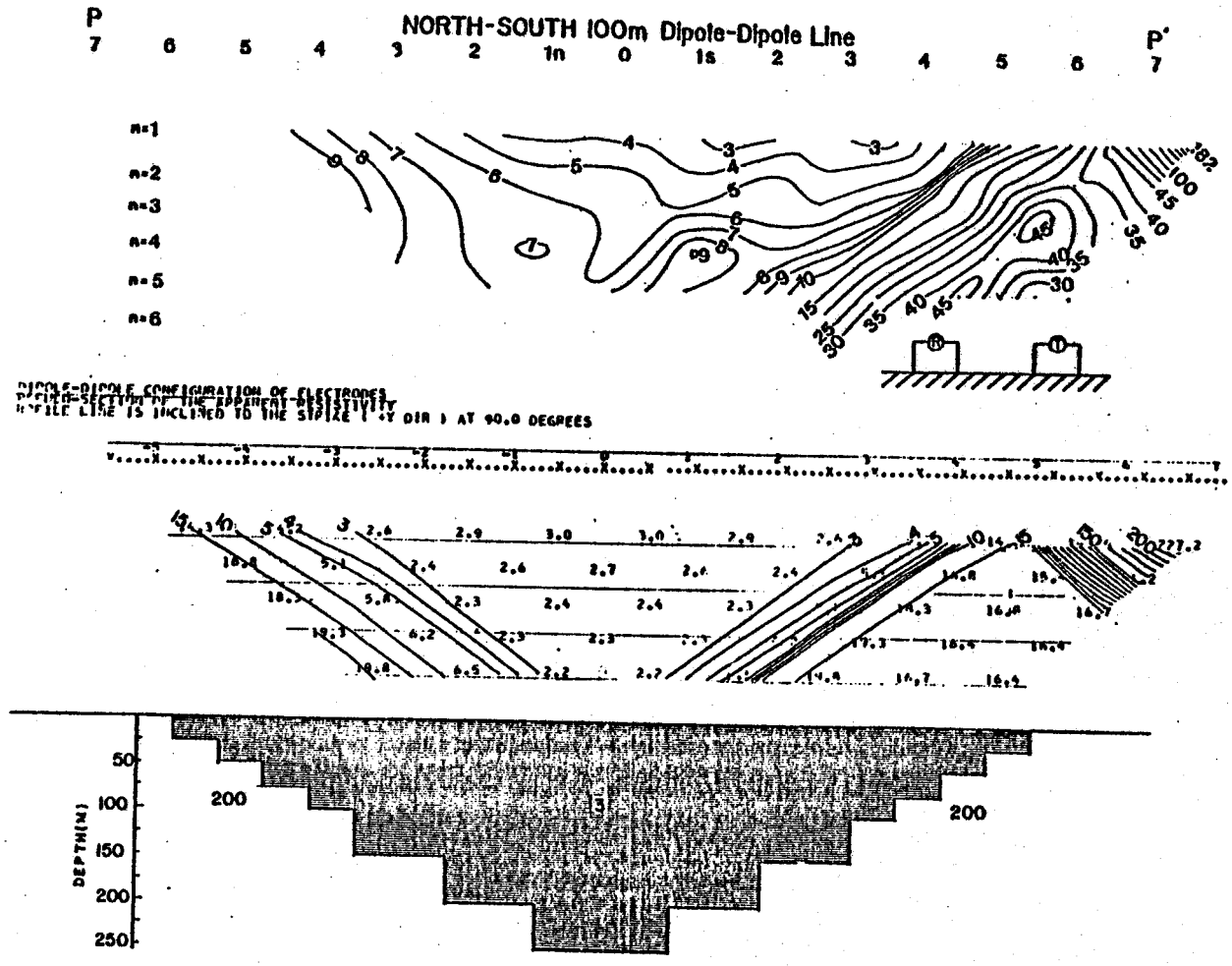

Figure 7a. Field data, N-S 100 m dipole-dipole pseudosection. Station numbers in hundreds of meters (e.g., 1S = 100 m south of origin).

Figure 7b. Two dimensional inverted cone model of a plume-type structure. The fit is not as good as the basic "pancake" model (Figure 3b). All values in Ω-m.

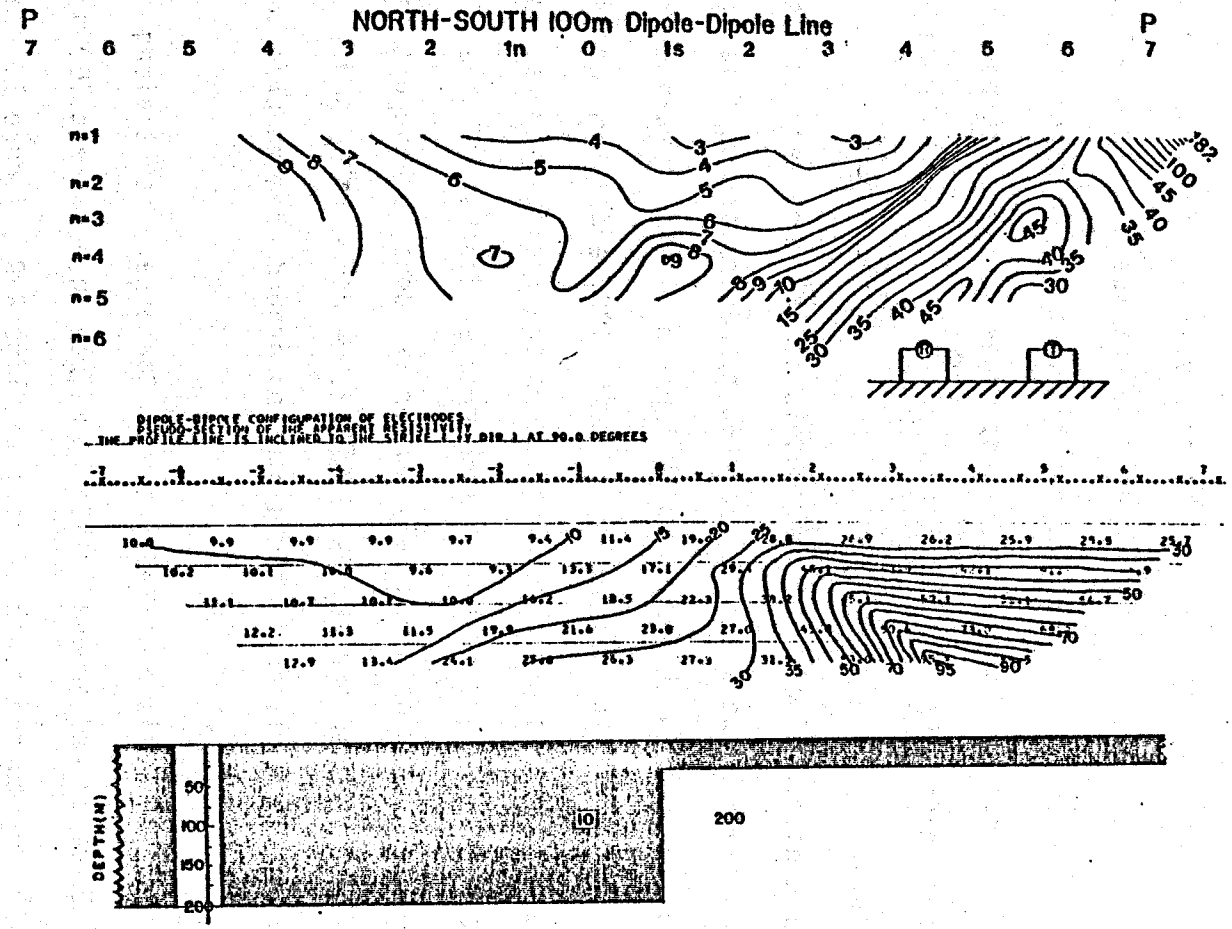

Figure 8a. Field data, N-S 100 m dipole-dipole pseudosection. Station numbers in hundreds of meters (e.g., 1S = 100 m south of origin).

Figure 8b. Two dimensional model with a buried fault offset 167 m corresponding to the Harding-Lawson model (1973). The fault model is inconsistent with the observed field data. All values in Ω-m.

line Q-Q', Figure 1. Figure 9 shows the field data and a theoretical computer model using a 6-layer earth. There is a dry surface layer of about 1 m thickness which was observed in the field to grade from soil into a blue clay which was saturated with hot water. The main feature of the model is a 40 m thick layer of resistivity 3.5 Ω-m, which is clearly a very hot water reservoir, with high salinity. Below the reservoir we find a 45 Ω-m section of sediments with low porosity and probably no hot water. Below 240 m the curve suggests a basement of 1000 Ω-m, but the last few data points may be affected by the lateral inhomogeneity of the edges of the disturbed ground. In any case these excellent data indicate a bottom to the shallow reservoir near 41 m depth.

Because the dipole-dipole computer models do not seem very sensitive to deeper reservoirs under the shallow (about 50 m) reservoir, we tried running the Schlumberger program with a 25 m thick layer of 1 Ω-m at various depths. Figure 10 shows the results of this layer at 75, 100, and 125 m depths. Clearly such a layer has a pronounced effect on the resistivity vs. spacing curves and could easily be detected at much greater depths. Thus a flat layered earth interpretation at anomaly number two does not support the suggestion of deeper reservoir layers. However, we did not run Schlumberger depth profiles at other places in the disturbed ground area to preclude such a possibility.

To test the hypothesis of a N-S-trending Quaternary fault along the west edge of the disturbed ground (Plate I) we ran an east-west 100 m dipole-dipole survey to the south of Pilgrim, line R-R', Figure 1. The mapped fault intersects the survey line at nearly a right angle in the vicinity of station 0. The pseudosection of the field data is shown in

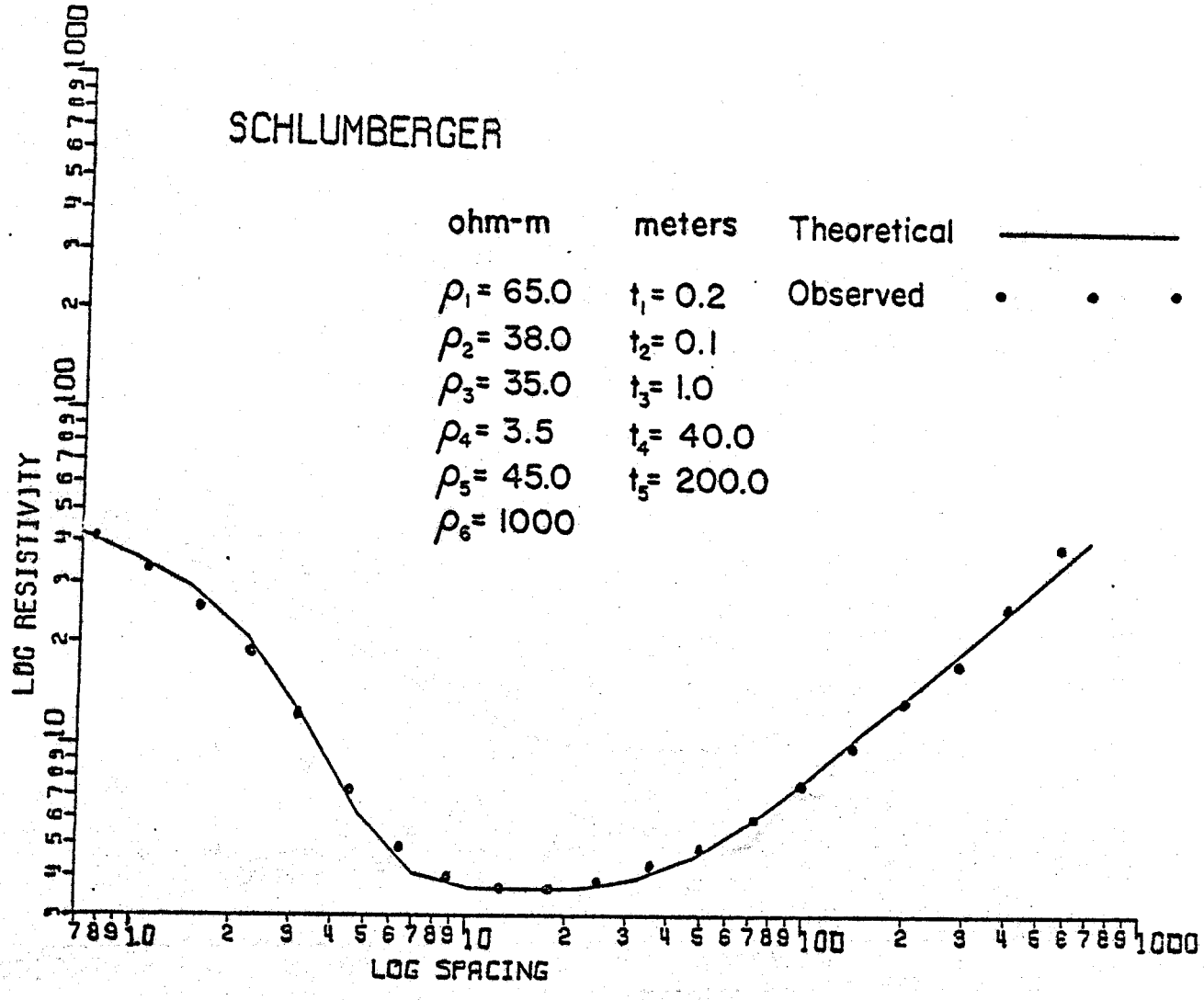

Figure 9. Field data points and calculated computer curve of a Schlumberger depth profile run east-west centered on ground temperature anomaly at 290 m S, 290 m W.

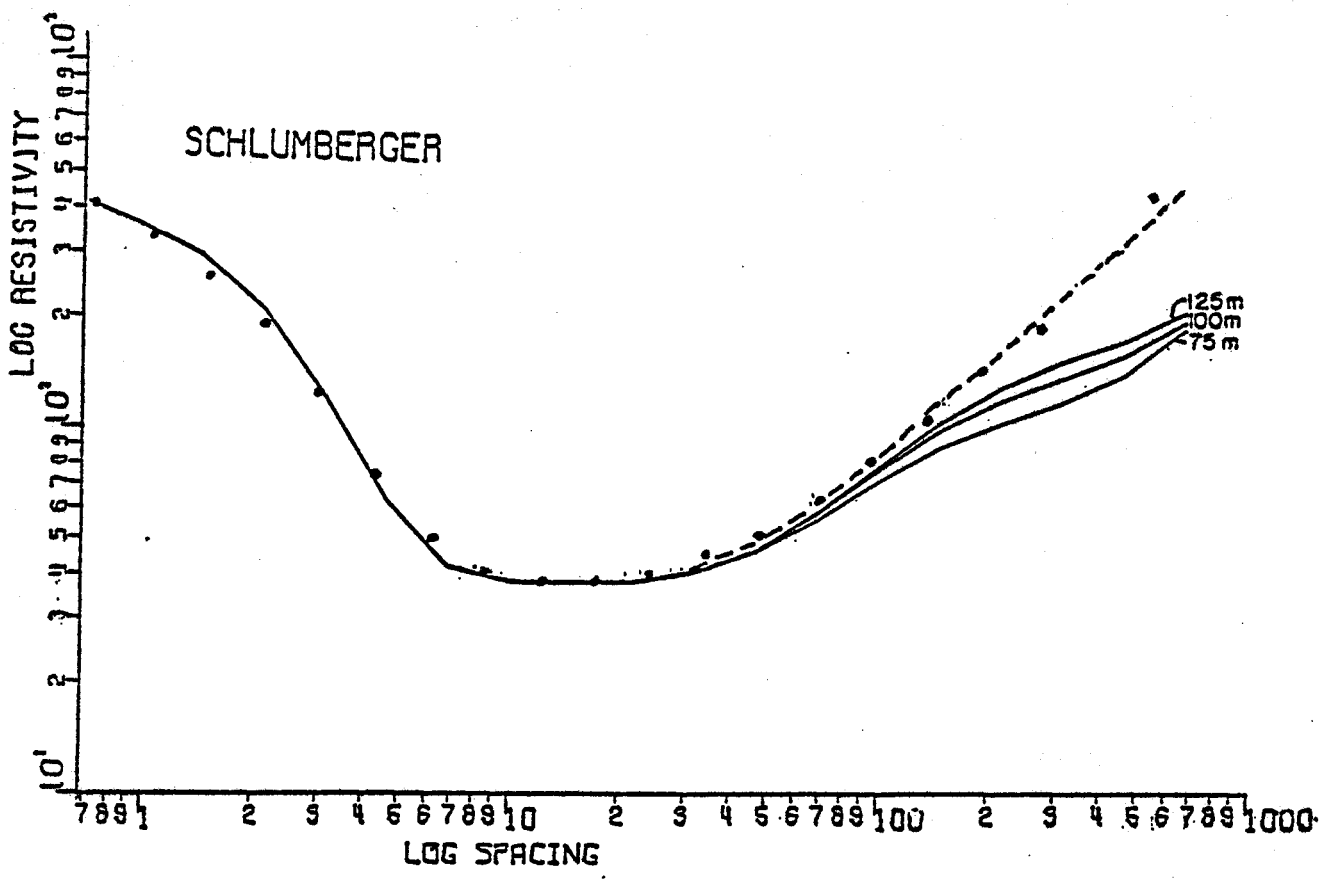

Figure 10. Schlumberger depth profile at ground temperature anomaly at 290 m S, 290 m W. With computer curve calculated for best fit dashed line, and for three cases of a 1 Ω-m, 25 meter-thick, deeper layer inserted at depths of 75 to 125 m.

Figure 11a. There is a clear difference in the surface resistivities across the line near station 1E (100 m east of origin). To the west we encountered very high resistivities of order 30,000 Ω-m, which we interpret as being very ice-rich permafrost. The permafrost east of the line has much lower resistivity and is also thinner.

The best computer model pseudosection is shown in Figure 11b. Many models were run attempting to duplicate all the features, and in general all agreed with a 100 m-thick section of permafrost of resistivity about 25,000 Ω-m to the west of station 0 and a 25 m-thick layer of permafrost of less ice content, 6000 Ω-m, to the east. We had to vary the near surface resistivity somewhat to duplicate the field values in the final models.

The most significant feature of the model is that underlying the permafrost on either side are sediments of resistivity 300 Ω-m. That is, the permafrost does not extend to basement, and water would be free to migrate in aquifers beneath the permafrost. The mapped fault is a reasonable explanation for the observed difference in surface resistivities, but no hot water is indicated by the resistivity data in this area. Apparently the fault is not serving as a conduit bringing hot water to near-surface levels in the vicinity of our resistivity profile.

We also ran a Schlumberger and a 10 m dipole-dipole survey in the region of the smaller thaw window NE of Pilgrim which produced 20°C temperatures at 4 meters depth. Plate I shows the configuration and location of this thaw window. Figure 12 shows the pseudosection. It shows a high resistivity near the surface (dry, sandy soil) underlain by a lower resistivity layer and then again higher. The resistivity data do not suggest hot saline water within a few tens of meters of the surface in this area.

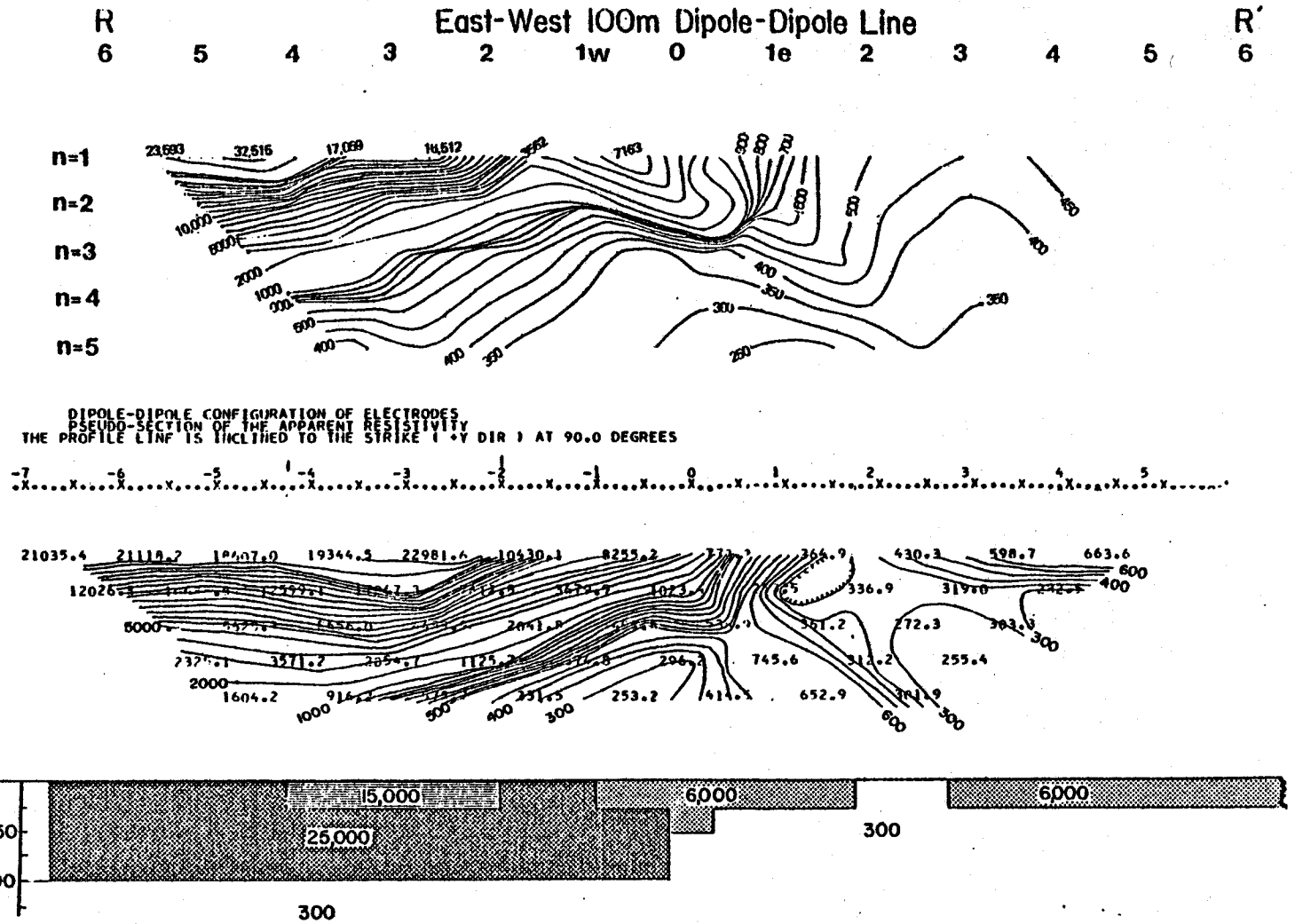

Figure 11a. 100 m dipole-dipole pseudosection line R-R' to test for a N-S trending Quaternary fault. Station numbers in hundreds of meters (e.g., 1S = 100 m south of origin).

Figure 11b. Two dimensional computer model shows thick ice-rich permafrost to the west and thinner permafrost to the east of the mapped fault at station 0.

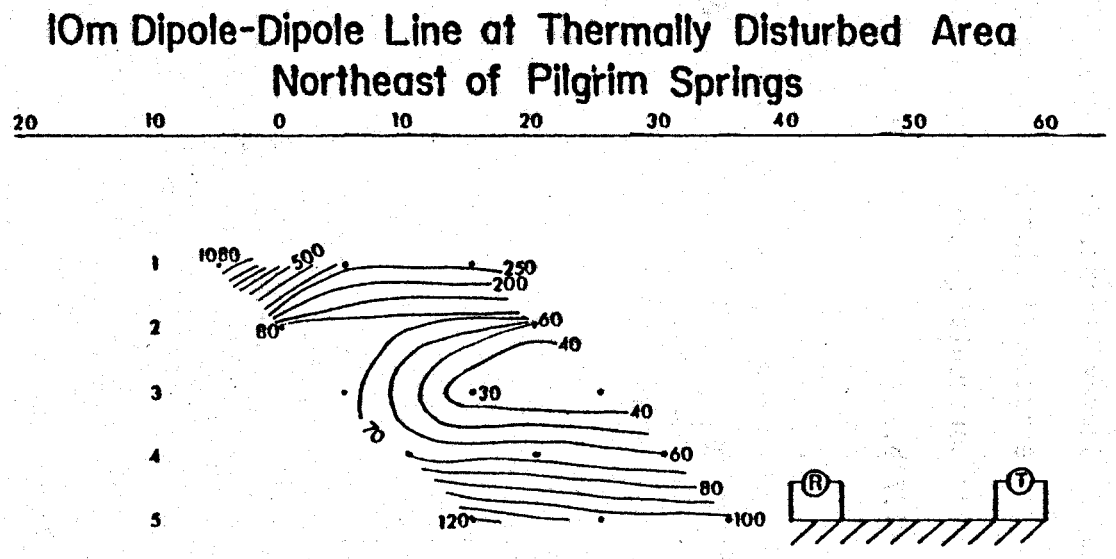

Figure 12. Pseudosection of 10 m dipole-dipole profile run NE-SW in the small thaw window NE of Pilgrim Hot Springs (Plate I).

REFERENCES

Dey, A., and H. F. Morrison, Resistivity modelling for arbitrarily shaped two dimensional structures, Engineering Geoscience and Lawrence Berkely Laboratory, University of California, 1975.

Zohdy, A. R., A computer program for the calculation of Schlumberger sounding curves by convolution, U.S. Geol. Survey Report, GD-74-010, 1974a.

Zohdy, A. R., A computer program for the automatic interpretation of Schlumberger sounding curves over horizontally stratified media, U.S. Geol. Survey Rept. GD-74-017, 1974b.

WATER AND HEAT FLOW MEASUREMENTS AND THEIR RELATIONSHIP TO POWER ESTIMATES AT PILGRIM SPRINGS, ALASKA

William Harrison and Daniel Hawkins

INTRODUCTION

To assess the power potential of a geothermal system it is important to map the temperature distribution of the area, both in plan view and in depth. It is also important to determine surface and ground water flow rates. Both types of measurements were made as part of the work described here. The procedures and results will be described below; as well as their implications for the power budget of the Pilgrim Springs area.

PROCEDURES AND RESULTS

Surface Measurements

The temperature of the hot water from the main hot springs area was determined to be 81°C and its flow rate to be 4.2×10^{-3} m^3/sec (0.15 ft^3/sec or 67 gallons/min). The uncertainty in the flow rate estimate is $\pm$ 30%. It was not feasible to measure the flow rate directly at the springs area. Instead, the flow rate of the stream draining the area was measured at the first good site about 150 m downstream, just below the confluence of a small cold water stream (Figure 1). Flow rate was determined by mapping the velocity over the stream cross profile with a small current meter. Temperature was also mapped and the average temperature

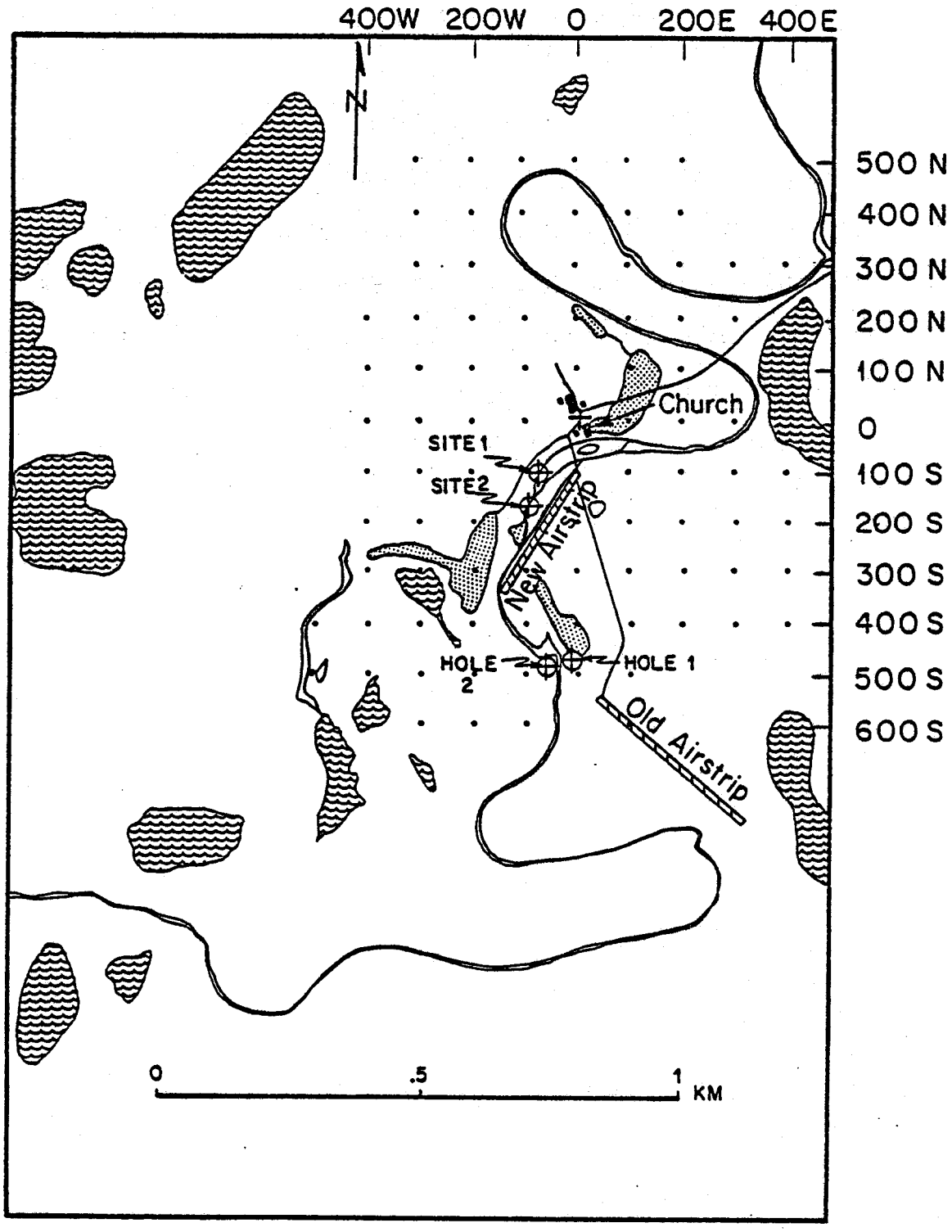

Figure 1. Stream gauging sites and hole locations. Stippled areas indicate agricultural fields. Wave patterns indicate lakes and ponds.

calculated. The average temperature of the cold stream was also determined. From this information the flow of water formerly at 81°C was calculated from the conservation of water and heat:

$$M_{HOT} + M_{COLD} = M_{COMBINED}$$

$$M_{HOT} (T_{HOT} - T_{COMBINED}) = M_{COLD} (T_{COMBINED} - T_{COLD})$$

where M stands for flow rate and T for temperature; T_{HOT} = 81°C. M_{COLD} can be eliminated and the flow of 81°C water (M_{HOT}) calculated from

$$M_{HOT} = M_{COMBINED} \frac{(T_{COMBINED} - T_{COLD})}{(T_{HOT} - T_{COLD})}$$

M_{COLD} also includes the cold water mixed in at the main hot springs area, and the most serious assumption--the one dominating the above uncertainty estimate of 30%--is that this cold water was at the same temperature as that measured in the cold stream.

The procedure was repeated at a second site about 100 m farther down stream just below the confluence of a second cold stream (Figure 1). At this site the ratio of original 81°C to cold water is less, but about the same flow rate of original 81° water was calculated, lending support to the validity of the main assumption. The measurements at this site can be interpreted in a second way, in which the hot water input at site 2 is the known output at known temperature from site 1. This over-determines the unknowns and the consistency found verifies that the approach contains no serious errors. The measurements and results are

summarized in Table 1. As the best estimate of M_{HOT}, the flow of 81°C water, we take 4.2×10^{-3} m/sec, which is slightly weighted in favor of site 1 because it is closer to the source.

The flow rate obtained is about 7 times that estimated by Waring in 1917. Neither the uncertainty of his estimate nor the possible variation of flow rate with season or surface water conditions are known. One possibility is that our value is higher because it is representative of the entire main hot springs area, but the difference could also represent a real secular change.

Borehole Measurements

Temperature, thermal conductivity and groundwater flow rate measurements were made in two holes, consisting of sections of 3/4" water pipe hand driven vertically into the ground to depths of 9 1/2 m. These were called holes 1 and 2, and their locations are shown on Figure 1. Temperatures were measured in both holes, and the results are shown in Figures 2 and 3. In both cases temperatures of roughly 80°C (176°F) are reached at 10 m, where the temperatures are still increasing. Strong convection in the water in the pipe in hole 1 caused scatter in the data, which is especially evident at 2.3 m depth. A more viscous fluid was used in hole 2, and the results are somewhat better. A damaged housing on the thermistor temperature sensor also contributed to the scatter. Calibration uncertainty could cause a systematic temperature error of about 2°C.

An attempt was made to measure the flow of ground-water perpendicular to holes 1 and 2 using a new thermal tracing technique (Harrison and Hawkins, to be published). A pair of wires is placed in the hole, and heated electrically. This heats the fluid in the hole, but with time, after the power has been turned off and the wire removed, the fluid cools off again.

TABLE 1*

	Site 1:	Site 2:	
Date:	June 19, 1979	June 19	June 23
$M_{COMBINED}$:	16.7×10^{-3} m^3/sec	21.5×10^{-3} m^3/sec	13.0×10^{-3} m^3/sec
$T_{COMBINED}$	31°	26°	36°
T_{COLD}	13°	13°	21°
T_{HOT}	81°	81°	81°
M_{HOT}	4.4×10^{-3} m^3/sec	4.1×10^{-3} m^3/sec	3.3×10^{-3} m^3/sec

*The measurement accuracy of the measured flow rate $M_{COMBINED}$ is roughly 10%. Temperatures are accurate to $\pm$ 1°C.

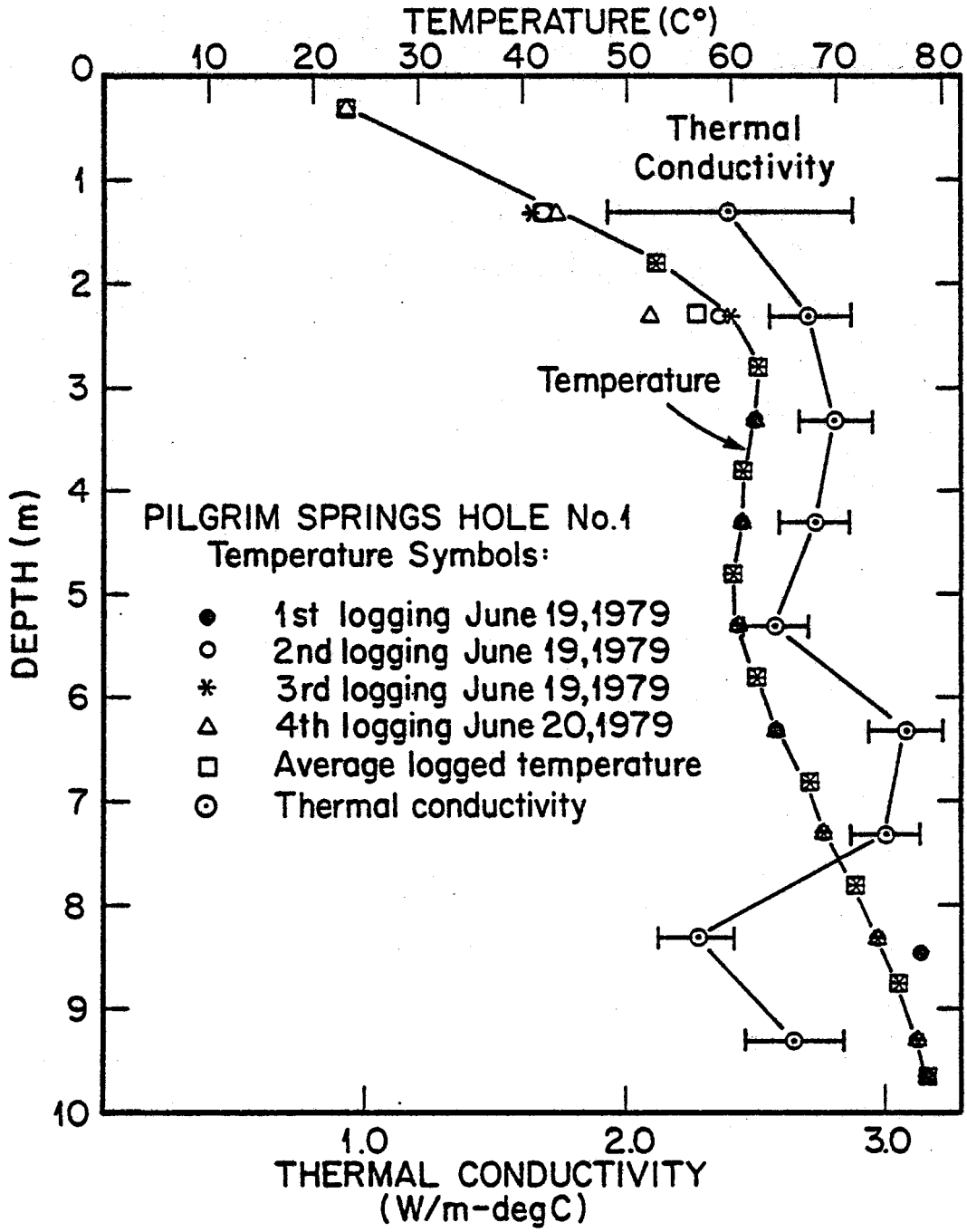

Figure 2. Dependence of temperature and thermal conductivity on depth in hole 1.

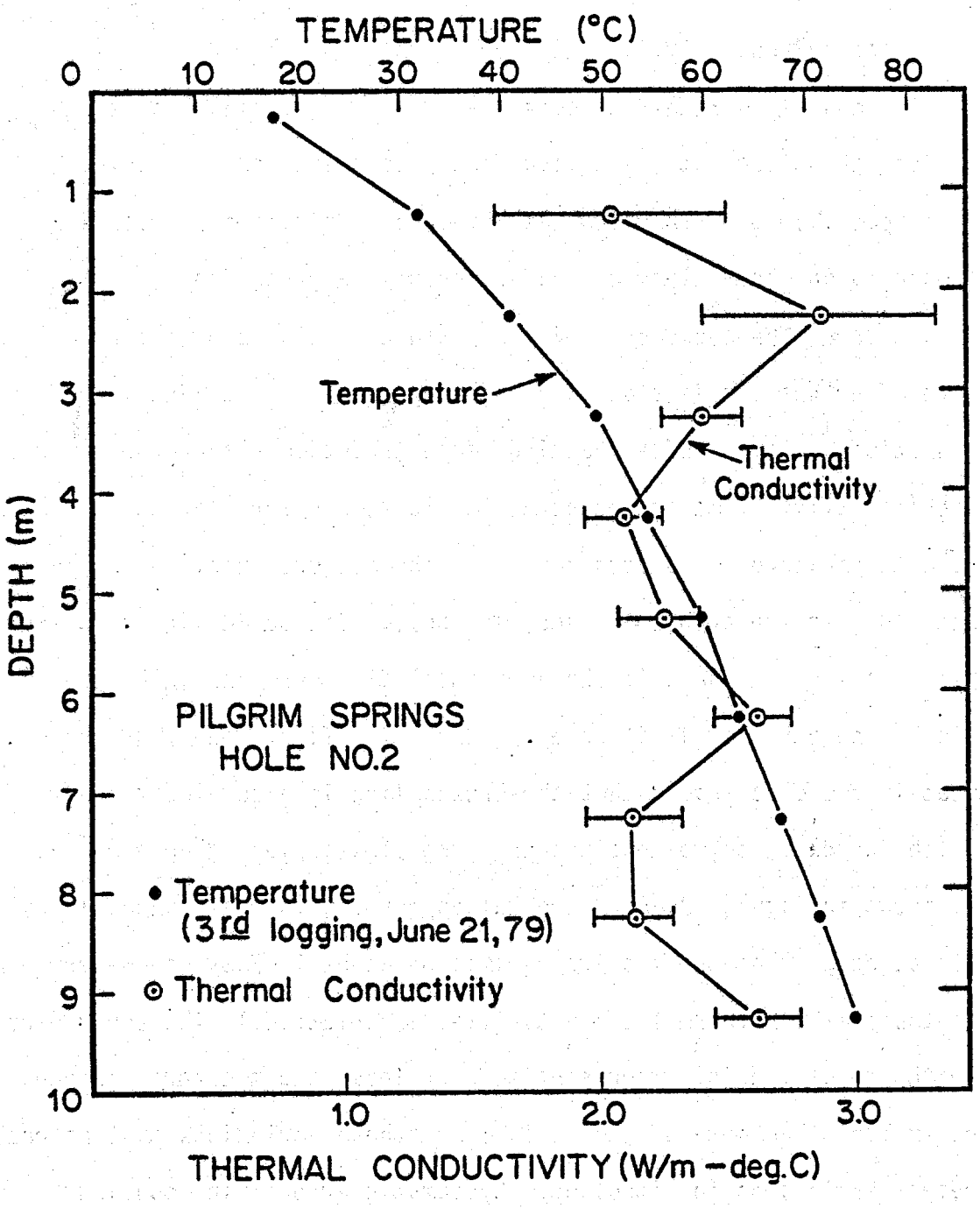

Figure 3. Dependence of temperature and thermal conductivity on depth in hole 2.

If water is flowing through the ground past the pipe, the rate of cooling will be faster because the moving water will help carry away the heat. This method was used in an attempt to measure the horizontal component of ground water motion. The technique also measures the thermal conductivity of the ground, an essential quantity in heat flow calculations.

Any horizontal flow rates at holes 1 and 2 were too small to be detected by this technique, at least given the problems discussed above. However, an upper limit to the flow was obtained. This limit varies somewhat depending upon the quality of measurements at a given depth, but it is typically 1 m/day. The approach is illustrated by the data of Figure 4. Temperature after heating is plotted vertically, and a convenient mathematical function of time t after heating began (and time s that the power was on) horizontally. Time increases to the left, and zero represents the undisturbed temperature. The dots represent the measurements, which have some scatter due to the problems discussed above. The solid line shows how the temperature should behave if the horizontal flow were zero; the broken line would be the behavior if it were 1 m/day. The first line fits the data better, but it could be argued that the broken line is also almost consistent with the data, so we conclude that the flow is less than 1 m/day.

Also shown in Figures 2 and 3 are values for the thermal conductivity. (It should be noted that the flow rate limit of about 1 m/day was determined at the depths at which thermal conductivities are plotted.) The error bars plotted with the data points represent more or less random errors. Since these are smaller than some of the variations, these variations must be real and represent variations in lithology. Systematic errors (introducing

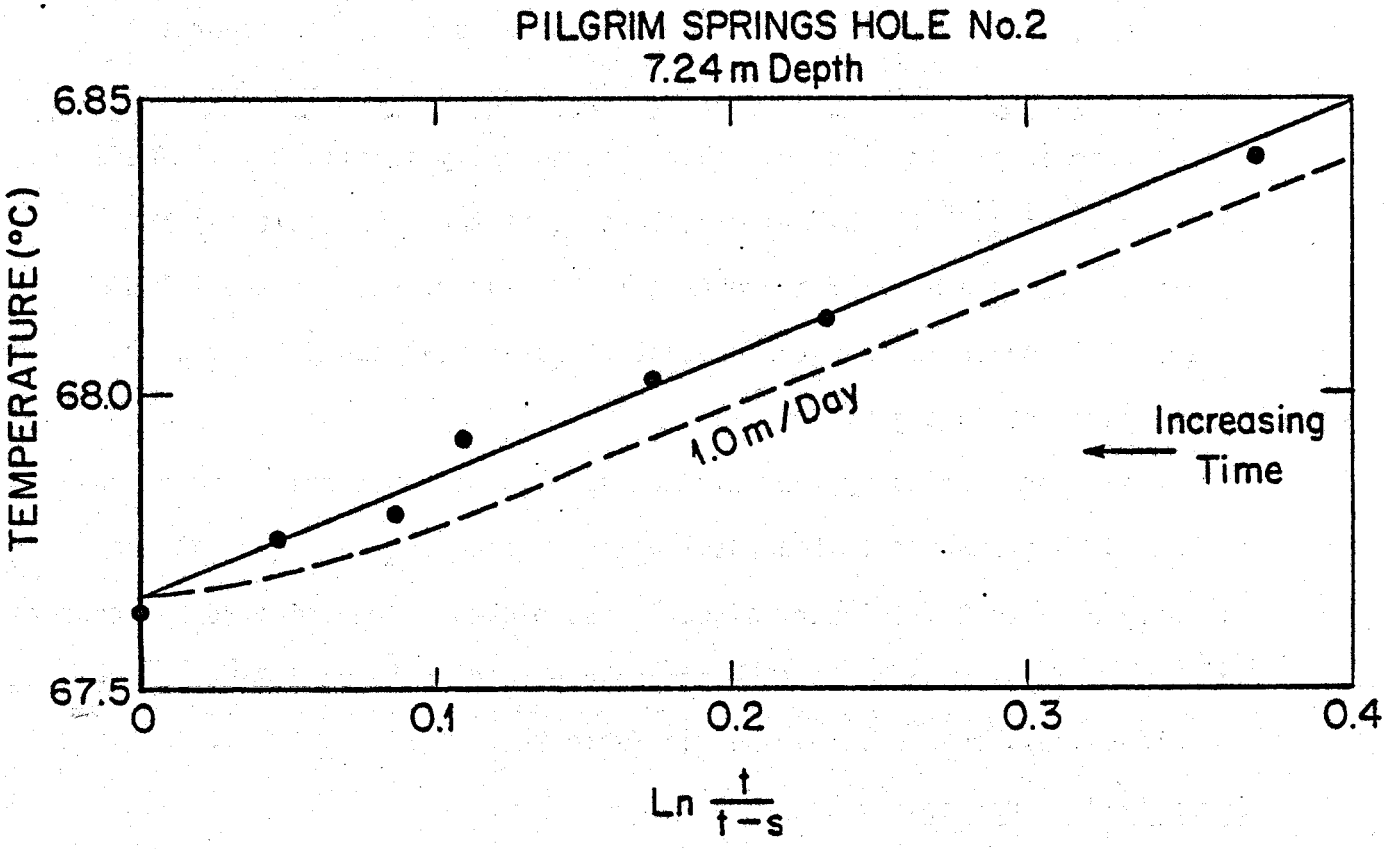

Figure 4. An example, at a particular depth (7.24 m), of hole cooling after heat was applied. The dots represent the data. The solid and broken curves are the theoretically expected cooling curves for water speeds of 0 and 1 m/day respectively.

a bias the same for all depths) are caused by uncertainty in heating power measurement, and may amount to 5 or 10% in addition to the errors plotted. The errors seem to be slightly larger in hole 2 because the "real" temperature changes (as opposed to those induced by us with our heating wire) were not as well measured.

DISCUSSION

Surface Measurements

The stream temperature and flow measurements permit an important quantity to be estimated--the power produced by surface flow from the main hot springs area. It turns out that this quantity is slightly ill-defined, but we make it definite by assuming that it is the power that can be supplied to a reservoir of approximately 0°C water, such as the Pilgrim River. This power is then the product of water heat capacity, flow rate, and temperature in deg C.

The power carried by the main hot springs 81°C water is thus calculated to be 1.4 MW (megawatt). The total power carried by the stream at the vicinity of site 2 is higher, since it has picked up heat from other sources which outweigh its losses to the atmosphere, and is about 2.2 MW.

These results are summarized in Table 2a.

Borehole Measurements

In addition to the horizontal ground water flow discussed earlier, a limit on the vertical flow can be estimated from the temperature profiles and the measured thermal conductivities. In the deeper part of hole 2 this vertical flow is less than 4 m/year; with a roughly similar value

TABLE 2a

SURFACE MEASUREMENTS

Water flow:

4.2×10^{-3} m^2/sec (67 gallons/minute) $\pm$ 30% of 81°C water from main thermal area

Heat flow:

1.5 MW (megawatts) carried by the 81°C water from main thermal area

2.2 MW carried by stream at site 2

TABLE 2b

BOREHOLE MEASUREMENTS

Water flow:

< 4 meters/year - vertical

< 1 meter/day - horizontal

Heat flow:

$\gtrsim$ 10 MW/m^2 (megawatts per square meter) - vertical

< 1000 W/m^2 - horizontal

applying for hole 1. The vertical heat flow can also be estimated, assuming it is mainly conductive. This is 12 and 9 W/m^2 for holes 1 and 2 respectively. If the flow is not completely conductive, as seems likely, these values could be somewhat larger. The horizontal component of heat flow, due to horizontal ground water motion of less than 1 m/day, would be less than 1 kW/m^2, assuming again that this goes to heating a large source of 0° water, such as in the Pilgrim River. These results are summarized in Table 2b.

The heat flow values are quite similar at both holes. If the vertical heat flow estimate were representative of the entire thermal area of roughly 1 square kilometer, the total vertical heat flow would be roughly 10 MW (megawatts). 10 MW is therefore the crudest order of magnitude estimate for the total thermal power currently being produced naturally at the surface of the area, and is roughly 4 times that carried by the stream at site 2.

Power Budget

10 MW is probably not a serious overestimate for the total surface heat flow because it is the same order of magnitude as the power carried off by the surface streams. However, it could well be a serious underestimate because it does not include the power carried off by groundwater. The main purpose of the boreholes was to estimate this power, but it is important to point out that at only 9.5 m they were too shallow to be likely to intercept any important aquifers. In fact, the groundwater component of the power budget appears to be very large (possibly greater than 300 MW), given the surface water power estimate from this work, and the Pilgrim River water temperature measurements discussed by Osterkamp and others in a subsequent section of this report.

ACKNOWLEDGEMENT

This work was partially supported by NSF grant number DPP-7728451.

REFERENCES

Harrison, W. and D. Hawkins, 1979, Hydrology Measurements at Pilgrim Hot Springs, 30th Alaska Science Conference, Sept. 19-21, 1979.

A RECONNAISSANCE STUDY OF THE HYDROTHERMAL CHARACTERISTICS AND ACCESSIBLE POWER OF PILGRIM SPRINGS, ALASKA

Thomas Osterkamp, Joan Gosink, Robert Forbes, Richard Gaffi, Janet Hanscom, Martha Kane, Camille Stephens and Jeff Kline[1]

INTRODUCTION

Pilgrim Springs is located in an area of thawed ground ≈ 1 1/2 km^2 in size bordered on the north by the Pilgrim River. The continuous permafrost in the general area is probably on the order of 100 m in thickness, judging from wells located at Nome and Kotzebue, and from electrical resistivity sounding measurements (Wescott et al., this report). The surface discharge of Pilgrim Springs appears to be ≈ 4 x 10^{-3} m^3 s^{-1} (Harrison and Hawkins, this report) at a temperature of 81°C. There are no apparent steam vents, geysers or other discharges present. As such, it is a pool-type hydrothermal system probably consisting of a heat source, heat sinks, recharge system, recirculation system and discharge system components. The purpose of this investigation was to carry out a reconnaissance study of these components. These data are to be combined with that of other geophysical and geological studies to serve as a guide for further studies and particularly for defining future drilling programs designed to evaluate the potential of Pilgrim Springs as a geothermal energy source.

The measurements reported here include soil temperature, apparent electrical conductivity of the soil-water system, electrical conductivity of groundwater samples and water samples from the Pilgrim River, saturated

[1]Alaska Division of Geological and Geophysical Surveys

hydraulic conductivity of the soil and groundwater flow characteristics (direction and velocity). Most of the measurements were performed on a grid consisting of NS (north-south) and EW (east-west) baselines as shown in Figure 1 with the origin at the basketball backboard pole in front of the old Catholic Church. Eleven EW lines were surveyed at 100 m intervals along the NS baseline; 4 to the N and 6 to the S. Two additional lines were investigated; line A from the above grid origin along a farm trail to the Pilgrim River and line B from 100S (100 m south of the origin) proceeding SSW down the middle of the new airstrip. A few conductivity measurements were made in permafrost terrain near 500E,400S (500 m east and 400 m south of the origin) and temperature profiles were also measured at a site ≈ 4 km NNE of Pilgrim Springs where some vegetative changes indicated warmer than normal ground.

TEMPERATURE MEASUREMENTS

Hydrothermal circulation of hot water in permafrost terrain produces thawed ground. The thawed area at Pilgrim Springs may be somewhat larger than the area outlined in Figure 1, which represents the area with the greatest disturbance (≈ 1 1/2 km^2), as estimated from changes in vegetation on an aerial photograph. Generally, there are large variations in the hydrological and thermal regimes within a hydrothermal system which are related to the underlying sources. Commercial development of these sources requires determination of their position, geometry, strength and internal flow characteristics. Soil temperature measurements are required as a first step in delineating these sources. A temperature survey of the shallow

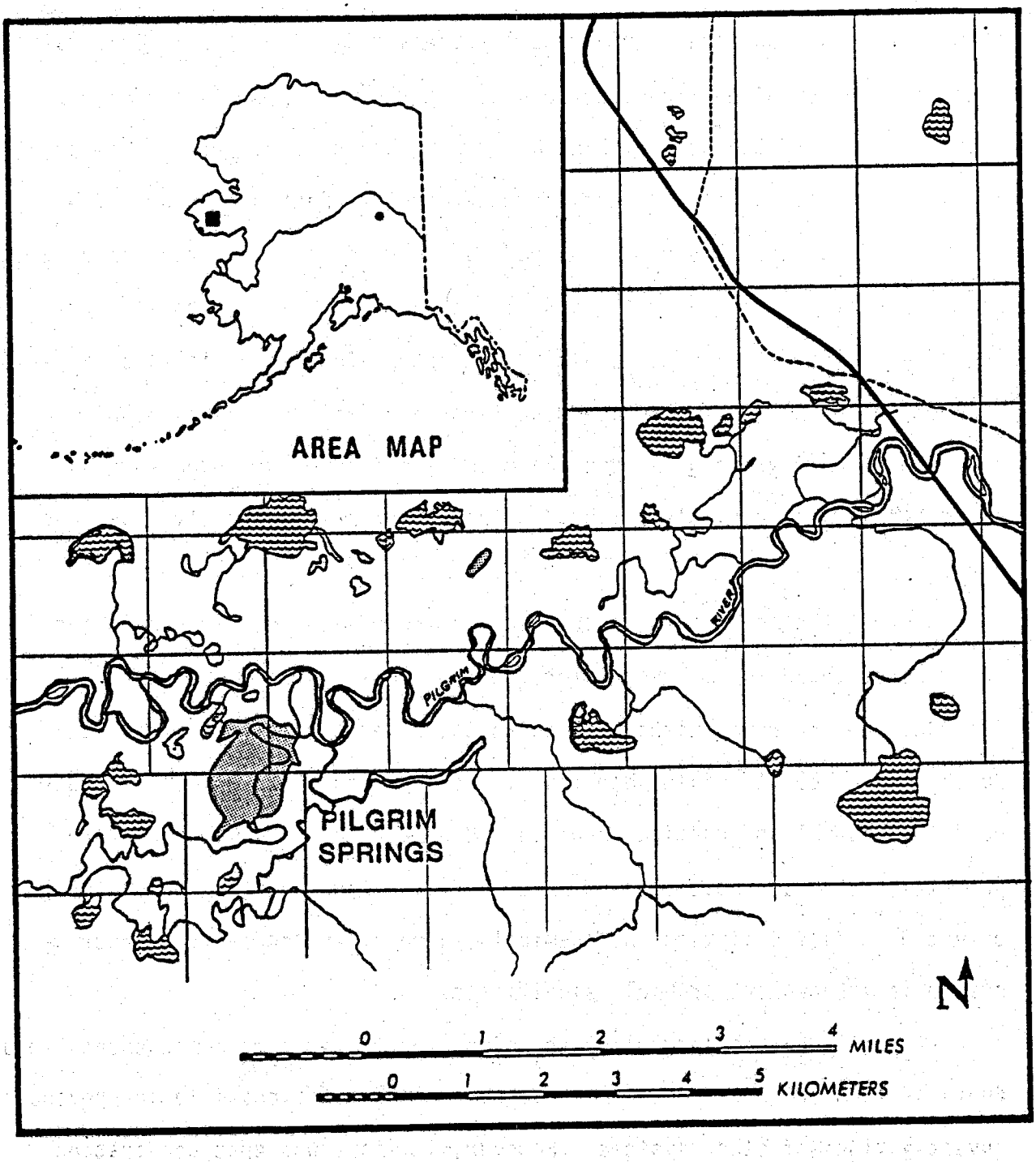

Figure 1. Map showing the Pilgrim Springs area, Pilgrim River and the Nome-Taylor Highway. The shaded area around Pilgrim Springs is the thawed area estimated from vegetative changes on an aerial photograph. The second, smaller thaw window about 3.2 km northeast of Pilgrim Springs is also shown.

near-surface (within 10 m) thermal regime of the more promising sites in the thawed area was conducted during the latter part of June, 1979. Temperature profiles were obtained from measurements made inside 1/2" diameter iron pipes driven into the soil by hand or by a mechanical driver. The temperatures were measured with a thermistor thermometer with an accuracy of N 1/2°C. Most of the measurements were made, periodically, at the tip of the pipe while it was driven into the soil. In a few cases, the pipes were logged after being driven to their total depth. Convection in these air-filled pipes was a problem which was overcome by filling the pipes with engine oil. A few profiles were measured with a much more precise wheatstone bridge and specially calibrated thermistor probe assembly on a long cable.

Most of the thawed ground area in the study site was flooded during break-up of the Pilgrim River prior to the time we arrived at the site. Although the river was within its banks there were still some wet areas during mid-June. It would seem that flooding by cold water would affect both the thermal and chemical regimes. However, only a few temperature profiles showed an indication of water infiltration into the soil. The effect of this flooding on the chemical regime of the soil-groundwater system is unknown but probably significant.

Attempts were made to place the pipes for temperature measurements to a depth of 10 m or more, since this had been found to be possible in previous investigations of other systems. However, it was found that penetration became increasingly difficult below 5 m and impossible below 10 m. This difficulty was attributed to changes in soil properties and was verified during subsequent drilling by the State of Alaska.

The distribution of temperatures at the 4 1/2 m depth was derived from about 70 temperature profiles and is shown in Figure 2. Generally, the lowest temperatures were found in the NW quadrant and the highest in the SW quadrant. Figure 2 shows 6 areas within the thawed region with 4 1/2 m temperatures > 50°C. Only the pool area near 30W,30S, had a flow of hot water to the surface. There are distinct differences in the size of these hot areas with the upper three about 500 m^2, the lower two about 10,000 m^2 and the far left area about 60,000 m^2. The lowest temperatures at the 4 1/2 m depth ranged near +10°C in the NW quadrant and the highest temperature, 96°C, was recorded in the SW quadrant at 276W,276S in an air filled pipe and changed to 87°C when the pipe was filled with oil at a later time.

The temperature profiles generally show increasing temperatures with depth, near the ground surface (within 1-2 m). At greater depths the thermal behavior was very complex, as shown in the four temperature profiles in Figure 3. The two profiles from 200W,100N and 420W,500S are outside of any of the 6 hot areas. The profile from 324W,276S is similar to other profiles just outside the hottest area and the profile from 124E,185S is on the edge of one of the hot areas. This last profile shows a gradient reversal which seems to indicate a lateral influx of hot groundwater above the 5 m depth, probably in a westerly direction away from the hot area. These temperature gradient reversals, zero gradients and large temperature variations over small depths are characteristic of areas where hot water from deeper sources is in convective motion toward the surface where it spreads laterally while mixing with cooler groundwater.

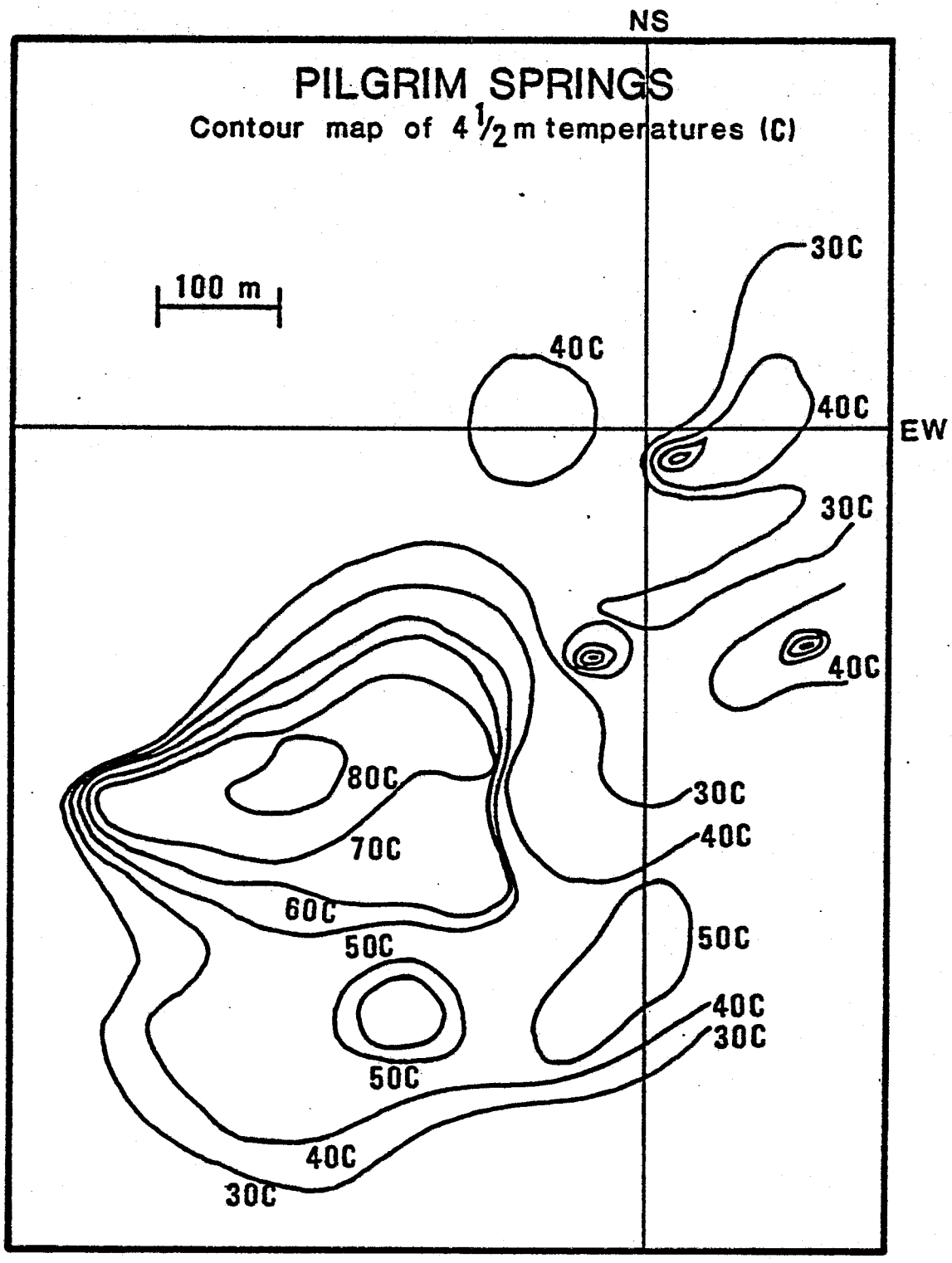

Figure 2. Contour map of ground temperature isotherms at 4 1/2 m depth. The numbers on the isotherms are temperatures in degrees Celsius.

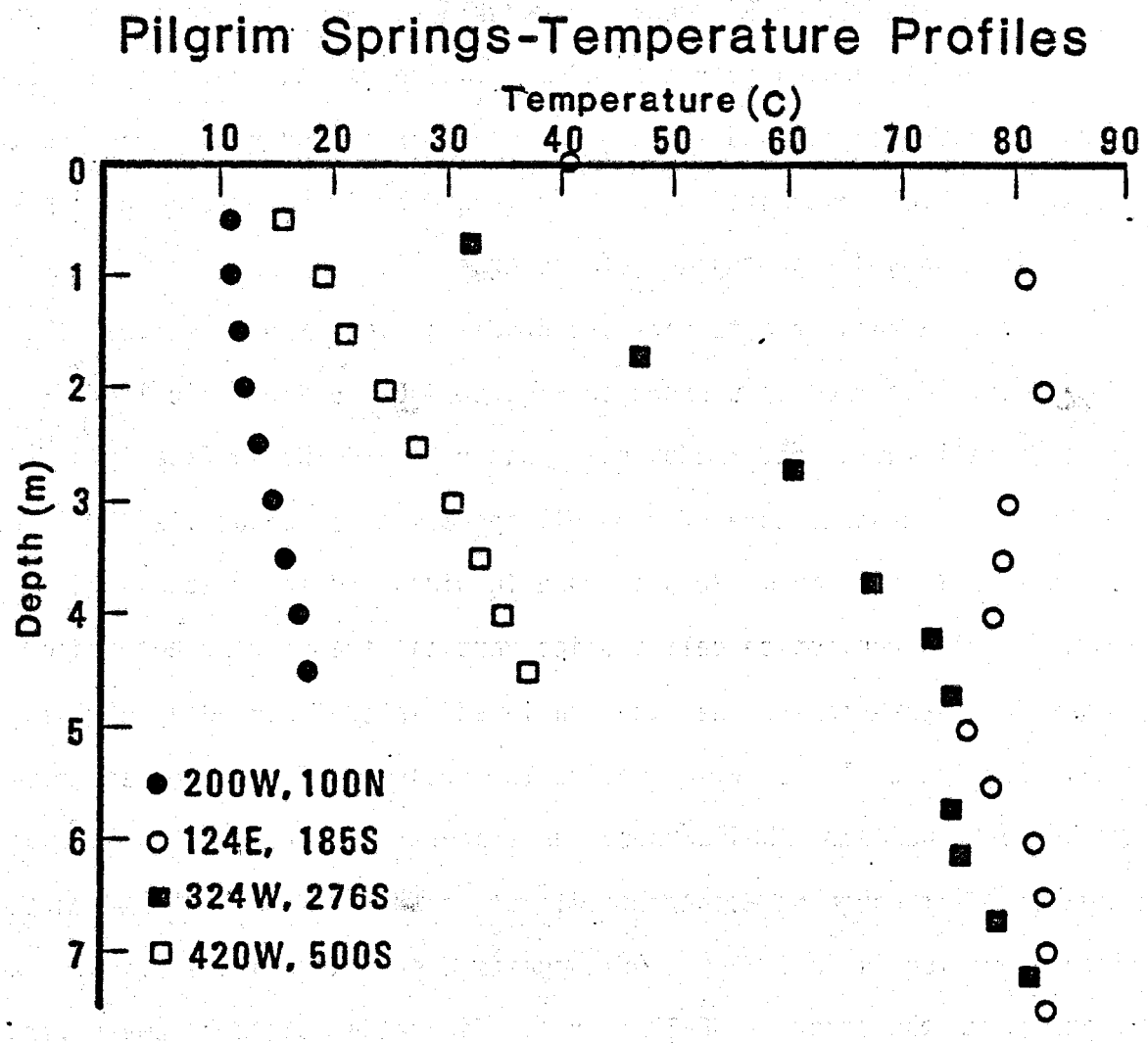

Figure 3. Some temperature profiles illustrating the complex thermal behavior of the Pilgrim Springs system.

Eight temperature holes were driven along the center of the new airstrip at a spacing of 20 m and Figure 4 shows the subsurface isothermal lines along this profile. There is a significant and well-defined heat source roughly between the 50 m and 130 m positions. At the 100 m position the temperature at the 5 m depth exceeds 75°C. A winter photograph shows bare, snow-free ground near the 100 m position and the vegetation there consisted of a sparse and short grass cover in a band running across the airstrip; which contrasted with the surrounding lush vegetation. This band is visible on a U-2 photograph of the area.

Figure 5 shows the temperature profiles along the airstrip. The temperature distributions shown in Figures 4 and 5 are typical of a convective cell moving hot and/or salty water toward the surface from a deeper source. The central core of the cell appears to be about 10-20 m in width and the whole cell about 80 m or more in width and somewhat asymmetric. The presence of a convection cell implies vertical transfer of hot and/or salty water from depth toward the water table and lateral spreading of this water away from the cell. It also implies the presence of a source and possible recharge mechanisms. While these temperature data are limited in depth, Figure 5, a through h, appears to illustrate these features. A tentative interpretation is that Figure 5f suggests a strong upward vertical water transfer on the order of 40-50 m yr^{-1}. Figure 5e suggests upward vertical water transfer on the order of 10 m yr^{-1}. Figures 5d and 5g suggest strong vertical transfer below the 3 1/2 m depth changing to lateral transfer or possibly combined lateral and vertical transfer over the 2-3 m depth. Conductive heat transfer occurs at the 20 m and 40 m positions as shown in

PILGRIM SPRINGS

Isotherms in a vertical section under the new airstrip

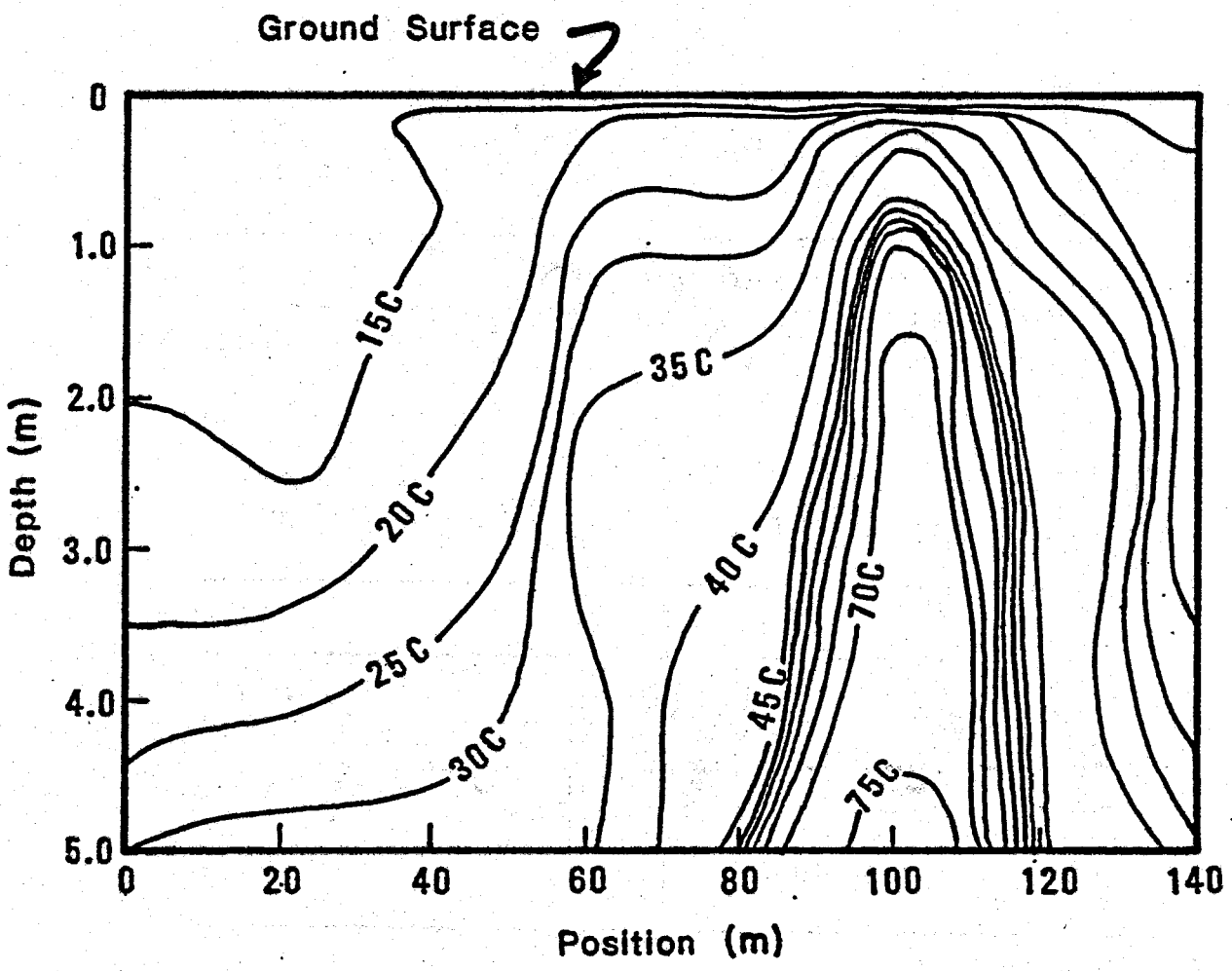

Figure 4. Contour map of the isotherms in a vertical section under the new airstrip. The zero position is at 00,100S. A convection cell appears to exist between the 50 m and 130 m positions.

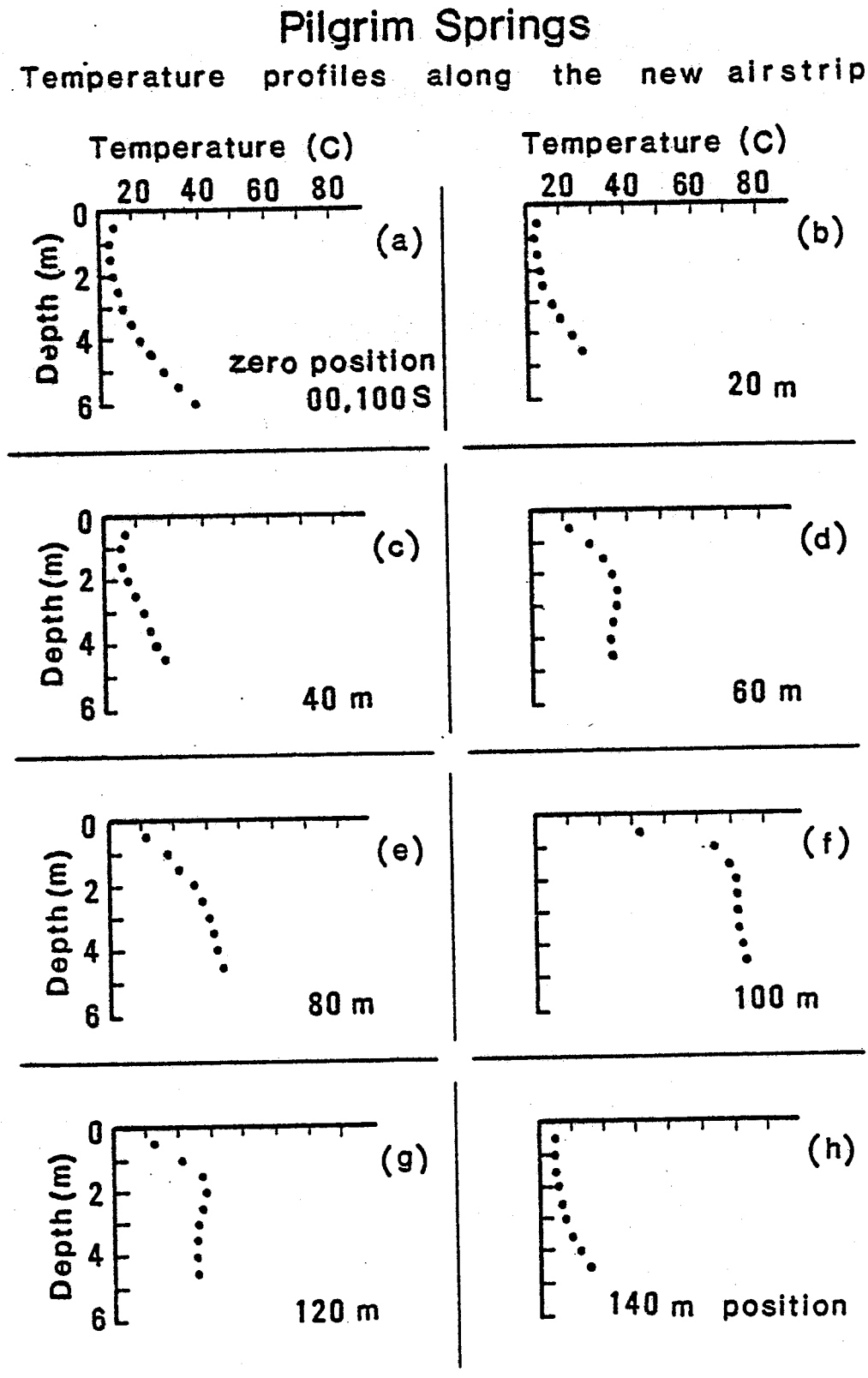

Figure 5. Temperature profiles along the new airstrip.

Figures 5b and 5c. Vertical infiltration of colder surface water into the soil at a velocity of ≈ 5 m yr^{-1} is illustrated in Figures 5a and 5h which suggests the presence of a near surface recharge mechanism (possibly flooding) for this convection cell. We would feel more comfortable with the above interpretation with deeper temperature measurements; however, it appears to be internally consistent and is also supported by the electrical conductivity data. Additional details of the interpretation are given in the hydrology section and a more complete analysis will be given in a subsequent report.

Other temperature profiles (24 total) also show evidence of convection cells and/or groundwater motion. Unfortunately these data are too sparse to have detected all the cells in the thawed area or to define cells as was done in the case of the cell along line B. Considering the size of the cell along line B and the spacing of our temperature grid survey it appears that many cells were not detected. This conclusion is supported by the shallow electrical conductivity measurements.

We also furnished temperature measuring apparatus and instructions to the Alaska Division of Geological and Geophysical Surveys (Mr. J. Kline), for the purpose of obtaining temperature measurements in two holes drilled during October and November 1979, at Pilgrim Springs. The first hole (PS-1-H) was drilled at 150W,200S to a depth of 49 m. Its position was decided on the basis of our temperature grid survey (Fig. 2). The second hole (PS-2-H) was drilled at 207W,258S to a depth of 46 m. Interpretation of the measured temperature profiles in these holes must be considered tentative since the holes had not equilibrated at the time the measurements were made. Also, the majority of the temperature data and drilling data are not available at this time.

PS-1-H flowed 90°C water at 200 gallons per minute (Kline, et al., this report) and the measured temperature profile suggests that this water probably came primarily from a layer centered about the 16-18 m depth and possibly from layers near the 28 m and 46 m depths. PS-2-H also flowed 90°C water, but at between 300 to 400 gpm (Kline, et al., this report), and the temperature profile suggests that this water probably came from layers near the 26 m and 39 m depths. The preliminary drilling logs suggest a layer of increased density and silica cementation in both holes near the 10 m depth (top of seismic layer 2, profiles B-B' and D-D', Kienle, et al., this report) which accounts for our difficulty in driving pipe to depths ≥ 10 m for the temperature grid survey. We are awaiting additional temperature data and drilling information to carry out a more detailed analysis.

ELECTRICAL CONDUCTIVITY MEASUREMENTS

The electrical conductivity of unfrozen soils depends primarily on the soil type, moisture content, temperature and purity of the groundwater. Purity refers to the amount of dissolved ions in the groundwater which can be characterized in a general way by its electrical conductivity. In a given type of saturated soil, the temperature and electrical conductivity of the groundwater determine the bulk electrical conductivity of the soil-water system. Conductivity increases with temperature and with increasing salt concentration so that a saturated soil with hot and/or salty water in the pores may be expected to have a higher conductivity than soils with cooler and/or less salty pore water. Therefore, it is reasonable to expect that *in situ* measurements of the electrical conductivity of a soil-water system would show that areas of hot and/or salty groundwater would have

corresponding high values of conductivity. Accordingly, a conductivity survey was carried out to try to detect these hot and/or salty areas. While deep conductivity measurements have been used to investigate hydrothermal systems, to our knowledge, this is the first time that shallow electrical conductivity measurements have been used to locate and define hot and/or salty groundwater sources near the ground surface (within 10 m).

These conductivity measurements were made with a magnetic induction (MI) method, a non-contact measurement. A magnetic dipole transmitter generates a primary field which induces eddy currents in the earth. These currents produce a secondary magnetic field detected by the receiver coil. The magnetic coupling between the primary and secondary fields is related to the earth conductivity. The instrument used for these studies was operated with the coils in the horizontal or vertical coplanar orientations at a height of ≈ 1 m above the ground surface. It senses the bulk apparent electrical conductivity of the soil-water system to an effective depth of ≈ 6 m in the horizontal coplanar coil orientation (σ_H) and ≈ 3 m in the vertical coplanar coil orientation (σ_V). Measurements were made at intervals of 10 m along the EW lines, NS baseline, line A, line B, and near 500E,400S. These data (≈ 2000 measurements) are summarized in the contour maps in Figures 6 and 7. Figure 6 shows the isoconductivity lines for σ_H and Figure 7 the isoconductivity lines for σ_V.

Since these conductivity measurements are a new technique for detecting hot and/or salty groundwater sources they should be compared to the temperature measurements to evaluate their usefulness and limitations. However, the conductivity measurements represent an averaging over the depth of penetration with the layers closer to the surface weighted more than underlying layers, and it is not totally clear what temperature function of

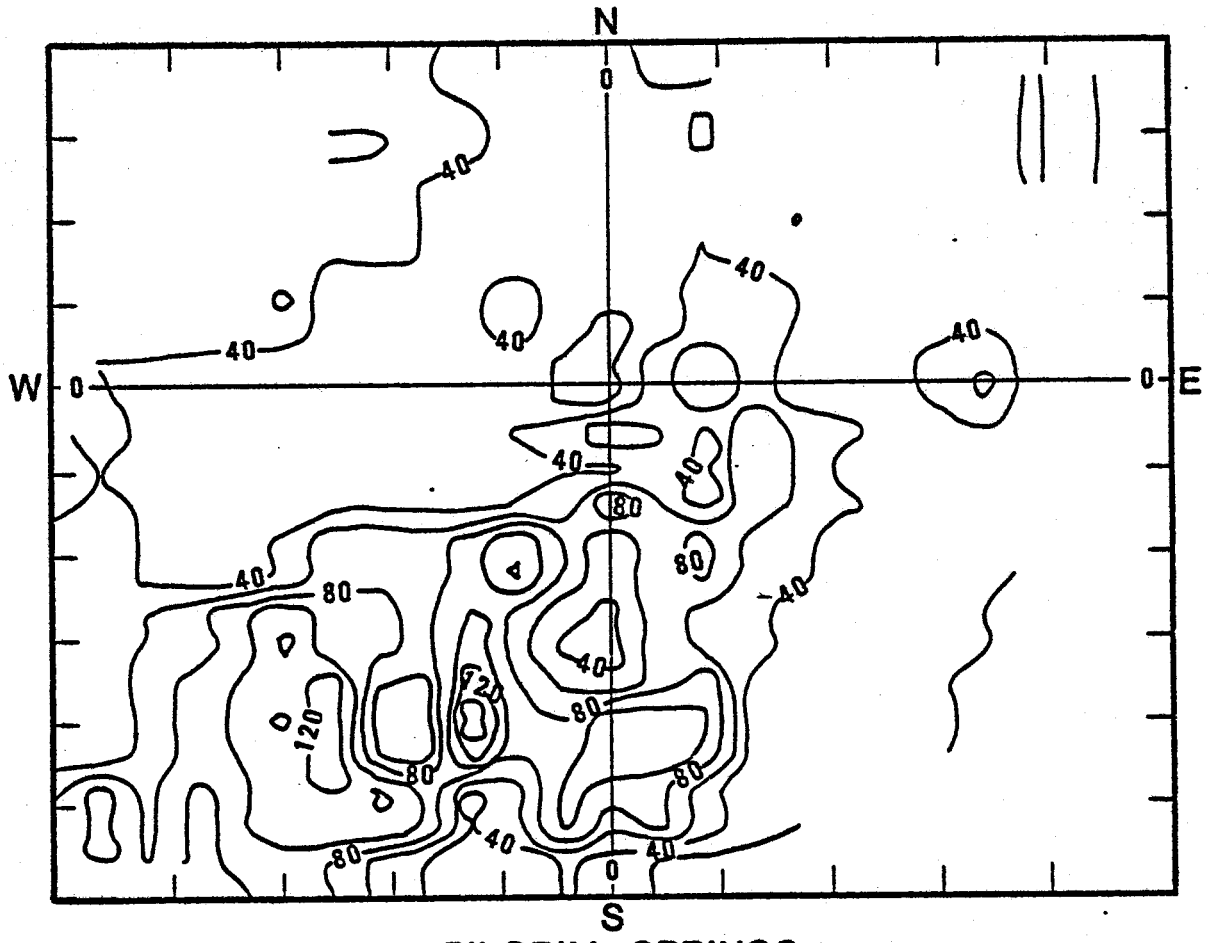

PILGRIM SPRINGS
Contour map of isoconductivity (mS-m^{-1}) lines for σ_H

Figure 6. Contour map of the isoconductivity lines at Pilgrim Springs for magnetic induction measurements with the horizontal coplanar coil configuration. The numbers have units of mS-m^{-1}.

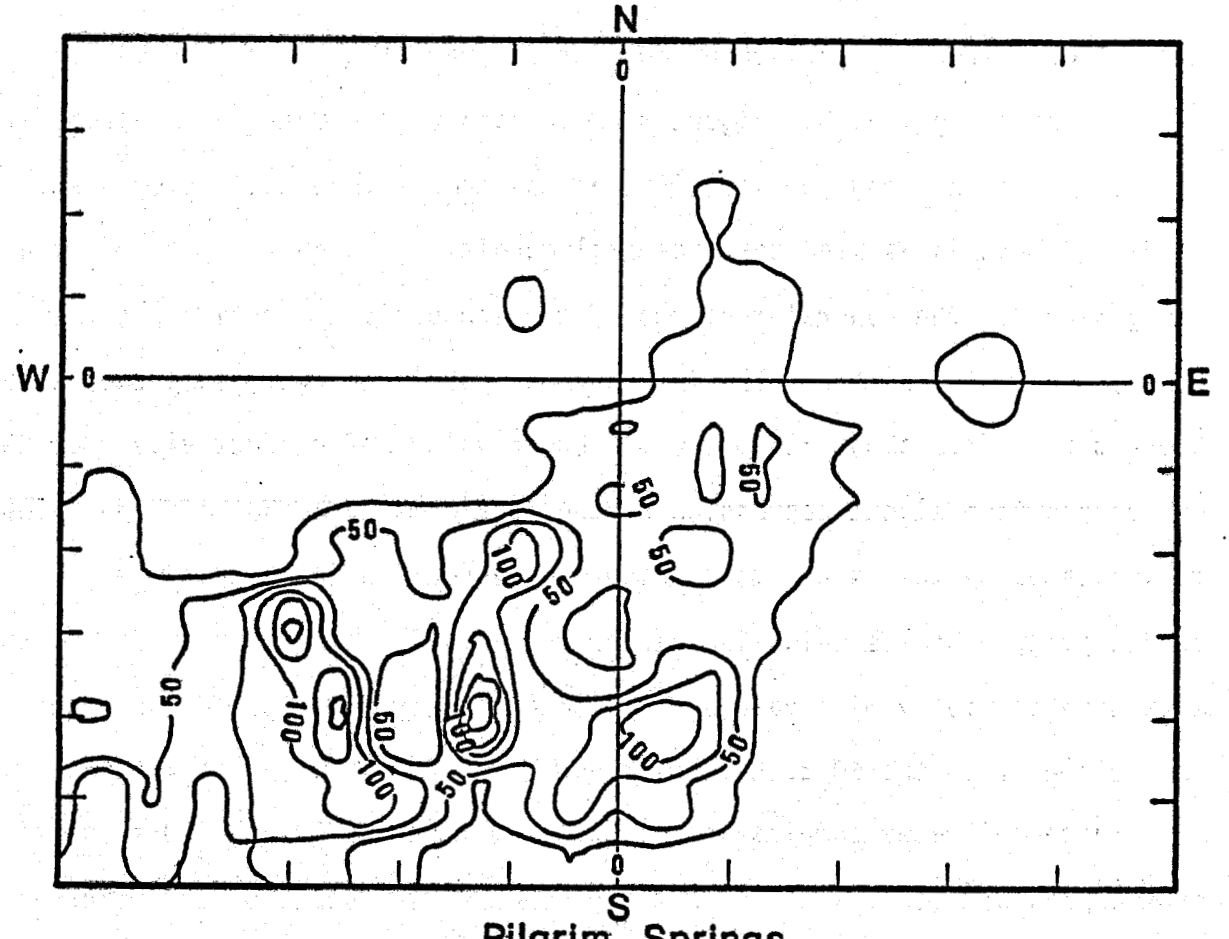

Pilgrim Springs

Contour map of isoconductivity ($mS\text{-}m^{-1}$) lines for σ_v

Figure 7. Contour map of the isoconductivity lines at Pilgrim Springs for magnetic induction measurements with the vertical coplanar coil configuration. The numbers have units of $mS\text{-}m^{-1}$.

a temperature profile should be used for comparison. The plotted contours of the conductivity data (Fig. 6 and 7) show that the high conductivity areas (i.e., hotter and/or saltier water) are primarily in the SW quadrant of the grid which is in general agreement with the contoured isotherms in Fig. 2. It should be remembered in comparing conductivity and temperature data that the density of measurements for the conductivity data is about 30 times that of the temperature data.

A more direct comparison of conductivity and temperature measurements can be made along line B. Figure 8 is a graph of the measured conductivity values σ_H and σ_V along the same line as the temperature measurements shown in Fig. 4. It is assumed that the soil conditions do not vary significantly along line B. The general features of the conductivity profiles and the isotherms are the same. There is a sharper peak near 100 m superimposed on a broad peak from about 50 to 130 m. Lower values of conductivity near 80 m correspond to a slight depression of the isotherms. The hot area near 100 m, indicated by the isotherms in Figure 4, appears as a peak in the conductivity profiles which is sharper for σ_V. The conductivity data also show some asymmetry with values decreasing rapidly from 120 to 140 m but much slower from the 60 to 0 m positions.

Three soilwater samples were taken from the 40, 100 and 140 m positions from depths between 1 and 2 m in the ground. These samples were returned to the laboratory for determination of their electrical conductivity. Values of 1.05, 1.12 and 0.765 S m^{-1} (0.95, 0.89 and 1.31 Ω-m) were measured at 25°C for the above respective positions. The latter value at the 140 m position is somewhat lower which may have contributed to the rapid decrease in conductivity at that end of the profile.

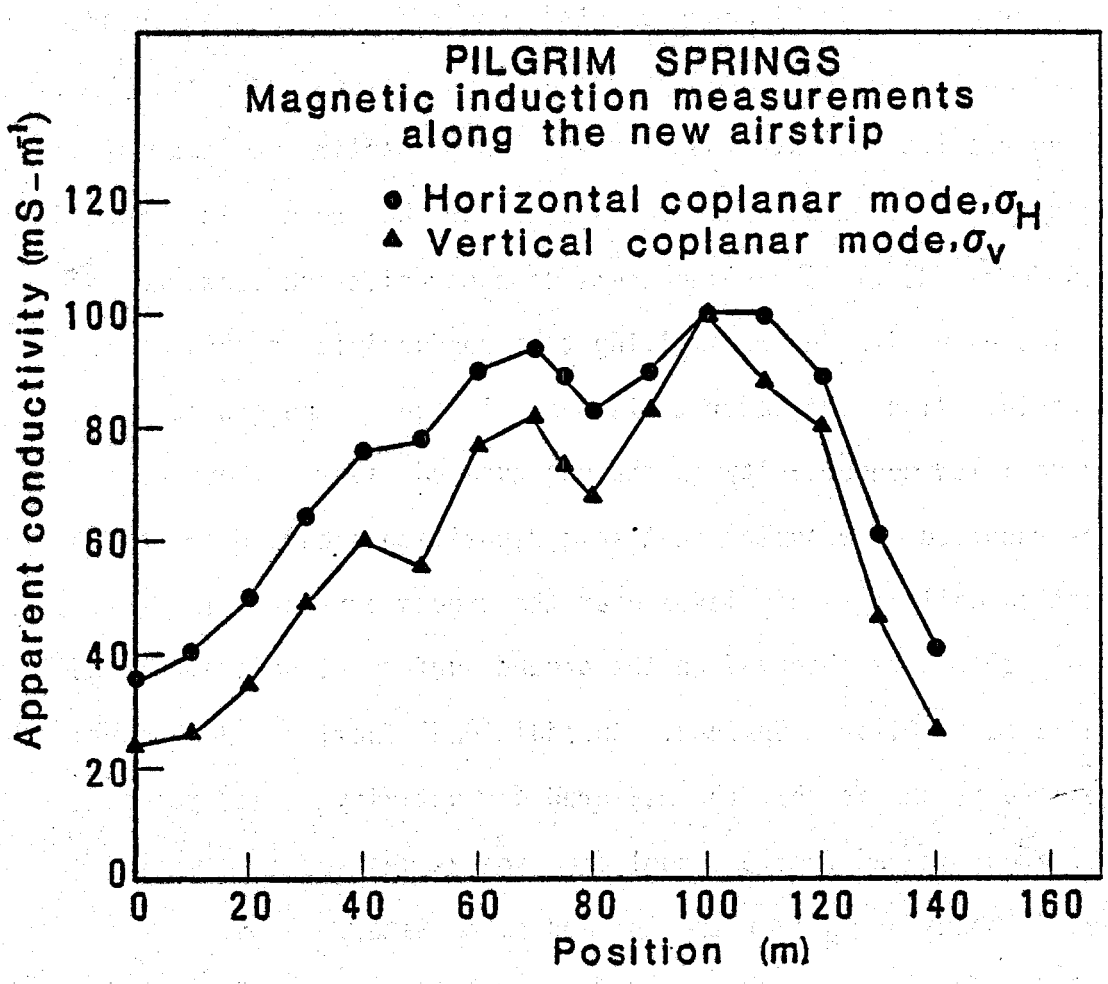

Figure 8. Magnetic induction measurements along the new airstrip.

A direct comparison of conductivity (or equivalently, resistivity) and temperature measurements along the same profile is shown in Figure 9, taken from a recent geophysical survey of the Chena Hot Springs area, Alaska (Osterkamp, et al., 1979). This figure demonstrates an excellent inverse correlation between ground resistivity and temperature.

Much more detailed information can be obtained by modeling the response of a layered earth to MI measurements. Layer thicknesses and conductivities can be adjusted to reproduce the measured values of conductivity. Our modeling results indicate that, at the 100 m position, a layer of very high conductivity soil exists near the surface of the ground with decreasing values downward. This finding seems to contradict the measured temperatures which increase with depth, implying that conductivities should also increase with depth. Also, the water table was ≈ 1 m below the ground surface implying a low conductivity in the unsaturated layer. These contradictions can be resolved by assuming that salt deposition occurs over the core of the convection cell in a thin layer near the ground surface. In fact, apparent salt deposits were observed on the ground surface at several places in the thawed area at Pilgrim Springs. An additional fact, which supports the above assumption, is that the measured conductivity values peaked sharply over the hot stream from the pool area and values for σ_V equalled or exceeded those for σ_H over the hot and salty water.

Our interpretation of the temperature and conductivity measurements along line B is that a convection cell brings hot and salty water to the surface in a plume near the 100 m position. Salt deposits occur near the ground surface over the plume, increasing the conductivity of the surface layer, which causes σ_V values to approach σ_H values. The underlying hot and

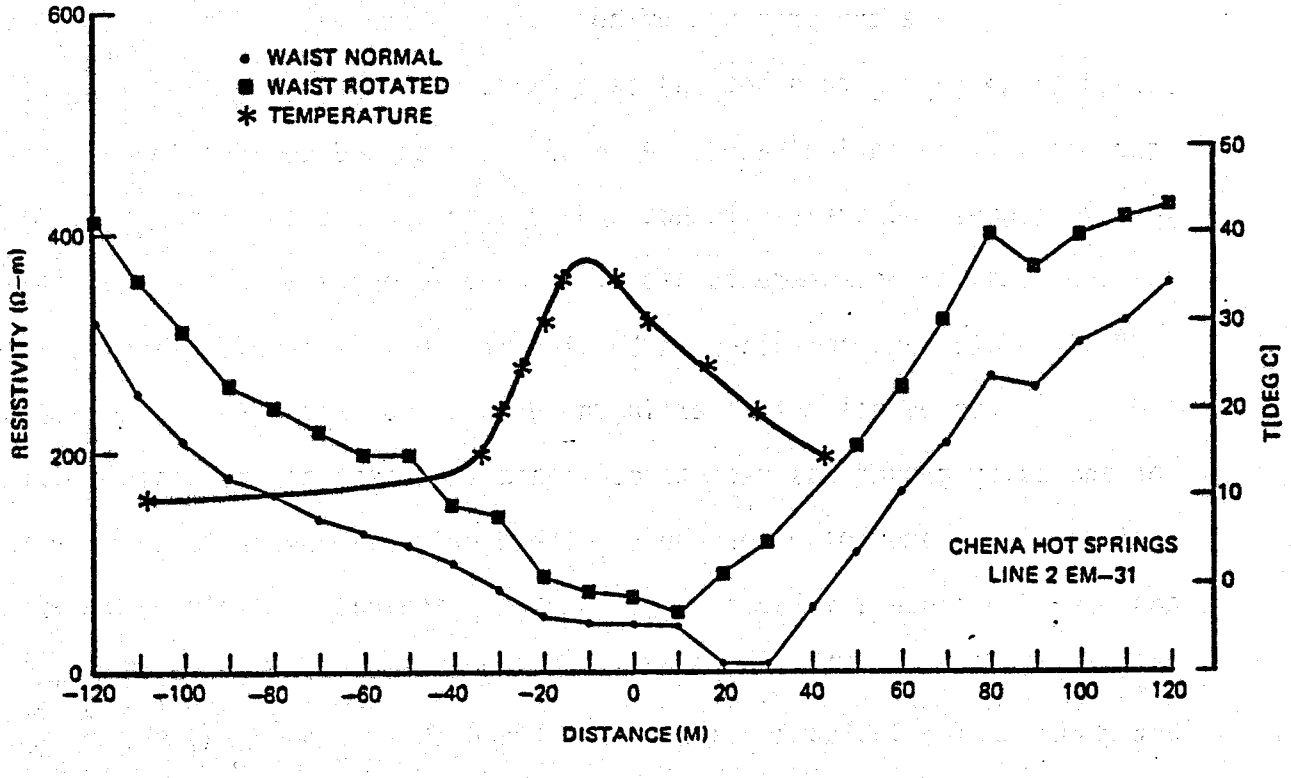

Figure 9. Comparison of magnetic induction and ground temperature measurements along the same profile at Chena Hot Springs, Alaska (Osterkamp, et al., 1979). Note excellent inverse correlation between MI and temperature data.

salty water in the soil produces peaks in both values and the asymmetry in the data implies that the ground water flow is asymmetric and primarily toward the N or NE.

These measurements and their interpretation suggest the use of conductivity measurements by the MI method to detect hot and/or salty areas near the ground surface in a hydrothermal system. Conductivity values substantially larger than background (roughly 15-40 mS-m^{-1} at Pilgrim Springs) indicate the presence of hot water. When values for σ_V equal or exceed those for σ_H then hot and salty water with probable salt deposition near the surface is indicated. Precise location and delineation of convective plumes and areas with hot groundwater appears to be possible from the conductivity measurements alone. Figure 10 shows an example of conductivity data obtained along an EW line at 400S. The criteria that $\sigma_H \geq$ 100 mS m^{-1} represents hot water in the ground and that $\sigma_V \geq \sigma_H$ represents hot and salty ground was used to delineate the position of possible convective plumes and hot water areas. These criteria appear to be somewhat conservative since a value of $\sigma_H \simeq 80$ mS m^{-1} indicates fairly warm ground ($\simeq$ 25°C at the 3 m depth) along line B. Using the above criteria, 5 areas of hot ground which includes 2 areas of hot and salty ground and the hot stream are found along the 400S line in Fig. 10. When these criteria are applied to all the conductivity data, 13 areas of hot ground and 7 areas of hot and salty ground were found <u>in addition</u> to those indicated in the temperature data of Figure 2. Using $\sigma_H \geq 80$ mS m^{-1} adds only a few more areas to the above total. It is not possible to determine the exact location and geometry of the convective plumes from our conductivity data without a more closely spaced grid survey of conductivity values; since there is no way to determine whether our present survey lines have passed directly over a plume

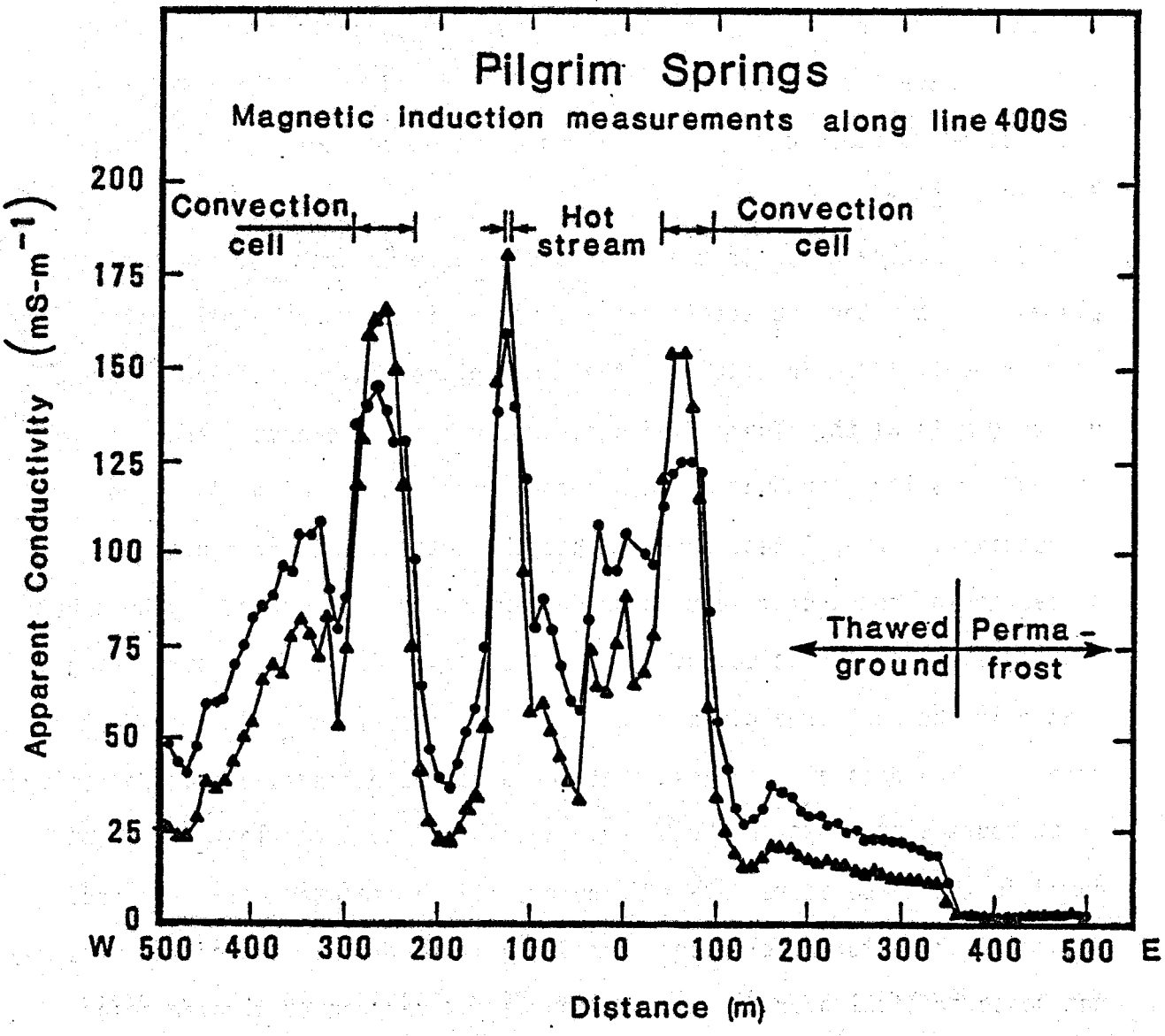

Figure 10. Magnetic induction measurements along line 400S which show what appear to be convection cells, the hot stream, hot ground and the boundary between thawed ground and permafrost.

or along the edge of one. However, a rough idea of the size of these hot and/or salty groundwater areas can be obtained by examining the width of disturbed ground in the more prominent peaks of our conductivity measurements. These widths ranged from 10 to 160 m for the hot ground; although most were < 100 m and the data further suggests that the 160 m value may have been a doublet. Areas with hot and salty groundwater which are assumed to represent the central core of the convection cells ranged from 10 to 40 m in width.

Our interpretation of the conductivity data is that the convective plumes of hot water sources in the Pilgrim Springs hydrothermal system range up to roughly 100 m in width and that some plumes have a hot and salty core up to 40 m in width. These findings, namely the large number and size of hot and/or salty groundwater areas encountered with a 100 m spacing of the conductivity survey lines, suggest that the total number of convective plumes moving hot and/or salty groundwater toward the surface may be about 2-3 times the number detected, probably about 40-60. This is surprising in that only the pool area gives rise to a flow of surface water away from the springs. The data also suggest that there may be extended hot and/or salty water sources at depth in the SW quadrant while the 3 smallest hot areas noted in the temperature data of Figure 2 may be isolated point sources. The implication for developmental drilling is that placement of the hole may not be so critical over an extended source but very critical over point sources.

Another application of the conductivity measurements is in detecting the boundary between the thawed ground and the surrounding permafrost terrain (i.e., delineation of the total area of thawed ground). Permafrost soils have ice in the soil pores rather than water which creates a strong

conductivity contrast between permafrost and unfrozen soil. The MI method of measuring conductivity was tested for detecting the transition from thawed soil to permafrost along line 400S (Fig. 10). From 160E to 340E σ_H decreased from 38 to 18 mS-m^{-1}, values typical of the background values in the thawed region. Between 340E and 370E there was a sharp decrease to 2.6 mS-m^{-1}, a value typical of permafrost terrain. The edge of the permafrost is predicted to be at 360E $\pm$ 10 m. While no temperature measurements were made in this area visual observations suggested that the portion of line beyond 370E was tundra permafrost. Thus, the MI measurements accurately delineate the boundary of the permafrost terrain with the thawed hydrothermal system. These measurements were made at a spacing of 10 m which could be reduced to obtain a more precise determination of the permafrost boundary.

The utility of these shallow conductivity measurements for delineating hot and/or salty ground water areas can be shown from the fact that the hottest site (near 300W,300S) was missed with our temperature grid survey. When high electrical conductivity values were noted at this site, we returned there to make the temperature measurements which proved to be the hottest temperatures measured during this field season. For reconnaissance studies of geothermal areas another favorable aspect of these shallow MI measurements is the large amount of data that can be gathered in a short time. It requires < 1 minute to make measurements at each position, the data reduction is simple and straightforward, and, if desired, modeling can yield additional information on the subsurface conditions.

HYDROLOGICAL MEASUREMENTS

Evaluation of a hydrothermal system like Pilgrim Springs requires a precise knowledge of the hot water sources, recharge, discharge and internal flow characteristics of the system, as noted previously. Detailed measurements of the hydrological characteristics of this system were beyond the scope of the present study. However, a few soil water samples were obtained along line B, as noted above, and also along the river at 24 points, as shown in Figure 11, for determination of their electrical conductivity. Two in situ measurements of the saturated hydraulic conductivity of the soil were carried out and an attempt was made to determine the volume of ground water flow at one site. In addition, vertical and horizontal ground water velocities were estimated from the measured temperature profiles.

Figure 11 shows the measured in situ temperatures in the Pilgrim River adjacent to and downstream from Pilgrim Springs. These temperatures were measured from a boat at a depth of $\sim$ 1/2 m below the water surface in the main part of the flow. The temperature measurement at station 3 was repeated, and again gave 6.5°C, after all the other measurements had been made. Water samples taken from the river at the sites noted in Fig. 11 were returned to the laboratory for determination of their electrical conductivity at 25°C. These data show a gradual increase in both water temperature and conductivity from a point just upstream of the Pilgrim Springs area to a point $\simeq$ 10 km downstream.

Water temperatures increase from 6.4°C to 7.9°C, or 1 1/2°C, between stations 1 and 16 on Figure 11. The corresponding increase in conductivity of the river water from stations 1 to 16 was 0.5 $mS\text{-}m^{-1}$. Assuming a river discharge of 50 $m^3\ s^{-1}$, this temperature change would involve a heat input

Pilgrim River

WATER TEMPERATURE AND ELECTRICAL CONDUCTIVITY MEASUREMENTS

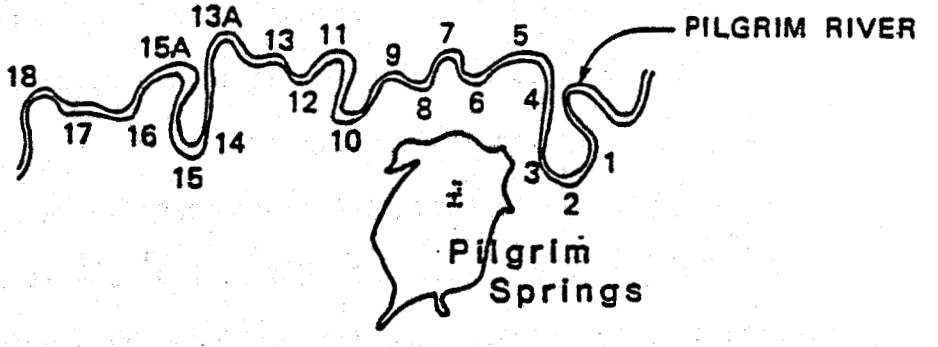

STATION	TEMPERATURE (C)	ELECTRICAL CONDUCTIVITY ($mS-m^{-1}$)
1	6.4	12.56
2	6.5	12.47
3	6.5	12.48
4	6.5	12.48
5	6.7	12.55
6	6.8	12.56
7	6.8	12.76
8	6.8	12.78
9	6.9	12.80
10	7.0	12.96
11	7.1	12.96
12	7.1	12.90
13	7.1	12.88
13A	7.5	12.93
14	7.6	12.96
15	7.7	12.94
15A	7.8	12.97
16	7.9	12.98
17 *	11.1	15.26
18	8.0	13.05

* THE HOT STREAM FROM PILGRIM SPRINGS ENTERS AT THIS STATION.

Figure 11. Measurements of water temperature and electrical conductivity of the Pilgrim River. A hot saline stream enters the river at station 17, causing the observed increases in temperature and conductivity.

of ≈ 300 MW! The temperature change associated with solar, evaporative and convective influx was estimated with the expressions given by Dingman, et al. (1969). The maximum temperature increase assuming a continuous 15°C air temperature was found to be 0.1°C. Air temperatures during the field program ranged from 4°C to a maximum of 15°C. A more reasonable estimate of air temperature at 10°C implies a negligible river temperature decrease. Calculations are given in Appendix A.

Calculations also show that an increase in water temperature of 1 1/2°C would require a groundwater influx of ≈ 1 m^3 s^{-1} at a temperature of 78°C. The conductivity increase could be produced by a groundwater influx of a few hundredths to a few tenths m^3 s^{-1} depending on the amount of salts in the incoming water. This mass influx required by the conductivity increase would heat the river a few tenths °C. These observations suggest that the rise in water temperature of the river must be primarily a result of heat transfer, rather than mass transfer, through the river bed.

There are several lines of evidence suggesting the presence of hot water under the river. The ≈ 1.5 km^2 size of the thaw area, the presence of numerous convection cells bringing hot water toward the surface and the large artesian flow from the 2 wells drilled in the area all suggest a good supply of groundwater to the thawed area. Yet, the surface discharge from Pilgrim Springs is very small. This would seem to imply a substantial groundwater discharge from the thawed area or possibly recirculation of the water. The Pilgrim River valley is generally underlain by permafrost so that the only possible near-surface flows must be in the thawed ground under the river channel or under the very small discharge stream from the Pilgrim Springs pool. We have not yet made any measurements in this discharge stream where it passes through permafrost terrain but some should be carried out in the future.

Shallow MI measurements along the trail between the old Catholic church and the Pilgrim River suggest that there is no permafrost present. This result implies that both groundwater recharge from the river to the thawed area and growndwater discharge from the thawed area to the river are possible. In addition, Wescott, et al. (this report) has discovered a highly conductive layer (159 $mS\text{-}m^{-1}$), about 50 m in thickness, between the depths of 15.5 and 69.5 m. This conductivity value is typical of measurements made over convective cells and the discharge stream from the pool. We suggest that there is a discharge of hot ($\approx$ 78°C) and salty groundwater in this layer and that the flow is to the Pilgrim River and then turns downstream for at least 10 km in a thaw bulb or thaw window under the river. It is also suggested that this discharge is capped by a semi-impermeable layer which prevents substantial flow of hot and salty water into the river itself.

As noted above, heating of the river water must be primarily by heat transfer through the river bed which could be conductive and/or convective transfer. Calculations based on a conductive model show that conduction cannot supply sufficient heat to the river so that convective heat transfer must be dominant. We have carried out calculations based on several convective heat transfer models which will be presented in a later report. We also note that it is theoretically possible for hot saline groundwater to enter the river through the bed and to flow along the river bed without mixing. This type of situation would significantly alter our interpretation. Further speculation is not justified at this time, however it should be noted that the discovery of what appears to be a substantial groundwater discharge from the Pilgrim Springs system has important implications for the mass and energy balance of the system, as will be discussed later.

It should also be noted that these temperature and conductivity measurements are point measurements. Since lateral dispersion in a river is such a slow process, these measurements do not represent the conditions in a cross-section nor the average conditions. Therefore the results should be treated with caution until a carefully designed experiment can be carried out. The results do imply that such an experiment would be worthwhile and that measurements should be made in the Pilgrim River system and in the system associated with the discharge stream from the pool area.

The saturated hydraulic conductivity governs transport of water through a soil matrix. Two determinations of this parameter were made near 25W,452S in the same hole; one at 2 1/2 m and one at the 4 m depth. These measurements were made by driving porous metal filters on the end of a 1/2" pipe into the soil to the desired depth and then recording the rate of change of water level in the pipe as groundwater flowed into the pipe through the filters. An example of the data, for the 2 1/2 m depth, is shown in Figure 12. The saturated hydraulic conductivity was calculated from

$$K = C \ln \frac{h_i/h_n}{\Delta t} \qquad (1)$$

where h_i is the water level at time t_i, h_n is the water level at time t_n, $\Delta t = t_n - t_i$ and C is a constant. The value found for K was 5.7×10^{-8} m s^{-1} at the 2 1/2 m depth and 1.2×10^{7} m s^{-1} at the 4 m depth. These values are typical for the near-surface soil conditions (silty and clayey sands) found at Pilgrim Springs.

Given the values of hydraulic conductivity above, the flux of water through the soil is

$$J = K \frac{dh}{dx} \qquad (2)$$

where dh/dx is the hydraulic gradient. An attempt was made to determine the gradient between two pipes placed 15 m apart on a line parallel to the stream near 25W,452S. However, the difference in the water levels between these two wells was too small to be measured with a hand-held level which indicates that the groundwater flow in a direction parallel to the stream was very small. This finding does not rule out ground water flow perpendicular to the stream. In fact, the measured temperature profile at this site shows what appears to be a combined vertical and lateral flow of ground water from a nearby convection cell. It appears that this flow must be in a direction perpendicular to the stream.

Estimates of the velocities of the groundwater flow can be obtained from the measured temperature profiles. The effect of water transport through the soil is to distort the temperature profiles from those of conductive profiles to other forms. We consider 3 cases of water transport; constant vertical transport, horizontal transport and combined vertical and horizontal transport. An outline of the methods will be presented and the details left to a later report. The theory used is a special case of the general theory for the problem of heat and mass transfer in a porous medium (e.g., Bear, 1972).

For the case of constant vertical flow of groundwater across a slab of thickness a, the one-dimensional, steady-state, heat transfer equation for a saturated, homogeneous porous medium is

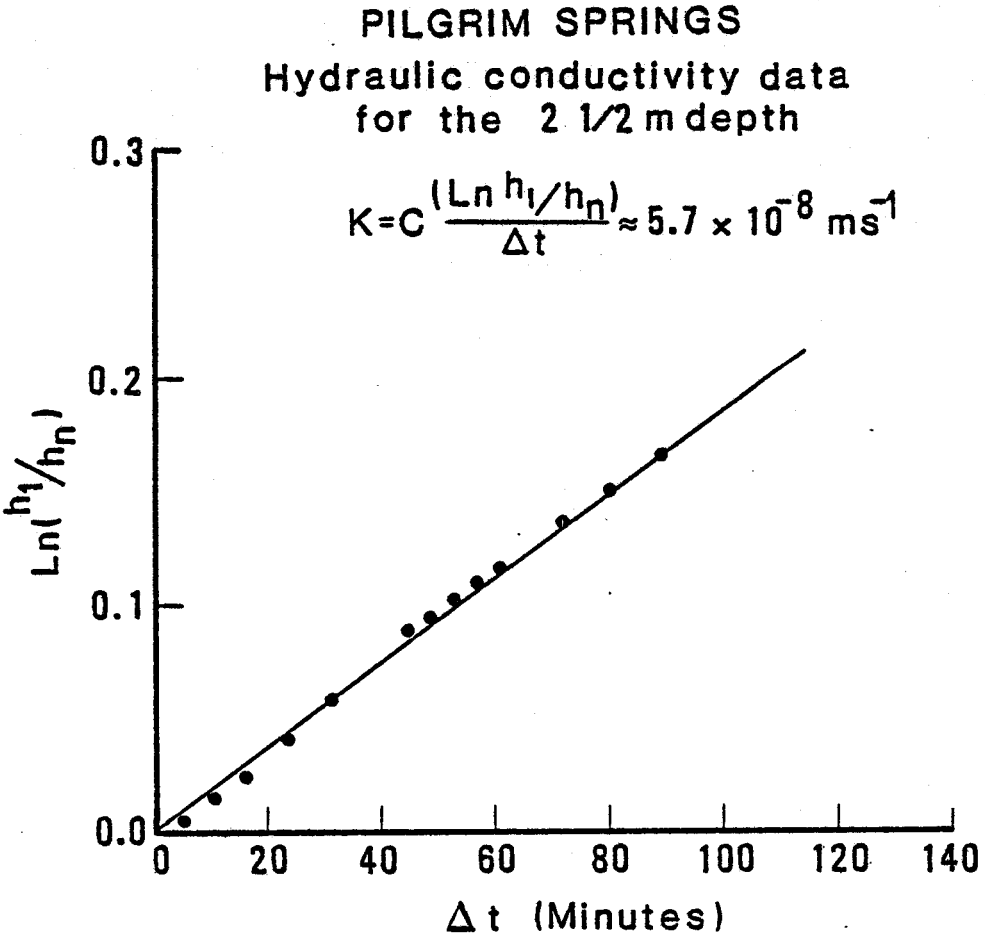

Figure 12. Hydraulic conductivity data at Pilgrim Springs near 25W,452S for flow to the well point at the 2 1/2 m depth.

$$\frac{\partial^2 T}{\partial z^2} - \alpha v \frac{\partial T}{\partial z} = 0 \qquad (3)$$

where T is the temperature, z is the vertical coordinate axis taken as positive downward, v is the constant vertical groundwater velocity and a is a constant involving the thermal properties and the porosity of the soil and groundwater. A solution of equation 3 with appropriate boundary conditions is

$$T(z) = T_o + \Delta T \frac{e^{-\alpha v z} - 1}{e^{-\alpha v a} - 1} \qquad (4)$$

where T(z) is the temperature profile, T_o is the temperature at the top of the layer and ΔT is the temperature difference across the layer. Figure 13 shows the behavior of T(z) for a vertical, flow of groundwater as a function of groundwater velocity. T(z) profiles to the left of the purely conductive case (v=0) represent infiltration velocities and to the right, upward convective velocities. Comparison of the measured temperature profiles with the T(z) in Figure 13 allows an estimate of the groundwater velocity. These comparisons have shown that vertical groundwater velocities in the upper 10 m of the Pilgrim Springs system are on the order of 1-50 m yr^{-1}. Specific values are given for some of the temperature profiles along line B (Figure 5) in the section on Temperature Measurements. It appears that the highest values occur in the cores of convection cells while the low values occur on the periphery of the cells. On either end of line B there was a downward groundwater flow of ≈ 5 m yr^{-1} (i.e., infiltration of groundwater) which may be a result of the flooding in the area mentioned earlier. Harrison and Hawkins (this report) estimate a vertical flow velocity < 4 m yr^{-1} in their hole 2. For comparison, we estimate a vertical flow velocity of 1-2 m yr^{-1} in this hole using equation 4 and Figure 13.

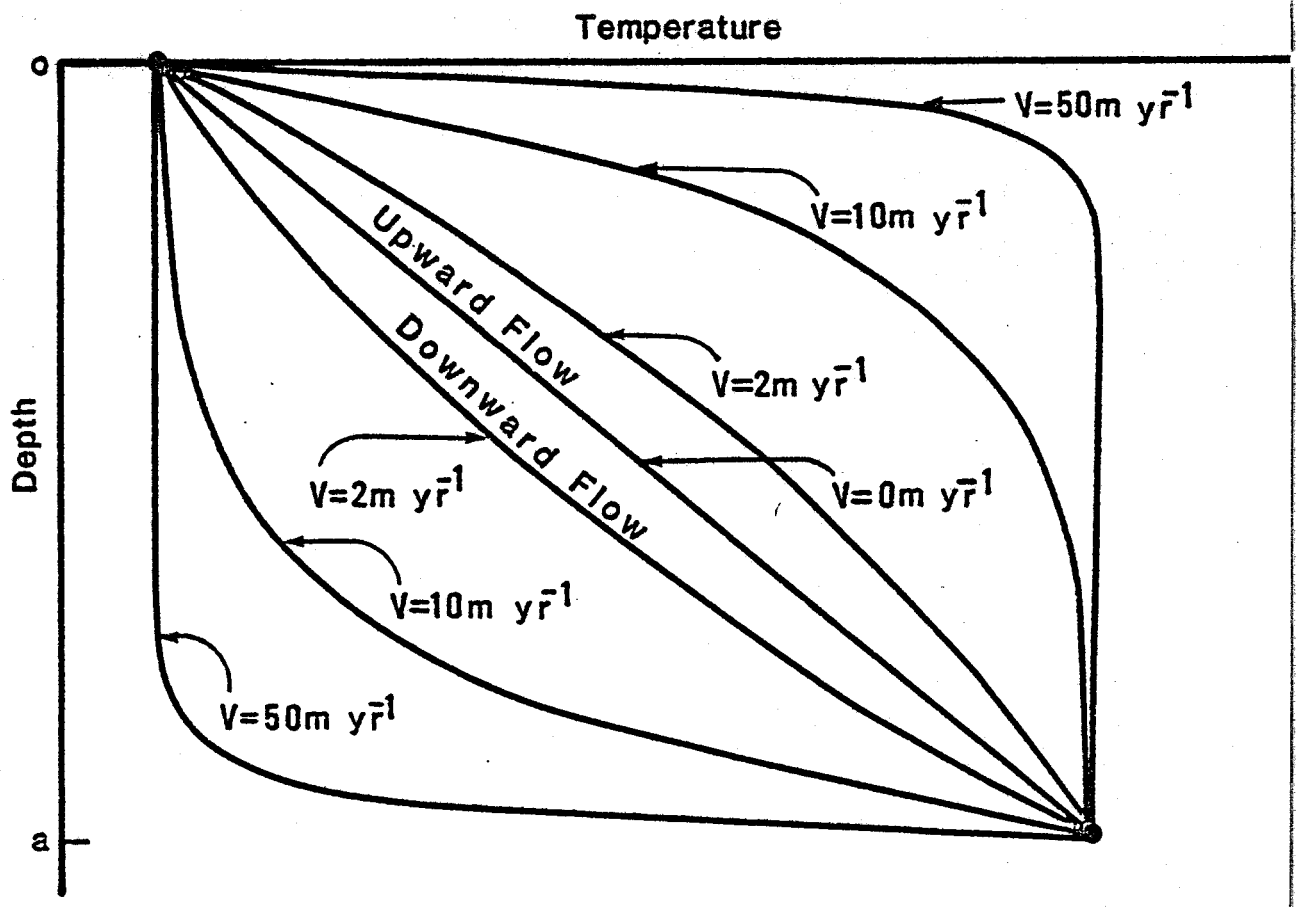

Figure 13. Calculated temperature profiles for a range of vertical flow velocities.

For the case of horizontal flow in an aquifer the 2-dimensional, steady-state heat transfer equation for a saturated, homogeneous and isotropic porous medium is

$$\frac{\partial^2 T}{\partial z^2} - \beta w \frac{\partial T}{\partial x} = 0 \qquad (5)$$

where w is the groundwater velocity in the horizontal (x-direction), β is a constant and z is the vertical coordinate. We have solved equation 5 for several functional forms of w and are presently analyzing the measured temperature profiles to determine the horizontal groundwater flow velocities. Results will be presented in a later report.

For the case of combined vertical and horizontal flow, the two dimensional, steady-state heat transfer equation for a saturated, homogeneous and isotropic porous medium is

$$\frac{\partial^2 T}{\partial z^2} - \gamma w \frac{\partial T}{\partial x} - \delta v \frac{\partial T}{\partial z} = 0 \qquad (6)$$

where w and v are the horizontal and vertical groundwater flow velocities and γ and δ are constants. We have solved equation 6 for both constant and variable velocities. Preliminary results from its application to holes near the edge of the agricultural field in the SE quadrant (Harrison and Hawkins hole 1 and our hole 25W,452S) indicate a vertical flow velocity of $\simeq$ 30 m yr^{-1} and a horizontal flow velocity of $\simeq$ 100 m yr^{-1}. For comparison Harrison and Hawkins (this report) estimate a horizontal flow velocity of $<$ 365 m yr^{-1} and a vertical flow velocity of $\lesssim$ 4 m yr^{-1}. However, their vertical flow estimate applies only to the lower part of their hole. Additional temperature profiles are being analyzed and the results will be presented in a subsequent report.

The results of flow velocity calculations using these equations must be treated with caution. Ambiguities exist when the temperature profiles are not those of steady-state heat transfer, when the soil properties change with depth, and, in general, when the assumptions for which the equations have been derived are violated. These ambiguities can bring the flow velocities into question; nevertheless, it seems possible to learn to recognize some of the "pure" cases in the data and to obtain a rough estimate of the flow velocities from them.

DISCUSSION, MODELS, ENERGY AND POWER

Conclusions based on this reconnaissance study of the thermal and hydrological characteristics of the Pilgrim Springs area must be treated with caution. The temperature measurements are sparse and shallow ($\lesssim$ 10 m depth) with the majority $\simeq$ 5 m in depth. Measurements in the Pilgrim River are exploratory in nature and we do not have a measurement of its discharge. Use of the MI method for shallow soil conductivity measurements in geothermal areas is new and there is a need for proper evaluation of its use and interpretation of the results in studies of hydrothermal systems. Nevertheless, while recognizing the hazards of premature generalization, it is necessary and desirable at this time to construct highly idealized models of the gross features of the Pilgrim Springs hydrothermal system. The details of these models will almost certainly be wrong, however, they should provide some guidance for future experimental designs and should serve to focus attention on what we believe are some of the more important parameters and processes.

Questions on the presence, distribution, location, size and geometry of convection cells in the thawed area at Pilgrim Springs derive their

importance from the effectiveness of these cells in transferring heat. Convective transfer of heat in cells can be several orders of magnitude greater than conductive heat transfer. Therefore, it is possible for the heat transfer to be dominated by convective cells even though they may only occupy a relatively small percentage of an area. The most direct evidence for the existence of these cells comes from the temperature data. Figures 4 and 5 show what appears to be a cell near the 100 m position along line B. As noted previously, other temperature profiles resemble those that would be expected in or near convection cells. The electrical conductivity data obtained with the MI method shows, by comparison with temperature data along line B and measurements made over the hot discharge stream from the pool area, the existence of many areas of hot and/or salty ground. These areas are tentatively interpreted as convection cells and the conductivity data have been used to determine their number, position, distribution, and size; to suggest that salt deposition occurs in the soil near the ground surface over the core of the cells; and to define asymmetry in the direction of water flow in the ground away from the cells. An alternative interpretation is that these hot ground areas, detected by the MI and temperature measurements, represent lateral flow of hot and/or salty water in old buried river channels. However, the preponderance of data seems to favor their interpretation as convective cells. A more detailed discussion of the structure and function of these cells will be given in a future report.

Information on the sources, sinks, distribution and fate of water involved in the Pilgrim Springs system must be obtained over annual cycles and interpreted before a detailed evaluation of its commercial potential can be accomplished. A "target" model of the water balance (one to shoot at) is proposed based on the fragmentary information from the temperature,

conductivity and hydrological measurements and their interpretation. Figure 14 illustrates the components of the model. The potential source components include rain, snow meltwater, floodwater, recharge from the river, subpermafrost recharge and hot and/or salty water from greater depths. Water can be lost from the system by evaporation, surface runoff, discharge from the hot stream and by discharge under the river and the hot stream. Only the discharge from the hot stream has been measured and it is not known if that flow varies annually. A few measurements of the other components would help to make crude estimates, however, the subpermafrost recharge and the hot and/or salty water from great depths will be very difficult to obtain as will the recirculation in the system. Subpermafrost water for recharge may be an important component of the system. There is some question whether or not the permafrost is continuous in the general area but, assuming that it is, it is very unlikely that percolation (e.g., through fractured granitic rocks) could be a source for the subpermafrost water. Water entering the rock would be expected to freeze, blocking off the infiltration channels. It appears to be more likely that the subpermafrost water enters the ground through thaw windows in the permafrost which exist under the river and lakes in the area. This type of recharge can also account for the artesian flow observed during the recent drilling program (Kline, et al., this report). Since the site is near the sea it would also be possible for sea water to penetrate under the permafrost through the thawed sea bed assuming there is no subsea permafrost. This last possibility might possibly explain the salty nature of the water from Pilgrim Springs; however, the geochemical and isotopic evidence does not appear to support the sea water hypothesis (Motyka, et al., this report).

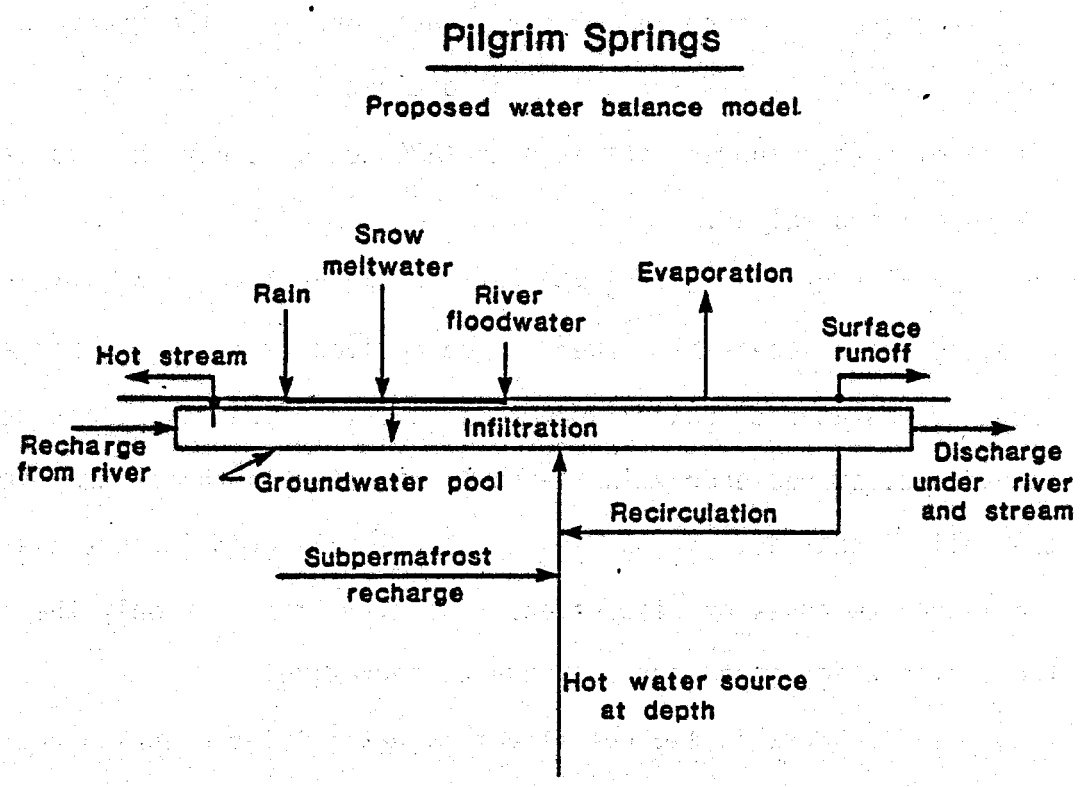

Figure 14. Proposed water balance model for Pilgrim Springs.

The above data and analyses allow a first crude estimate of the accessible power in the upper 50 m of the Pilgrim Springs hydrothermal reservoir. The accessible power (Muffler, 1979) represents the power stored in the soil and water, the power lost by natural heat transfer processes at the upper surface of the reservoir, and the power lost by discharge of groundwater from the upper 50 m of the reservoir. These estimates are referenced to 0°C which is a few degrees above the mean annual ground temperature of the surrounding permafrost terrain. The mean annual air temperature at Pilgrim Springs is also close to 0°C (-3.5°C at Nome). Referencing these power estimates to 15°C would reduce them to 2/3-3/4 of the calculated values.

Based on the above fragmentary data and analyses, we believe, at this time, that the accessible power can be derived from the discharge of the hot pool, groundwater discharge under the river, natural heat loss to the atmosphere, stored energy in the soil and water in the system, and possibly the well discharges. It is assumed that the Pilgrim Springs system is stable for purposes of discussion. Again, we consider only the top 50 m of the system which makes our estimate conservative.

The discharge in the hot stream from the Pilgrim Spring pool is equivalent to roughly 2 MW (Harrison and Hawkins, this report) assuming the energy of the discharge water to be extracted at 0°C.

The groundwater discharge under the river supplies ≃ 300 MW to the river over a ≃ 10 km distance. This discharge may continue farther downstream however there are no measurements to support this supposition. Also, this groundwater discharge would surely carry more energy than that given off to the river so that its accessible energy would be greater than 300 MW.

The natural heat loss from the Pilgrim Springs thawed area was estimated from the temperature profiles to be about 17 MW during late June. This value would be expected to be greater at times when the surface temperature of the ground was colder (i.e., during fall, winter and spring).

Stored energy in the system includes that stored in hot soil and in the hot water in the thawed area. It is estimated to be at least 400 MW . yr (i.e., 20 MW for 20 years).

It is not known if the well discharge from the two drilled wells can be added to the spring discharge and the groundwater discharge under the river, however, the well discharge is equivalent to ≅ 14 MW.

The components of the accessible power are summarized in Table 1 and it appears that the minimum total accessible power is ≈ 350 MW. This estimate does not include the accessible power in the layer of hot water and sediments under the river nor that carried off beyond 10 km downstream by flow in this layer. Also, it does not consider any flow at depths below 50 m. Given these considerations, it seems reasonable that the total accessible power in the Pilgrim Springs system may be on the order of 500 MW.

The beneficial power, which is the fraction of accessible power that could be directly applied to non-electric uses, was estimated using a geothermal recovery factor of 0.25 and a beneficial heat utilization factor of 0.24 (Muffler, 1978). Use of these factors yields a beneficial power estimate of ≈ 30 MW (Table 1).

Such a large estimate for the accessible power should not result in unbridled optimism for the Pilgrim Springs system. This is a low-grade power that would yield ≈ 30 MW for space heating, agricultural purposes, and other direct uses. Special technology would be required to produce

TABLE 1

PILGRIM SPRINGS POWER ESTIMATES[1]

Accessible Resource Base (Muffler, 1979) for Upper 50 Meters of Reservoir Referenced to 0°C[2].

Discharge of hot stream (Harrison and Hawkins, this report)		~2 MW
Discharge under the Pilgrim River		>300 MW
Well discharge (?)		~14 MW
Natural heat loss		≥17 MW
Stored energy (400 MW · yr = 20 MW for 20 yrs)		~20 MW
	Total	~350 MW
Best estimate		~500 MW

Beneficial Power [Power available for direct (nonelectric) use, assuming a utilization factor of 0.24 and a geothermal recovery factor of 0.25 (Muffler, 1979)].

(500 MW) (.25) (.24) = 30 MW

Electrical Power

Estimation of the electrical power potential must depend on engineering parameters associated with special technologies required for electrical generation in intermediate-temperature, liquid-dominated geothermal systems. It is therefore premature to attempt a quantitative estimate of electrical power potential at this time, except to state that it will probably be a small fraction of the beneficial power estimate.

[1]These power estimates are preliminary, based on reconnaissance-level hydrologic measurements, and should be treated with caution until they can be tested by the more extensive field studies proposed in the final section of this report.

[2]Referencing the above power estimates to 15°C would reduce them to 2/3-3/4 of the above values.

electricity and only a small fraction of the 30 MW beneficial heat estimate could be produced as electrical power. However, it should be noted that we have only studied the top layer (50 m) of this system and have found a good flow of hot water. It is possible that future geophysical and geochemical surveys, together with deeper exploratory drilling, may result in the discovery of deeper, hotter reservoirs--possibly containing wet steam. The net result of these reconnaissance--level investigations is that they strongly suggest that more detailed work on the Pilgrim Springs system is justified. Recommendations for follow-on geophysics, hydrology, exploratory drilling, and geochemistry are given in the following section (Turner, et al., this report).

ACKNOWLEDGEMENTS

In addition to funding from DOE and the State of Alaska, this research was supported with funds from the National Science Foundation, Division of Polar Programs, Polar Earth Sciences Section (DPP77-20462); U.S. Department of Labor under the Comprehensive Employment and Training Act; and by the State of Alaska, Department of Regional and Community Affairs. We also want to acknowledge the help of D. Hawkins, A. Lockhart, R. Fisk, and J. Peace in performing some of the measurements.

APPENDIX A

Calculation to determine net heat flux from the ground to the Pilgrim River:

The net heat flux from the ground to the river is given by the product of the river discharge times the temperature increase:

$$\dot{H} = \rho\, c_p\, j\, D_o\, \Delta T$$

where $\dot{H}$ = net heat flux

ρ = water density = 1 gm cm^{-3}

c_p = specific heat of water = 1 cal $(gm\ °C)^{-1}$

D_o = river discharge ≈ 50 $m^3\ s^{-1}$

ΔT = temperature increase = 7.9°-6.4° = 1.5°C

j = mechanical equivalent of heat = 4.184 joules cal^{-1}

$$\dot{H} = \frac{1\ gm}{cm^3} \cdot 10^6\ \frac{cm^3}{m^3} \cdot 1\ \frac{cal}{gm°C} \cdot 4.184\ \frac{joules}{cal} \cdot 50\ \frac{m^3}{s} \cdot 1.5°C$$

$$\dot{H} = 3.14 \cdot 10^8\ \text{joules}\ s^{-1}$$

$$\dot{H} = 314\ \text{MW}$$

Calculation to determine maximum surface heating of the Pilgrim River due to meteorological input:

Dingman, et al. (1969) specify straightforward expressions for heat gain at the water surface due to radiative, evaporative and convective flux Assuming an average wind speed of 5 m s^{-1}, and clear sky conditions,

$$\dot{Q}_s = -220.9 + 56.27\ (T_a - T_w)\ [\text{cal}\ (cm^2 day)^{-1}]$$

where $\dot{Q}_s$ = net heat gain per unit area of the river

T_a = air temperature, assumed to be +15°C.

T_w = water temperature, assumed to be +6°C.

then, $\dot{Q}_s$ (T_a = 15°C) = 263 cal $(cm^2 day)^{-1}$

This heat is transferred to the river through its water surface area equal to the width of the river (∿ 25 m) times the affected reach (∿ 6 miles = 9656 m) yielding a net heat input of

$$\dot{H}_s = 3.075 \cdot 10^7 \text{ joules } s^{-1}$$

Assuming that this heat input is continually absorbed by the river we can estimate the associated river temperature rise from

$$\dot{H}_s = \rho \, c_p \, j \, D_o \, \Delta T$$

$$3.075 \cdot 10^7 \frac{\text{joules}}{s} = 1 \frac{g}{cm^3} \cdot 10^6 \frac{cm^3}{m^3} \cdot 1 \frac{cal}{g°C} \cdot 4.184 \frac{\text{joules}}{cal} \cdot 50 \frac{m^3}{s} \quad \Delta T$$

which yields $\Delta T = .15°C$

Note that this estimate assumes a continuous air temperature of 15°C, the maximum daytime temperature recorded during field investigations. For an average daily air temperature of 10°C, the Dingman expression predicts negative surface heat gain, and subsequently, a river temperature decrease!

REFERENCES

Bear, J., 1972, "Dynamics of Fluids in Porous Media", American Elsevier Publishing Company, Inc., 52 Vanderbuilt Ave., New York, NY.

Dingman, S. L., and Assur, A., 1969, "The Effects of Thermal Pollution on River Ice Conditions. Pt. II: A Simplified Method of Calculation", Corps of Engineers, U.S. Army, CRREL Research Report 206 Pt. II, Hanover, New Hampshire.

Muffler, L. J. P., editor, 1979, Assessment of Geothermal Resources of the United States--1978, U.S. Geol. Survey Circular 790, 163 pp.

Osterkamp, T., R. Gaffi and C. Stevens, Shallow electrical conductivity measurements, in: Wescott, E.M. and D. Turner, eds., "A Geological and Geophysical Study of the Chena Hot Springs Geothermal area, Alaska, preliminary report, Geophysical Institute, Univ. of Alaska, prepared for Division of Geothermal Energy, U.S. Dept. of Energy, Cooperative Agreement DE-FC07-79ET27034, 55 pp., 2 plates, 1979.

CONCLUSIONS AND RECOMMENDATIONS FOR PHASE-TWO GEOPHYSICS, HYDROLOGY, EXPLORATORY DRILLING, AND GEOCHEMISTRY AT PILGRIM SPRINGS, ALASKA

Donald L. Turner, Robert B. Forbes, Thomas Osterkamp,
Eugene Wescott and Juergen Kienle

CONCLUSIONS

Our reconnaissance-level studies suggest that the Pilgrim Springs area is underlain by an intermediate-temperature, liquid-dominated geothermal system (Muffler, 1979) of substantial magnitude. Initial exploratory drilling has confirmed the presence of the shallow, ≈ 1-1.5 km^2 hot water reservoir delineated by our geophysical surveys. Large artesian flow rates of 200 and 300-400 gallons/minute of 90°C water indicate that at least one good aquifer is present at shallow depths within this reservoir. Resistivity surveys suggest that the shallow reservoir is approximately 50 m thick. Deeper hot water reservoirs may also be contained in the thick sedimentary section identified by the seismic and gravity surveys, but they have not as yet been located by our initial resistivity surveys.

Our analysis indicates that the power presently being dissipated from the upper 50 m of this geothermal system is a minimum of 350 megawatts (MW), with more than 300 MW of this amount in subsurface groundwater discharge beneath the Pilgrim River. The accessible resource base (Muffler, 1979) for the upper 50 m of the system referenced to 0°C is estimated at 500 MW. The beneficial power (Muffler, 1979) available for direct (nonelectric) use is estimated at 30 MW.

These power estimates are referenced to 0°C, the approximate mean annual ground temperature in the unthawed region surrounding Pilgrim Springs, and a value close to the mean annual air temperature (-3.5°C at Nome). Referencing these estimates to 15°C would reduce them to 2/3-3/4 of the above values.

The available evidence indicates that the geothermal system at Pilgrim Springs is not likely to have steam temperatures at depth which are adequate for economic production of electricity using conventional steam turbine generation technology. Pilgrim Springs does appear to have excellent potential for the production of hot water for direct heat applications and, perhaps, an as yet undetermined quantity of relatively low-temperature steam. Such a system is capable of generating moderate amounts of electricity for local community use, particularly if Rankin-cycle turbines are used. These turbines utilize an organic working fluid, such as isobutane, which flashes to vapor at a temperature well below the boiling point of water. The organic fluid is heated by passing through a heat exchanger coupled to the geothermal system.

Estimation of the electrical power potential of Pilgrim Springs must depend on engineering parameters associated with this special technology, as well as ultimate reservoir temperatures and production parameters which are presently unknown. It is therefore premature to attempt a quantitative estimate of electrical power potential at this time, except to state that it will probably be a small fraction of the 30 MW beneficial power (non-electric) estimate.

Further discussion of engineering applications is beyond the scope of this report. Engineering, developmental, and economic studies should be initiated as soon as the next phase of geophysics, hydrology, exploratory drilling, and geochemistry are completed and the extent and magnitude of the hydrological and thermal regimes in the geothermal resource have been delineated.

We emphasize that many measurements in this report are preliminary, based on reconnaissance-level studies, and that our conclusions should be viewed with caution. Their primary use should be to focus attention on the more important features of the geothermal system. Finally, they indicate that more detailed work should be done to arrive at a more complete and refined estimate of the Pilgrim Springs geothermal system.

RECOMMENDATIONS

The next phase in the assessment and development of the Pilgrim Springs geothermal system should consist of hydrothermal studies of the Pilgrim River, more extensive geophysical surveys, further exploratory drilling, drill hole logging and hydrologic studies, and geochemical studies of drill hole and river water samples. Considerable care should be exercised in the time-sequencing of this work in order to derive maximum benefits and information from it. Our specific recommendations are as follows:

1. Hydrothermal Studies of the Pilgrim River

This project should have the highest priority because of its direct relationship to the power estimates discussed above. It should consist of carefully designed studies to carry out precise measurements of the river temperature distribution, electrical conductivity of the river water, river discharge, chemical analyses of the river water, shallow temperature measurements in the bottom of the river, and drilling of two 75 m holes along the river. The above measurements should be carried out on several cross-sections of the river. The drilling should include sampling, petrographic, lithologic, hydrologic, chemical and thermal studies. A preliminary assessment of the hot discharge stream and possible associated groundwater flow should also be done.

2. Geophysical Surveys

a. Deep seismic refraction and reflection surveys should be run prior to drilling to determine depth to crystalline basement. At present we only know from seismic and resistivity evidence that basement lies at a minimum of 200 meters below the surface. The gravity data suggest the possibility of basement depths on the order of 500 m in an area about 4 km southwest of Pilgrim Springs (-15 mgal closure on gravity map). The results of the seismic survey, further resistivity surveys and geothermometry (discussed below) can be used to determine the choice of the drill rig necessary to reach target depths.

b. Long-spread (deep penetration) Schlumberger resistivity soundings should be made in the area of the -15 mgal gravity closure to look for possible deep, hot brine layers in what appears to be the deepest part of the Pilgrim River valley sedimentary basin. This will require a higher-powered transmitter than has previously been used in order to achieve the necessary signal penetration through permafrost.

c. An east-west, dipole-dipole resistivity survey should be made to define the eastern and western limits of the shallow geothermal reservoir.

d. A long-spread N-S Schlumberger sounding should be made near the center of the disturbed ground to look for deeper hot brine layers.

e. A long-spread Schlumberger sounding should be made to the north of the Pilgrim River and at a point several km downstream to locate the hot ground water flow suggested to be heating the Pilgrim River.

f. A controlled-source, audio magneto-telluric survey line should be run across the Pilgrim thermal anomaly in an attempt to energize the possible deep conduit along the long axis of the thaw elipse with a perpendicular electric dipole located towards the NE thaw window. This might well show up the location of a planar-type deep conduit system (requires high-power transmitter).

g. A shallow magnetic induction survey should be run to more accurately define the area of thawed ground surrounding Pilgrim Springs.

h. Computer modelling of gravity data should be done prior to drilling to help define more accurately the thickness of valley fill sediments over crystalline basement.

3. Exploratory Drilling

Recommended drilling sites have been selected based primarily on the existence of favorable geophysical anomalies, at the same sites, in the ground temperature, ground conductivity and deep resistivity surveys. Individual resistivity and conductivity profiles, as well as convection cell analyses were integrated with contoured data in plan view in order to arrive at these recommendations. Supporting data from all other aspects of the Pilgrim Springs study were also considered (bedrock and surficial geology, seismic and gravity data, etc.). We recommend:

a. Drilling and flow testing of two 200 m test holes centered at 290 m S, 290 m W and 20 m S, 20 m E as shown on Figure 1. Deeper holes would, of course, be desirable and drilling should ideally be extended to maximum practical depths allowed by the drill rig and drilling budget, assuming geologic indications are favorable at depth during the actual drilling. Flow tests

should include gas sampling and analysis to help determine the nature of the geothermal system and the extent to which artesian flow may be caused by gas drive.

b. Detailed lithologic logging of these holes to determine stratigraphy, reservoir characteristics and temperature profiles.

c. Water sampling and geochemical analyses from above holes, including geothermometry and oxygen isotope studies to determine deep reservoir temperatures and ultimate source of water (e.g., seawater vs. meteoric water). Detailed geochemical and geothermometric analyses of water samples from the first two deep test holes should be completed before final drilling decisions are made for any subsequent deep holes; e.g., a deeper test hole would be appropriate if geothermometry indicates a sufficiently attractive (hot) deep reservoir temperature.

d. Detailed temperature logging of all holes and analysis of temperature data, including estimations of vertical and horizontal groundwater flow velocities from the temperature profiles.

e. Detailed petrographic analysis of cuttings from the first two test holes should be completed to evaluate the possibility of hydrothermal cementation (e.g., siliceous caps, etc.).

f. Drilling a series of 6 shallow (75 m) step-out holes designed to help determine the extent of the geothermal reservoir. Recommended locations for the first three of these holes are

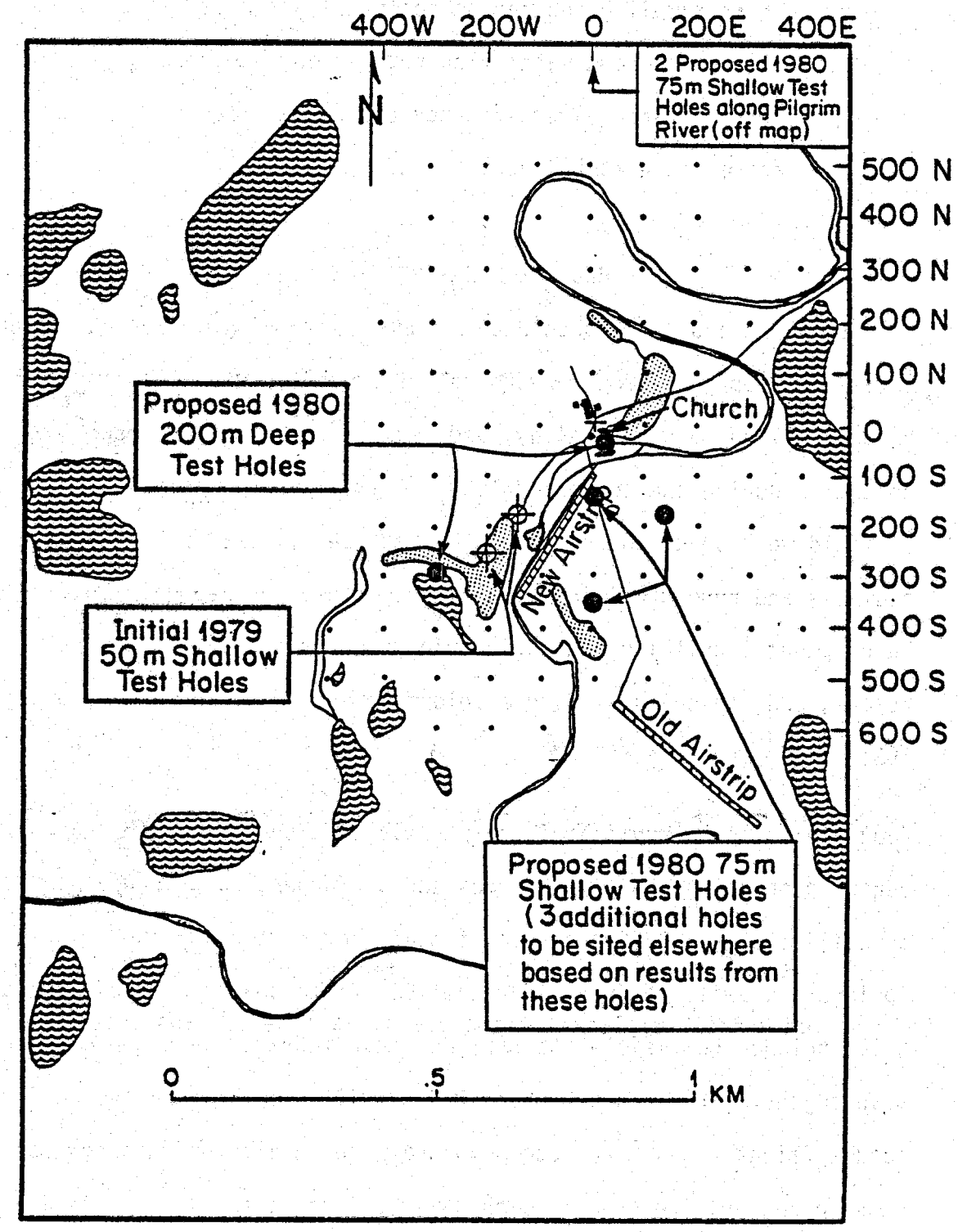

Figure 1. Proposed 1980 exploratory drill hole locations. Stippled areas indicate agricultural fields. Wave pattern indicates lakes and ponds.

shown on Figure 1. Locations for the remaining three holes should be decided after on-site analysis of the results of the first three holes.

g. Water sampling and geochemical analyses from above holes.

h. The undisturbed water flow rate in any aquifers located by drilling should be estimated by thermal tracing or other appropriate techniques.

RECOMMENDED WORK SCHEDULE

Drilling equipment should be brought in to Pilgrim Springs prior to break-up in spring, 1980. Hydrothermal studies of the Pilgrim River, geophysical surveys, hydrology, and exploratory drilling should be conducted during the summer of 1980. A preliminary analysis and report of field work should be completed by December 1, 1980. Final data analysis and report writing should be completed by February 15, 1981. Developmental drilling and engineering studies based on the final report, and agricultural site development should begin in the spring of 1981.

Footnote: The Geophysical Institute has just been informed that our recent proposal to NASA (R. Forbes and D. Turner, Co-principal investigators) to utilize their WB57F research aircraft for a study of the Pilgrim Springs area will be funded for the 1980 field season. Data to be acquired will include the visible, thermal and near infrared, and x-band radar wavelengths. Ground truth thermal data will also be acquired during the actual flight times. We recommend that the results of this new remote sensing cooperative program with NASA be integrated with the results of

the proposed 1980 geophysical, hydrological, drilling and geochemical studies discussed above in order to further improve our understanding of the Pilgrim Springs geothermal system.

REFERENCES

Muffler, L. J. P., editor, 1979, Assessment of Geothermal Resources of the United States--1978, U.S. Geol. Survey Circular 790, 163 pp.

PILGRIM SPRINGS GEOTHERMAL ENERGY EXPLORATION PROJECT

Sponsored by the U.S. Department of Energy and the Alaska State Division of Energy and Power Development

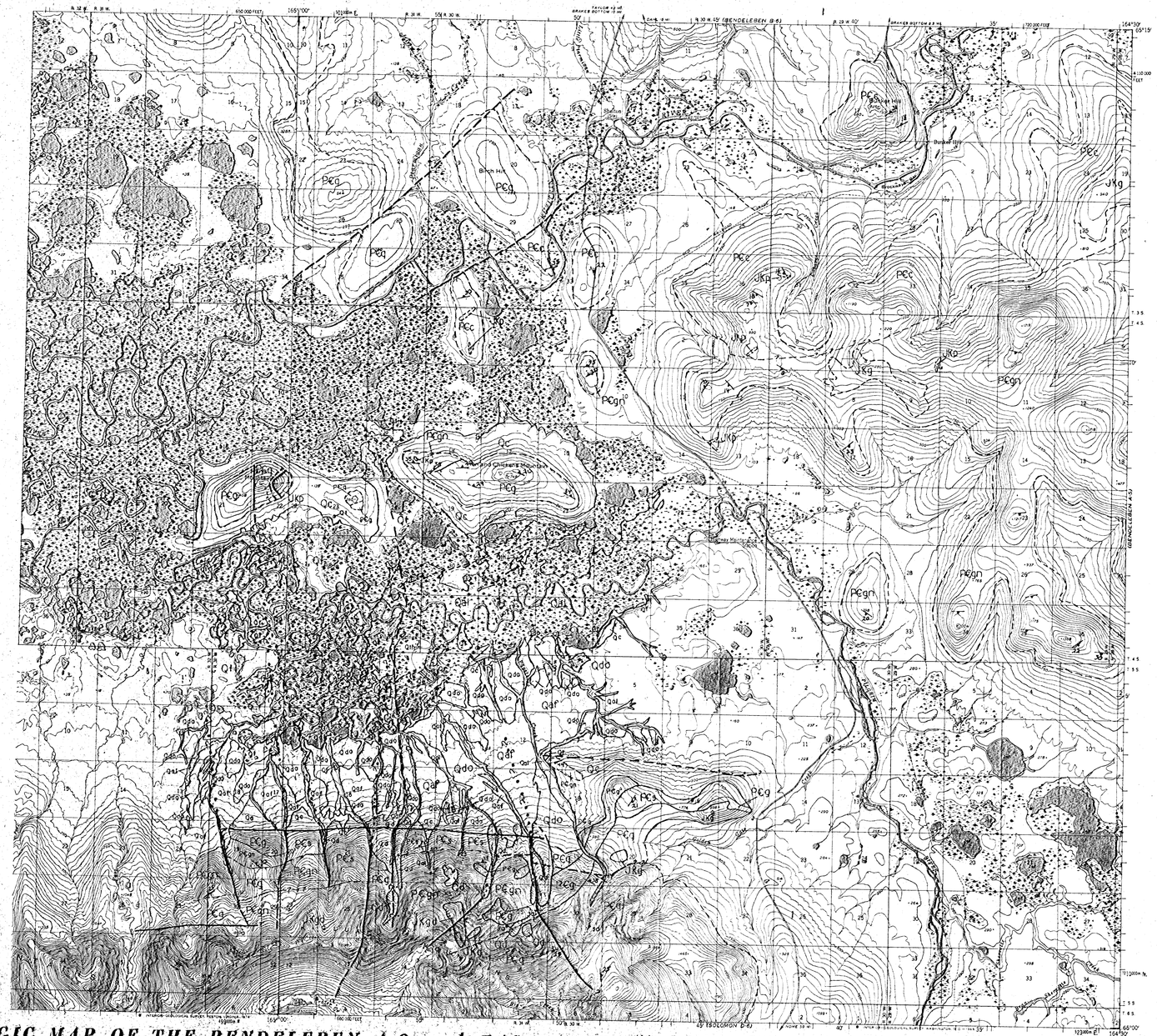

EXPLANATION

SURFICIAL DEPOSITS

- Qal — Alluvial deposits of recently active streams: includes floodplain, overbank and backwater or slough deposits
- Qaf — Alluvial fan deposits
- Qc — Colluvial deposits (undifferentiated): includes solifluction, landslide, frost creep talus and rubble sheet deposits as well as mixed colluvial and fluvial deposits of fans emanating from steep, ephemeral streams on mountain slopes
- Qe — Eolian sand and loess deposits, mapped where > 1.5m thick
- Qt — Alluvial and lacustrine (?) terrace deposits: composed of sand with minor silt, organic, and gravel layers; ice wedges and lenses common; subject to rapid thermal erosion and subsidence
- Qth — Areas of geothermally thawed permafrost
- Qd — Glacial drift (undifferentiated)
- Qdo — Outwash gravels: from outwash fans, plains and terraces graded to moraines in the Kigluaik Mountains and upper Pilgrim River valley

QUATERNARY

INTRUSIVE IGNEOUS ROCKS

- JKg — Biotite quartz-monzonite and granite: massive to weakly foliated, locally alaskite
- JKgd — Biotite granodiorite: massive, with abundant monazite and sphene
- JKp — Biotite granite pegmatite dikes and lenses: tourmaline locally abundant

JURASSIC – CRETACEOUS ?

METAMORPHIC AND INTRUSIVE ROCKS

- PCg — Gneissose granite: weakly to moderately foliated biotite granite with some compositional layering; local occurences of sillimanite, garnet and inclusions of adjacent pelitic schists
- PCs — Chlorite-biotite schist: fine-grained with well developed foliation, locally containing epidote, may be retrograded higher grade assemblages
- PCgn — Pelitic gneiss and schist: dominantly biotite paragneiss with subordinate layers of sillimanite-garnet gneiss
- PCq — Metaquartzite: dominantly graphitic quartzite with minor biotite and sillimanite bearing variants
- PCc — Calc-silicates: diopside-carbonate-quartz rocks; with intercalated biotite paragneiss, marble, and rare amphibolite

PRECAMBRIAN

———?——— Contact

Dashed where approximately located; short dashed where indefinite, gradational, or inferred from aerial photographs; dotted where concealed; queried where doubtful

———?——— Fault

Dashed where approximately located; short dashed where indefinite, gradational, or inferred from aerial photographs; dotted where concealed; queried where doubtful

30 — Strike and dip of foliation

1 0 1 2 3 4 MILES

1 0 1 2 3 4 5 KM

SCALE

Geology modified in part from Sainsbury, et al. (1969) and Salnsbury (1972, 1974, 1975)

References:

Hudson, T., 1977, Geologic map of the Seward Peninsula, Alaska, U.S. Geol. Survey Open-File Rept. 77-796A

Salnsbury, C. L., R. Kachadoorian, T. Hudson, T. E. Smith, T. R. Richards and W. E. Todd, 1969, Reconnaissance geologic maps and sample data, Teller A-1, A-2, A-3, B-1, B-2, B-3, C-1, and Bendeleben A-6, B-6, C-6, D-5, D-6 quadrangles, Seward Peninsula, Alaska, U.S. Geol. Survey Open-File Rept. 377

Salnsbury, C. L., 1972, Geologic map of the Teller quadrangle, western Seward Peninsula, Alaska, U.S. Geol. Survey map I-685

Sainsbury, C. L., 1974, Geologic map of the Bendeleben quadrangle Seward Peninsula, Alaska: The Mapmakers, Anchorage

Salnsbury, C. L., 1975, Geology, ore deposits, and mineral potential of the Seward Peninsula, Alaska, U.S. Bur. Mines Open-File Rept.

GEOLOGIC MAP OF THE BENDELEBEN A-6 and EASTERN PART OF THE TELLER A-1 QUADRANGLES, ALASKA

Bedrock Geology by Donald L. Turner, Samuel Swanson, Robert B. Forbes and Danita Maynard, Geophysical Institute, University of Alaska, Fairbanks

Surficial Geology by Jeffrey T. Kline, Richard D. Reger and Rena McFarlane, Alaska State Division of Geological and Geophysical Surveys

1979